

A nuclear magnetic resonance study of plant-water relationships



0000 0248 1295

BIBLIOTHEEK
LANDBOUWUNIVERSITEIT
WAGENINGEN

U10951

Promotor: dr. T. J. Schaafsma,
hoogleraar in de moleculaire fysica

Co-promotor: dr. H. van As,
universitair hoofddocent

NNO8201, 1176

J. E. A. Reinders

A nuclear magnetic resonance study of plant-water relationships

Proefschrift

ter verkrijging van de graad van
doctor in de landbouwwetenschappen,
op gezag van de rector magnificus,
dr. C. C. Oosterlee,
in het openbaar te verdedigen
op woensdag 11 november 1987
des namiddags te vier uur in de aula
van de Landbouwniversiteit te Wageningen.

ISN 293631

STELLINGEN

- 1 Met behulp van NMR is het in principe mogelijk onderscheid te maken tussen het effect van weerstandsverandering in wortel, respectievelijk blad op opwaarts watertransport van de plant.
(Dit proefschrift, hoofdstuk 7).
- 2 Het aantal gevonden exponenten bij een analyse van spinrelaxatiecurves in biologische systemen is niet noodzakelijkerwijze gerelateerd aan het aantal fysisch onderscheidbare waterfrakties.
(Dit proefschrift, hoofdstuk 4).
- 3 Om spin-spinrelaxatietijden van biologische systemen te kunnen vergelijken is het noodzakelijk de pulsrepetitietijd te kennen. Deze wordt ten onrechte vaak niet vermeld.
(P.A. Bottomley, T.H. Foster, R.E. Argersinger and L.M. Pfeifer, 1984. Med. Phys., 11, 425-48).
- 4 Het is voor real-time NMR flowmetingen van tijdsafhankelijke stroming in het algemeen noodzakelijk het spinrelaxatiegedrag van de vloeistof te kennen.
(H. Van As, J.E.A. Reinders, J.E.M. Snaar, 1987. Abstracts 1987 European Workshop on Magnetic Resonance in Medicine, London).
- 5 Uit de door M. Drews bepaalde volumetrische en lineaire snelheden in intacte augurkenplanten kan een effectief doorstroemd oppervlak worden berekend dat ca. 100x groter is dan het totale oppervlak van de doorsnede van xyleemvaten in deze planten. Dit is waarschijnlijk te wijten aan een onjuiste bepaling van de lineaire snelheid.
(M. Drews, 1982. Arch. Gartenbau, Berlin 30, 1, 27-38).
- 6 Het model van Windsor et al. voor het mechanisme van de primaire ladingsscheiding in de reactiecentra van fotosynthetische bacteriën is in strijd met de grootte van het waargenomen magneetveldeffect op de tripletopbrengst van de primaire donor.
(M.W. Windsor, 1986. J. Chem. Soc., Farad. Trans. 2, 82, 2237-43).

7 In hun model voor de heterogene reacties in systemen voor fotochemische waterstofproductie uit water verwaarlozen Miller et al. ten onrechte de aanwezigheid van buffer in deze systemen.

(D.S. Miller, A.J. Bard, G. McLendon, J. Ferguson, 1981. J. Am. Chem. Soc., 103, 5336-41).

8 De behandeling door de KNAU en de daaruit voortvloeiende prestaties van twee Nederlandse topatleten tijdens de wereldkampioenschappen atletiek in Rome, illustreren dat te ver doorvoeren van het gelijkheidsprincipe het leveren van goede prestaties in de weg staat.

9 Het wetsvoorstel betreffende voorwetenschap bij handel in effecten op de beurs bevat onvoldoende garanties om misbruik van voorkennis daadwerkelijk te voorkomen.

(Voorstel artikel 336a, Wetboek van Strafrecht).

Stellingen behorende bij het proefschrift:

"A Nuclear Magnetic Resonance Study of Plant-Water Relationships".

Johan Reinders, 11 november 1987.

Aan mijn ouders
Aan Adelheid

VOORWOORD

=====

Het onderzoek waarvan de resultaten in dit proefschrift zijn vastgelegd is uitgevoerd op de Vakgroep Moleculaire Fysica in de periode 1983 - 1987. Hoewel alleen mijn naam op de voorzijde van dit boekwerk prijkt, hebben ook vele anderen aan de totstandkoming ervan een bijdrage geleverd.

Allereerst wil ik Henk Van As bedanken, met wie ik altijd met zeer veel plezier heb samengewerkt en die altijd bereid was mij met raad en daad bij te staan. Zijn bijdrage aan dit proefschrift is onontbeerlijk geweest.

Ook wil ik professor Schaafsma bedanken, die altijd een rotsvast vertrouwen heeft gehad in de mogelijkheden van de techniek en veel energie heeft gestopt in het creëren van de juiste (o.a. financiële) randvoorwaarden, die noodzakelijk waren voor een succesvol verloop van het onderzoek. Zijn belangrijke inhoudelijke bijdragen aan het proefschrift wil ik ook niet veronachtzamen.

Voor de talrijke technische aspecten van het onderzoek is de hulp van Adrie de Jager onontbeerlijk geweest.

Zonder Ron Lukassen en Gerrit Polder had ik de (vele) verschillende computers nooit datgene kunnen laten doen wat ik wilde.

Bij name van Siert Zijlstra, Dick Visser en Ton den Nijs wil ik het Instituut voor de Veredeling van Tuinbouwgewassen bedanken voor het kweken van de komkommer- en augurkenplanten, die ik bij mijn experimenten heb gebruikt.

De werkplaats van Fysische en Kolloïdchemie bedank ik voor de bouw van de rf probe en de tekenkamer en de afdeling fotografie in het Bio-technion voor de nette weergave van de tekeningen in dit proefschrift.

Jannie Bijl en Riet Mes wil ik bedanken voor het geduld waarmee ze delen van dit proefschrift hebben getypt op de tekstverwerker.

Johan Reinders,

21 september 1987

CONTENTS

=====

<u>LIST OF ABBREVIATIONS AND FREQUENTLY USED SYMBOLS</u>	xiii
<u>CHAPTER I</u>	
1 INTRODUCTION	1
References	6
<u>CHAPTER II</u>	
2 THEORY	7
2.1 Introduction	7
2.2 Basic NMR Theory	7
2.3 Relaxation mechanisms	11
2.4 Relaxation in biological systems	13
2.5 Theory of NMR techniques	16
2.5.1 Flow measurements	16
2.5.2 T_2 -measurements	19
2.6 Water potential and (relative) water content	20
2.6.1 Water potential	20
2.6.2 Water content	23
2.6.3 Relationship between water potential and water content	23
2.7 Relationship between P_w , R_w , Ψ and proton spin relaxation times	26
2.8 Water flow through plants	30
2.9 References	31
<u>CHAPTER III</u>	
3 MATERIALS AND METHODS	34
3.1 Introduction	34
3.2 Computer-controlled experiments	34
3.3 Outline of equipment	36
3.3.1 Lock system	37
3.3.2 NMR probe	37
3.3.3 Linear Variable Differential Transformer (LVDT)	41

3.4 Plant material	41
3.5 Acknowledgements	44
3.6 References	44
<u>CHAPTER IV</u>	
4 PROTON SPIN RELAXATION AND DIFFUSION OF WATER IN TRANSPORT VESSELS OF PLANTS	45
4.1 Introduction	45
4.2 Theory	46
4.3 Materials and methods	49
4.4 Results and discussion	50
4.5 Diffusion in a spherical geometry	56
4.6 References	57
<u>CHAPTER V</u>	
5 ANGULAR AND FIELD STRENGTH DEPENDENCE OF ^1H NMR SPECTRA OF THE CUCUMBER STEM	59
5.1 Introduction	59
5.2 Theory	60
5.3 Materials and methods	61
5.4 Results	62
5.5 Discussion	63
5.6 Conclusions	66
5.7 Acknowledgements	66
5.8 References	66
<u>CHAPTER VI</u>	
6 EVALUATION OF THE NMR METHODS AND CALIBRATION	67
6.1 Introduction	67
6.2 Flow measurements	67
6.2.1 Flow profiles	68
6.2.2 Effect on the flow-curves of relaxation times T_1 and T_2 of flowing water	74
6.2.3 Local field inhomogeneity, off-resonance effects and stationary water signals	82
6.2.3.1 Effect of local field gradients on NMR	

flow signal	82
6.2.3.2 Effect of off-resonance on NMR flow curves	83
6.2.3.3 Contributions of stationary water to the flow signal	84
6.2.4 The accuracy of NMR flow measurements, a summary	86
6.2.4.1 Relationship \bar{v} vs. $1/t_m$; the calibration constant K_v	86
6.2.4.2 Relationship Q vs. \dot{S}_0 ; the calibration constant K_q	87
6.2.5 Calibration procedures	87
6.2.6 Discussion of the accuracy and limitations of NMR flow measurements	89
6.3 Measurement of water content and water potential	90
6.3.1 Transverse relaxation time	91
6.3.2 Initial height (A_0)	93
6.3.3 Experimental calibration curves and conclusions	94
6.4 References	95
 <u>CHAPTER VII</u>	
7 EXPERIMENTS ON INTACT PLANTS	96
7.1 Introduction	96
7.2 Water balance in Cucumis plants, measured by Nuclear Magnetic Resonance, I. (submitted to Journal of Experimental Botany)	97
7.3 Water balance in Cucumis plants, measured by Nuclear Magnetic Resonance, II. (submitted to Journal of Experimental Botany)	116
7.4 Miscellaneous experiments	131
7.5 References	139
 <u>SUMMARY</u>	140
 <u>SAMENVATTING</u>	144
 <u>CURRICULUM VITAE</u>	148

LIST OF ABBREVIATIONS AND FREQUENTLY USED SYMBOLS

=====

A (m^2)	= (vessel)wall area (Chapter 4)
A (m^2)	= area available for flow (§ 2.5, Chapters 6,7)
A_r (m^2)	= area of root membrane through which water flows
A_0 (arb.un.)	= initial amplitude of T_2 -curves
B (T(esla) or G(auss))	= magnetic field strength
B_x, B_y, B_z (T or G)	= magnetic field strength along x, y and z axis respectively
B_0 (T or G)	= laboratory magnetic field strength
B_1 (T or G)	= magnetic field strength of rf pulse
B_{loc} (T or G)	= local magnetic field strength
c ($mol \cdot l^{-1}$ (=M))	= concentration
\vec{C}	= torque
CPMG	= Carr-Purcell-Meiboom-Gill
γ ($rad \cdot s^{-1} \cdot G^{-1}$)	= gyromagnetic (magnetogyric) ratio
γ_H ($= 2.6752 \cdot 10^4 \text{ rad} \cdot s^{-1} \cdot G^{-1}$)	= gyromagnetic ratio of proton
γ_S ($rad \cdot s^{-1} \cdot G^{-1}$)	= gyromagnetic ratio of electron
d (m)	= thickness of bound water layer
D ($m^2 \cdot s^{-1}$)	= diffusion constant
D_p ($m^{-1} \cdot s^{-1}$)	= $-dP/(4 \eta \, dy)$
δ	= chemical shift
$\delta(A)$	= delta function of A
Δh (m)	= difference in height
Δ_S (m)	= difference in stem thickness
ΔV ($kg \cdot m^{-3}$)	= difference in water vapour concentration between leaf air space and air

$\Delta\delta$	= difference in chemical shift
E ($\text{kg}\cdot\text{s}^{-1}$)	= rate of transpiration (Chapter 7)
E (J)	= energy (§ 2.2)
f (Hz, s^{-1})	= frequency
FETS	= Fast Exchange Two State
FID	= Free Induction Decay
g ($=9.8 \text{ m}\cdot\text{s}^{-2}$)	= gravitational constant
G ($\text{G}\cdot\text{m}^{-1}$)	= magnetic field gradient
g_s ($\text{m}\cdot\text{s}^{-1}$)	= $1/r_s$ = stomatal conductivity
$G(\tau)$	= auto correlation function
h (m^{-1})	= H/D (Chapter 4)
h ($= 6,6256\cdot 10^{-34} \text{ J}\cdot\text{s}$)	= Planck's constant (Chapter 2)
\hbar ($\text{J}\cdot\text{s}$)	= $h/2\pi$ (Chapter 2)
H ($\text{m}\cdot\text{s}^{-1}$)	= sink strength parameter
η ($\text{N}\cdot\text{s}\cdot\text{m}^{-2}$)	= viscosity
θ	= angle
I	= angular momentum
I_n (arb.un.)	= intensity of component n
J_0, J_1	= Bessel functions of first kind and order zero and one respectively
$J(\omega)$	= spectral density function
K_q ($\text{m}^3\cdot\text{s}^{-1}\cdot(\text{arb.un.})^{-1}$)	= constant relating Q and \dot{S}_0
K_v (m)	= constant relating v and $1/t_m$
κ ($\text{m}^3\cdot\text{s}^{-1}\cdot\text{bar}^{-1}$)	= hydraulic conductance

L (m)	= length rf coil
L_r ($m \cdot s^{-1} \cdot bar^{-1}$)	= root permeability coefficient
L_s ($m \cdot s^{-1} \cdot bar^{-1}$)	= stomatal permeability coefficient
LVDT	= Linear Variable Differential Transformer
n (arb.un. $\cdot m^{-3}$)	= spin density
\vec{M} (arb.un.)	= $\sum \vec{\mu}$ = magnetization vector
M_{eq}	= equilibrium magnetization
$\vec{\mu}$ ($A \cdot m^{-1}$, arb.un.)	= magnetic moment
μ_0 ($J \cdot mol^{-1}$)	= chemical potential of water at STP
μ_w ($J \cdot mol^{-1}$)	= chemical potential of water
M_s (mol)	= moles of solute
NMR	= Nuclear Magnetic Resonance
P (bar, $N \cdot m^{-2}$)	= pressure
P_b	= fraction bound water
P_f	= fraction free water
P_i	= fraction of component i
$P(R)$	= probability distribution of radius R
P_r	= root pressure
P_w	= water content
$P(v)$	= probability distribution of velocity v
Π (bar)	= osmotic pressure
Q ($m^3 \cdot s^{-1}$)	= volume flow rate (flux)
Q_p	= quality factor of rf probe
r (m)	= distance or radial vector
r_b ($s \cdot m^{-1}$)	= boundary layer resistance
r_c ($s \cdot m^{-1}$)	= cuticular resistance
rf	= radio frequency

rh	= relative humidity
r_s ($s \cdot m^{-1}$)	= stomatal resistance
R ($=8.3 J \cdot K^{-1} \cdot mol^{-1}$)	= gas constant (§ 2.6)
R ($s \cdot m^{-1}$)	= resistance for transpiration (Chapter 7)
R', R ($s \cdot bar \cdot m^{-3}$)	= hydraulic resistance (§ 2.8)
R (m)	= radius (§ 2.7, Chapter 4)
Re	= Reynolds number
R_d	= water deficit
R_w	= relative water content
R_w^*	= $R_w \times 100\%$
R_1 (s^{-1})	= $1/T_1$ = longitudinal relaxation rate
R_2 (s^{-1})	= $1/T_2$ = transverse relaxation rate
$R_2(av)$ (s^{-1})	= $1/T_2(av)$
$R_2(e)$ (s^{-1})	= $1/T_2(e)$
R_{2i} (s^{-1})	= $1/T_{2,i}$
ρ ($kg \cdot m^{-3}$)	= density
S_0 (arb.un.)	= initial slope of flow curves
$S(t)$ (arb.un.)	= signal intensity as a function of time
STP	= Standard Temperature and Pressure (25°C, 1 bar)
σ	= reflection coefficient
t (s)	= time
t_m (s)	= time at which extremum occurs in flow curve
T (K)	= absolute temperature
T_b (s)	= T_1 or T_2 of bound water
T_f (s)	= T_1 or T_2 of free water
T_i (s)	= T_1 or T_2
T_{in} (s)	= initial decay time
$t_{\frac{1}{2}}$ (s)	= time required for FID to decay to half its initial value
T_1 (s)	= longitudinal relaxation time

T_2 (s)	= transverse relaxation time
$T_2(av)$ (s)	= average transverse relaxation time derived from 3-components analysis
$T_2(e)$ (s)	= transverse relaxation time defined as time at which T_2 -curve has decayed to 1/e times its initial value
T_{2b}, T_{1b} (s)	= T_2 respectively T_1 of bound water
T_{2f}, T_{1f} (s)	= T_2 respectively T_1 of free water
$T_{2,i}$ (s)	= transverse relaxation time of i'th component
$T_{2,n}$ (s)	= decay time of n'th root (Chapter 4)
τ (s)	= time between rf pulses in a flow experiment
τ_b (s)	= average residence time in fraction b
τ_c (s)	= rotation correlation time
τ_f (s)	= average residence time in fraction f
τ_m (bar)	= matric suction
τ_p (s)	= length of a pulse
2τ (s)	= time between 180° rf pulses in CPMG experiment
U ($\text{kg}\cdot\text{s}^{-1}$)	= rate of uptake
v ($\text{m}\cdot\text{s}^{-1}$)	= linear flow rate
\bar{v} ($\text{m}\cdot\text{s}^{-1}$)	= average linear flowrate
V_w ($\text{m}^3\cdot\text{mol}^{-1}$)	= molar volume of water
W_b (kg)	= weight of bound water
W_d (kg)	= dry weight
W_f (kg)	= weight of free water
W_{fr} (kg)	= fresh weight
W_t (kg)	= turgescent weight
Ψ (bar)	= plant water potential
Ψ_c (bar)	= Ψ at closed stomata
Ψ_l (bar)	= leaf water potential

Ψ_m (bar)	= matric potential
Ψ_o (bar)	= osmotic potential
Ψ_p (bar)	= pressure potential
Ψ_s (bar)	= water potential of soil or Steiner solution
Ψ_z (bar)	= gravitational potential
ω (rad·s ⁻¹)	= angular frequency
ω_0 (rad·s ⁻¹)	= larmor precession frequency
∇^2	= $\partial^2/\partial x^2 + \partial^2/\partial y^2 + \partial^2/\partial z^2$

CHAPTER I

=====

1. Introduction

The water status of plants is of extreme importance for their 'normal' functioning. Water deficits influence the behaviour of a plant at all levels of organization: metabolism, physiology, morphology and phenology are all affected [1]. Water is by far the most important solvent for biologically relevant solutes, and is the medium in which many biological reactions take place. The mineral nutrients needed for growth, and the organic products of photosynthesis are transported throughout the plant in aqueous solution. Water can also be considered as part of the plant structure, because it serves as an electron- and hydrogen donor in photosynthesis, and its protons, thus, are part of the carbohydrates produced by a plant. Because of its large specific heat, water in plants reduces fluctuations in tissue temperature, while its high latent heat of evaporation allows transpiration to keep tissue temperature below damage levels in hot climates, and the high latent heat of fusion reduces low temperature damage in environments that have freezing temperatures during part of the day. Because of its contribution to turgor, water is a very important supporting structure, especially in non-woody plants [2,3].

Several methods are used to study plant-water relationships. In the list below we will only be concerned with individual plants or plant organs, and not with canopies.

For the determination of the rate of water flow through a plant the following techniques have been used [4,5]:

- Injection and monitoring of dyes or radio-active tracers. Their rate of transport is followed by monitoring the moving front, and is assumed to be equal to the rate of water flow.
- Heat pulse method [6]. A heat pulse is applied to a plant stem, and its speed of movement is monitored upstream and downstream from the site where the pulse is applied. The unbalance indicates the velocity of water flow through the plant stem.

- Magnetohydrodynamic technique [7,8]. The plant is placed in a magnetic field perpendicular to the stem. The flow of conducting fluid (water) through the stem then causes a voltage perpendicular to both flow direction and magnetic field. This voltage is proportional to the velocity of the stream.
- Lysimeter, or weight balance technique [9]. During a sufficiently short period loss of weight of the plant and soil per unit time equals the rate of transpiration, if the change of weight due to growth can be neglected.
- Evaporation measurement. The loss of water vapour per unit time into an air stream flowing through a chamber containing all or a part of a plant is measured.

Techniques frequently used to measure water vapour in an airstream are (see e.g. [10]):

- dry- and wet bulb temperature;
- dew point;
- infrared gas analysis (IRGA);
- electronic relative humidity (rh) sensor;
- changes in thermal conductivity of the air due to changes in water vapour concentration (katharometer).

For the determination of water potential [Chapter 2] the following techniques are used [11]:

- Pressure chamber or pressure bomb. A leaf or shoot is excised and sealed into a pressure chamber with its cut end outside. The chamber is slowly pressurised until water appears at the cut end. The gas pressure is then equal, but opposite in sign, to the water potential of the leaf or shoot at the time of excision, provided the osmotic potential of the xylem fluid is negligible.
- Thermocouple psychrometer. A (small) chamber containing a Peltier psychrometer thermocouple is sealed onto a plant. After a suitable period of equilibration, chamber temperature and either the dew point or wet bulb temperature of air in the chamber is determined. Water potential can then be calculated, assuming the chamber and its contents to be isothermal.
- Gravimetric vapour exchange. Replicate leaf discs are weighed, then

left for several hours up to a day in separate vapour equilibration jars containing a graded series of osmotic solutions. The disks are then weighed again. The water potential of the leaf is equivalent to the osmotic pressure of the solution which causes no change in weight.

Water content, or the amount of water present in the tissue has been measured with the following techniques:

- Dendrometer [12], which measures the thickness of a leaf or stem. This device can be used to determine changes in water content, provided growth is accounted for.
- β -gauge (see e.g. [10]). The absorption of β -particles by a tissue (usually a leaf) is monitored. This is a measure for the thickness of the water layer, and thus for the total amount of water. It is accurate for measuring changes, not for absolute values.
- Attenuation of microwaves [13]. The absorption of microwaves by a tissue is monitored. Similar to the β -gauge technique, this is a measure for the amount of water.
- Measurement of dielectric constant [14]. The tissue is used as a dielectric medium in a capacitor. The capacitance increases with the amount of water in the tissue between the two plates.
- Measuring fresh and dry weight of a tissue. From these data the water content can be calculated [15].

All of the above mentioned techniques measure only a single variable: either water content, water potential, linear volume flow or volumetric water flow. Also many of the techniques are invasive or destructive. This does not apply to the NMR technique described below, and used in this thesis.

The measurement of water flow using pulsed Nuclear Magnetic Resonance (NMR) has been conducted at the Department of Molecular Physics since 1974 [4,16-22]. The method (denoted as Repetitive Pulse (RP) method) was well developed using model systems and computer calculations [17,18]. It has been shown that volumetric and linear flow of water in xylem vessels can be measured in cucumbers, gherkins and pumpkins [4,19]. The method has been successful in detecting pulsatile flow in human

fingers [4,22,25], even spatially resolved with a resolution of ca. 0.5 mm [20,21]. Also for the measurement of flow in large trees NMR has shown promising results [23].

For over 25 years NMR has been used to obtain information on the water content of biological tissue [5]. In this thesis both the signal amplitude [5] and relaxation rates (see e.g. [24]) are used for this purpose.

Except for the presence of a magnetic field gradient in the direction of flow, the RP flow method very much resembles the so-called Carr-Purcell-Meiboom-Gill (CPMG) method used to measure transverse relaxation rates (R_2) (see Chapter 2), and only minor changes in the instrumental settings are required to change from RP-flow to CPMG- R_2 measurements. Because both methods require only a few seconds measuring time, it is possible to do real-time measurements of water flow and water content with an unusually short time-resolution and high repetition frequency. Additionally, neither method affects the plant in any way, since the protons of the water molecules are used as a monitor, and an appropriate system design allows measurement on intact plants without mechanical or electrical contact between plant and instrument.

Thus, NMR has the following advantages as a monitor of the plant water status:

- It is non-destructive and non-invasive.
- It permits measurements of linear water flow, volumetric water flow, as well as water content.
- From a combination of volumetric and linear flow rate the effective total cross-sectional area available for flow can be calculated.
- It has a high time resolution, thus allowing for real-time, semi-continuous measurements of water flow and water content.

Disadvantages of the NMR method are:

- Intrinsic low sensitivity of NMR. Provided sufficient attention is paid to data acquisition and processing, the method can be made sensitive enough to obtain physiologically relevant data.
- High cost of NMR equipment as compared to the alternative equipment, described above, to monitor the water status. At the

Department of Molecular Physics a miniaturized, portable version of the NMR flow meter has been developed, for which the cost factor is considerably reduced.

Following the 'pioneering study' by Van As [4], demonstrating that the RP NMR method could be used to measure water flow in plants, this thesis is a further exploration of the application of NMR to study the water status of plants. One of the goals of the work presented in this thesis was to obtain a better definition of the reliability and accuracy of the data on the plant water status, using NMR. Although this study did not aim at obtaining novel data in the field of plant physiology, the interpretation of the NMR results heavily leans on the use of models from that field. Some of the properties of the NMR method (e.g. measurement of water potential and volumetric flow rate in a single experiment) permit the construction and testing of models for the plant water status, which are inaccessible using any other single method in existence. A second goal of this work is therefore to evaluate the significance of the data obtained by the NMR method in the field of plant physiology.

Part of the work described in this thesis was dedicated to the improvement of the equipment and experimental procedures. The study of the magnetic properties of the plant tissue (Chapter 5) and of the xylem vessels (Chapter 4), as well as the study of flow profiles (Chapter 6) are examples of this work. Another part of this work emphasises physiology, using NMR techniques as a monitor. The experiments described in Chapter 7, in which environmental changes were imposed on a plant in a controlled atmosphere made it possible to formulate a model of the water balance of plants.

We finally conclude that NMR can be a valuable technique in the study of plant-water relationships. Of the measured parameters the linear and volumetric flow rates can most reliably be determined. This can still be improved by further suppression of the stationary-water signal. R_2 , obtained from transverse magnetization decay curves, yields the most interesting information with respect to the water content, although the exact relationship between R_2 and water content/potential is still far from elucidated, and only relatively large changes in water

potential can be reliably detected. Comparison of NMR with other methods, such as those mentioned above, is useful and necessary for improving the accuracy and reproducibility of the NMR technique.

References

- [1] J.B. Passioura, 1982. "Physiological Plant Ecology II. Encyclopedia of Plant Physiology", Vol. 12B. Chapter 1. Lange et al. eds. Springer Verlag, Berlin.
- [2] P.S. Nobel, 1974. "Introduction to Biophysical Plant Physiology". W.H. Freeman and Company, San Francisco.
- [3] F.B. Salesbury and C. Ross, 1969. "Plant Physiology". Wadsworth Publishing Company, Inc., Belmont, California.
- [4] H. Van As, 1982. Ph.D Thesis. Agricultural University, Wageningen.
- [5] B. Slavik, 1974. "Methods of Studying Plant Water Relations". Ecological Studies, Vol. 9. Springer Verlag, Berlin.
- [6] K. Schurer, H. Griffioen, J.G. Kornet and G.J.E. Visser, 1979. *Neth. J. Agric. Sci.*, 27, 136-141.
- [7] D.W. Sheriff, 1972. *J. Exp. Bot.*, 23, 1086-1095.
- [8] D.W. Sheriff, 1974. *J. Exp. Bot.*, 25, 675-683.
- [9] P. Tegelaar, A.F. van der Wal, 1974. *Neth. J. Pl. Path.*, 80, 77-84.
- [10] Z. Sestak, J. Catsky and P.G. Jarvis, 1971. "Plant Photosynthetic Production. Manual of Methods". Dr. W. Junk N.V., Publishers, The Hague.
- [11] H.H. Wiebe, G.S. Campbell, W.H. Gardner, S.L. Rawlins, J.W. Cary and R.W. Brown, 1971. "Measurement of Plant and Soil Water Status". Utah State University, Logan, Utah.
- [12] W.G. Gensler, 1986. "Advanced Agricultural Instrumentation Design and Use". Gensler ed. Martinus Nijhoff Publishers, Dordrecht.
- [13] W.R.N. Edwards and P.G. Jarvis, 1982. *Plant, Cell and Environment*, 5, 271-277.
- [14] D.W. Sheriff, 1975. *J. Exp. Bot.*, 26, 645-650.
- [15] R.O. Slatyer, 1967. "Plant-Water Relationships". Academic Press, London.
- [16] M.A. Hemminga, P.A. de Jager and A. Sonneveld, 1977. *J. Magn. Res.*, 27, 359-370.
- [17] P.A. de Jager, M.A. Hemminga and A. Sonneveld, 1978. *Rev. Sci. Instr.*, 49, 1217-1218.
- [18] M.A. Hemminga, P.A. de Jager, 1980. *J. Magn. Res.*, 37, 1-16.
- [19] H. Van As and T.J. Schaafsma, 1984. *Biophys. J.*, 45, 469-472.
- [20] H. Van As, T.J. Schaafsma, P.A. de Jager and J.M. Kleijn, 1984. *Ann. Radiol.*, 27, 405-413.
- [21] H. Van As, J.M. Kleijn, P.A. de Jager and T.J. Schaafsma, 1985. *J. Magn. Res.*, 62, 511-517.
- [22] H. Van As, A.A.M. Brouwers and J.E.M. Snaar, 1985. *Arch. Int. Physiol. Biochem.*, 93, 87-95.
- [23] G. Byrne, 1987. CSIRO Division of Forest Research, Canberra, Australia. Personal communications.
- [24] G.D. Fullerton, J.L. Potter and N.C. Dornbluth, 1982. *Magn. Res. Imag.*, 1, 209-228.
- [25] H. Van As, 1987. Dutch Patent Application, no. 8700700.

CHAPTER II

=====

2 THEORY2.1 Introduction

This chapter contains the theory necessary for an understanding of the experiments described in the chapters 3-7. The theory deals with NMR (sections 2.2 - 2.4) and techniques (section 2.5), as applied to flow and relaxation times. The relation between NMR parameters and water content or water potential is described in sections 2.6 - 2.8.

2.2 Basic NMR theory

In this paragraph a short introduction to NMR theory is given. More extensive descriptions can be found in several textbooks [e.g. 1,2,3]. Nuclei of elements containing an odd number of neutrons or protons contain an intrinsic angular momentum \vec{I} (spin) as well as a magnetic moment ($\vec{\mu}$) related by [1]:

$$\vec{\mu} = \gamma \hbar \vec{I} \quad (2.1)$$

in which γ = gyromagnetic ratio, a constant for a given nucleus, and $\hbar = h/2\pi$, with h = Planck's constant, and \vec{I} represents the spin. When such a nucleus is placed in a static magnetic field \vec{B}_0 (conventionally chosen in the z-direction) an interaction energy E between \vec{B}_0 and $\vec{\mu}$ occurs, given by

$$E = - \vec{\mu} \cdot \vec{B}_0 \quad (2.2)$$

The torque \vec{C} acting on $\vec{\mu}$ is given by:

$$\vec{C} = \vec{\mu} \times \vec{B}_0 \quad (2.3)$$

The torque results in a precession of $\vec{\mu}$ around \vec{B}_0 with an angular frequency $\vec{\omega}_0$ (in rad/s), where:

$$\vec{\omega}_0 = -\gamma \vec{B}_0 \quad (2.4)$$

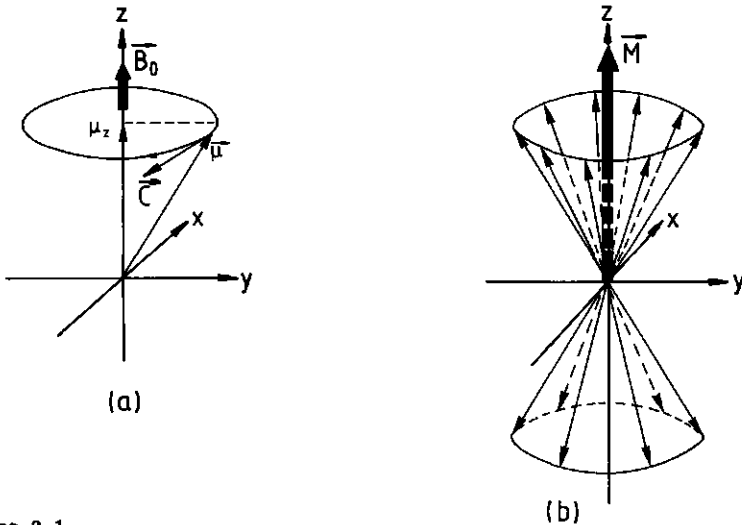


Figure 2.1

fig. 2.1a. Precession of a magnetic moment $\vec{\mu}$ about a static magnetic field \vec{B}_0 in the z-direction with frequency ω .; μ_z is the z-component of $\vec{\mu}$.; \vec{C} represents the torque $\vec{\mu} \times \vec{B}_0$.

fig. 2.1b. Precession of an ensemble of identical magnetic moments of nuclei with $I=1/2$. The net macroscopic magnetization (\vec{M}) is directed along \vec{B}_0 .

as shown in Fig. 2.1a. From quantum mechanics it follows that the component of \vec{I} parallel to \vec{B}_0 can only have $2I+1$ values, given by:

$$I_z = -I, -I+1, \dots, I-1, I \quad (2.5)$$

For a proton (^1H), the only nucleus considered in this thesis, $I=1/2$, leading to two allowed values of I_z and thus of μ_z , given by:

$$\mu_z = \pm \gamma \hbar / 2 \quad (2.6)$$

using eq. (2.2), and $B_0 =$ length of \vec{B}_0 :

$$E = \pm \frac{1}{2} \gamma \hbar B_0 \quad (2.7)$$

In Fig. 2.1b spins occupying both states (denoted by "up" and "down") are shown. Since the energy of the spins in the "up" position ($\vec{\mu}$ parallel with \vec{B}_0) is lower than of those in the "down" position ($\vec{\mu}$ antiparallel with \vec{B}_0),

the "up" position has an excess population of spins. The vector sum of all individual $\vec{\mu}$'s therefore results in a net magnetization vector \vec{M} , parallel to \vec{B}_0 . In thermal equilibrium $M_z = M_0$ and $M_{x,y} = 0$.

After \vec{M} is tipped away from the z-axis (by applying a second magnetic field \vec{B}_1 , perpendicular to \vec{B}_0 and oscillating at $\vec{\omega}_0$), it starts precessing around \vec{B}_0 with Larmor frequency $\vec{\omega}_0$. In descriptions of NMR-experiments commonly a frame of reference (x', y', z') is defined, which rotates around z with angular frequency $\vec{\omega}_0$ in the, hitherto used, laboratory frame (x, y, z). The z' axis in the rotating frame coincides with the z axis of the laboratory frame. This means that \vec{M} and \vec{B}_1 are stationary in the rotating frame. \vec{B}_1 is applied through a radio frequency (rf) coil and affects \vec{M} in an analogous way as \vec{B}_0 :

$$\vec{\omega}_1 = -\gamma \vec{B}_1 \quad (2.8)$$

in which $\vec{\omega}_1$ is the angular frequency resulting from the interaction of the spins with \vec{B}_1 . In pulse experiments \vec{B}_1 is turned off after \vec{M} has rotated through a desired angle α (e.g. 90° or 180° ; the corresponding rf pulses are referred to as 90° or 180° pulses, respectively):

$$\alpha = \gamma B_1 \tau_p \quad (2.9)$$

in which τ_p = pulse length, in our experiments of the order of microseconds. In Fig. 2.2 the effect of a 90° ($\pi/2$) and 180° (π) pulse along the x' -axis on \vec{M} is shown in the rotating frame of reference (i.e. \vec{B}_1 was di-

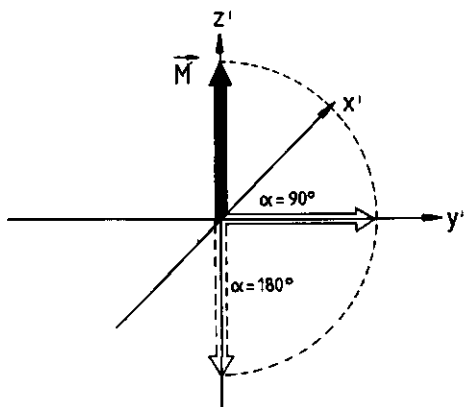


Figure 2.2
Effect on \vec{M} of a 90° and 180° rf pulse applied along the x' -axis of the rotating frame (x', y', z').

rected along the x' -axis), resulting in a magnetization directed along y' ($\vec{M}_{y'}$) and $-z'$ ($\vec{M}_{z'}$) respectively. \vec{M} has now been tipped away from its equilibrium position, which is along $+z'$. Return to the equilibrium state is caused by nuclear magnetic relaxation processes governed by the differential equation:

$$d\Delta M(t)/dt = -M(t)/T_1 \quad (2.10)$$

in which T_1 = the characteristic time constant for the relaxation process and

$$\Delta M(t) = M(t) - M_{eq} \quad (2.11)$$

with M_{eq} = equilibrium magnetization. Two time constants can be distinguished:

- 1) T_1 , spin-lattice- or longitudinal relaxation time: time constant for the return of M_z to its equilibrium value ($M_{eq} = M_0$);
- 2) T_2 , spin-spin- or transverse relaxation time: time constant for the return of $M_{x'}$ and $M_{y'}$ to their equilibrium value. For both $M_{x'}$ and $M_{y'}$: $M_{eq} = 0$.

From eqs. (2.10) and (2.11) the following can be deduced:

$$dM_{x'}(t)/dt = -M_{x'}(t)/T_2 \text{ or } M_{x'}(t) = M_{x'}(0) \exp(-t/T_2) \quad (2.12a)$$

$$dM_{y'}(t)/dt = -M_{y'}(t)/T_2 \text{ or } M_{y'}(t) = M_{y'}(0) \exp(-t/T_2) \quad (2.12b)$$

$$d(M_{z'}(t) - M_0)/dt = -(M_{z'}(t) - M_0)/T_1 \text{ or}$$

$$M_{z'}(t) = (M_{z'}(0) - M_0) \exp(-t/T_1) + M_0 \quad (2.12c)$$

The spin-lattice relaxation time T_1 characterizes the exchange of energy between the spin system and the degrees of freedom of the lattice whereas the spin-spin relaxation time T_2 characterizes the exchange of magnetic energy inside the spin system, i.e., without a net change of the equilibrium magnetization. T_2 characterizes the mean lifetime of the spins in a given energy state, due to the exchange of magnetic energy between the spins.

2.3 Relaxation mechanisms

As stated in the previous paragraph, the direction of \vec{M} (or $\vec{\mu}$) can be changed by applying a magnetic field \vec{B}_1 . Relaxation processes can be considered as originating from time dependent magnetic fields inside the sample that change the direction and amplitude of \vec{M} , and thus the amplitudes of \vec{M}_x' , \vec{M}_y' and \vec{M}_z' . T_2 processes are those in which M_x' and/or M_y' are changed. This can be brought about by magnetic fields in the directions y' and/or z' (changing M_x') and x' and/or z' (changing M_y'). T_1 processes are those in which M_z (= M_z') is changed. This can only be brought about by magnetic fields in x' and/or y' directions. This means that T_1 relaxation can only be effective with magnetic fields within the sample at angular frequency ω_0 (to have a stationary component along x' and/or y'), whereas T_2 relaxation can additionally be induced by slowly rotating magnetic fields (having components along $z'=z$). Magnetic fields with frequency components around $2\omega_0$ are also effective in T_1 and T_2 relaxation, as follows from more detailed relaxation theory [1-3]. In water the most important nuclear magnetic relaxation mechanism (and the only one discussed here) is the magnetic dipole-dipole interaction [1-3]. The magnetic moments of neighbouring water protons give rise to the magnetic fields responsible for relaxation. The local magnetic field (B_{loc}) induced by a spin $\vec{\mu}_1$ at the position of another spin is given by:

$$B_{loc} = \mu_1 (3\cos^2\theta - 1)/r^3 \quad (2.13)$$

in which r = distance between the two spins and θ = angle between \vec{B}_0 and the vector \vec{r} connecting both spins. Due to thermal motion of the molecules B_{loc} varies in time. In order to be effective for relaxation, B_{loc} must have frequency components of 0, ω_0 and $2\omega_0$ rad/s, as explained before. The power available at a particular frequency in the fluctuating B_{loc} is given by the spectral density function $J(\omega)$, which is the Fourier transform of the autocorrelation function $G(\tau)$, measuring the persistence of the fluctuations of motion. Frequently $G(\tau)$ drops off exponentially with a decay time τ_C , which is called the correlation time. In many cases, τ_C uniquely defines $J(\omega)$ for the local field.

For translational motion τ_C can be considered as the time needed for a

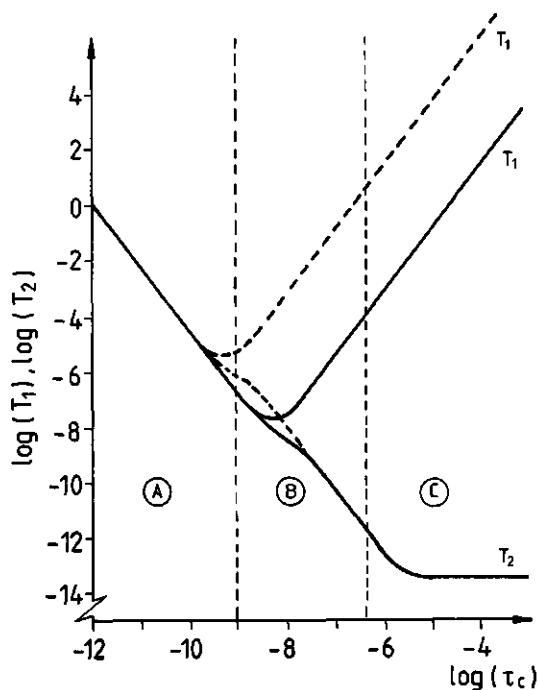


Figure 2.3

Dependence of the relaxation times T_1 and T_2 on the correlation time τ_c for two resonance frequencies:

---: 200 MHz, —: 20 MHz.

Three regions are defined with respect to the 20 MHz curves:

- A) rapid motion;
- B) motional narrowing;
- C) rigid lattice.

Ordinate and abscissa values as well as boundaries between the three regions are only approximate.

molecule to make a displacement corresponding to its diameter. Similarly, for rotational motion, τ_c can be viewed as the time needed to make a rotation through an angle of one radian. If we assume a mono-exponential auto-correlation function with correlation time τ_c characterizing molecular rotation, the dipole-dipole interaction for 2 identical nuclei with $I=1/2$ in one and the same molecule (e.g. water) gives rise to intramolecular nuclear spin relaxation, with relaxation rates [2]:

$$(1/T_1)_{\text{intra}} = (3\gamma^4 n^2 / 10r^6) [\tau_c / (1 + (\omega_0 \tau_c)^2) + 4\tau_c / (1 + 4(\omega_0 \tau_c)^2)] \quad (2.14a)$$

$$(1/T_2)_{\text{intra}} = (3\gamma^4 n^2 / 20r^6) [3\tau_c + 5\tau_c / (1 + (\omega_0 \tau_c)^2) + 2\tau_c / (1 + 4(\omega_0 \tau_c)^2)] \quad (2.14b)$$

where r is the internuclear distance and τ_c is the rotational correlation time. For the translational motions involved in intermolecular interactions of water molecules, the general expressions for $(1/T_1)_{\text{inter}}$ and $(1/T_2)_{\text{inter}}$ are similar [4] to eqs. (2.14a,b). The rotational correlation time τ_c must

then be replaced by the translational correlation time [2]. Eqs. (2.14a,b) are depicted in Fig. 2.3. In this figure, A indicates the region of rapid motion for which $\omega_0\tau_C \ll 1$ and $T_1 = T_2 \sim 1/\tau_C$. B indicates the region of "motional narrowing" for which $T_1 > T_2$. C indicates the "rigid lattice" region for which $T_1 \gg T_2$. For this region eq. (2.14b) does not apply anymore, because molecular fluctuations are too slow to time average the nuclear spin-spin interactions. For long τ_C spin-spin relaxation becomes non-exponential and independent of τ_C , as has been observed for ice (see e.g. [4]). The dashed line indicates the relaxation behaviour at a larger value of ω_0 than for the fully drawn line. The correlation time τ_C increases with decreasing temperature.

2.4 Relaxation in biological systems

At room temperature τ_C for water molecules is of the order of 10^{-12} s, which falls, for usual NMR frequencies ($10^6 - 10^9$ Hz), in region A of Fig. 2.3. Therefore for bulk water at room temperature $T_1 = T_2$. Relaxation times of water in biological systems are frequently found to be shorter than for bulk water, measured at the same temperature. Additionally, T_1 is usually larger than T_2 . The relaxation curves in general are not mono-exponential for these systems as they are for bulk water. It is generally accepted that this is due to macroscopic and microscopic sample heterogeneity [4-12]. Water in different tissue types and, within one tissue type, different cell types, has different correlation times and thus different relaxation times. Also within a certain cell type various cell organelles and macromolecules are responsible for the existence of various water fractions. The observed relaxation rate, is then a (complex) combination of the relaxation rates of the various water fractions, in which factors like the relative amount of water in a certain fraction and the relaxation rate and residence time of a molecule in this fraction should be considered [10].

A common way to describe relaxation in heterogeneous systems is due to Zimmermann and Brittin [13]. If we consider two water fractions b and f with relaxation times T_b and T_f , relative populations P_b and P_f ($P_b + P_f = 1$), and average residence times τ_b and τ_f of the protons in fraction b and f before transfer occurs to the other fraction, the magnetization decay

following a pulse is given by [10]:

$$M(t)-M_0 = (M(0)-M_{eq})(P_{f'} \exp(-t/T_{f'}) + P_{b'} \exp(-t/T_{b'})) \quad (2.15)$$

where:

$M(0)$ = magnetization at a time immediately following the pulse at $t = 0$;

$$1/T_{f'} = C_1 - C_2 \quad (2.16a)$$

$$1/T_{b'} = C_1 + C_2 \quad (2.16b)$$

$$P_{b'} = 1/2 - [(P_b - P_f)(1/T_f - 1/T_b) + 1/\tau_f + 1/\tau_b]/4C_2 \quad (2.16c)$$

$$P_{f'} = 1 - P_{b'} \quad (2.16d)$$

in which

$$C_1 = (1/T_f + 1/T_b + 1/\tau_f + 1/\tau_b)/2 \quad (2.17a)$$

$$C_2 = [(1/T_b - 1/T_f + 1/\tau_b - 1/\tau_f)^2 + 4/\tau_f\tau_b]^{1/2}/2 \quad (2.17b)$$

Furthermore $P_b/P_f = \tau_b/\tau_f$.

The following cases can be distinguished:

- 1) $\tau_f, \tau_b \gg T_f, T_b$ (slow exchange). This results in $P_{f'} = P_f$, $P_{b'} = P_b$, $T_{f'} = T_f$ and $T_{b'} = T_b$. A biexponential curve is obtained for which the relative amplitudes correspond to the relative amounts of water in both fractions. The decay times represent the relaxation times of both individual fractions.
- 2) $\tau_f \gg T_f, T_b \gg \tau_b$. Under these conditions, the decay curve is again biexponential with $T_{f'} \approx T_f$, $T_{b'} \approx \tau_b$, $P_{b'} \approx P_b \ll 1$, and $P_{f'} \approx P_f \approx 1$. This situation corresponds to a very short residence time of water molecules in the bound phase, presumably due to weak bonding. Under strong bonding conditions the labels f and b in the abovementioned results should be interchanged.
- 3) $\tau_f, \tau_b \ll T_f, T_b$ (fast exchange). A mono-exponential curve is obtained for which the decay rate is the weighted average of the relaxation rates of both fractions:

$$M(t)-M_0 = (M(0)-M_0) \exp(-t(P_f/T_f + P_b/T_b)) \quad (2.18)$$

This is referred to as the fast exchange two state (FETS) model.

It is obvious from the above that the interpretation of relaxation data is rather complex, due to the large number of parameters involved. Even for as few as two states, the relaxation curve is determined by 6 different parameters, and generally additional assumptions on the (relative) values are required to interpret the data. Frequently these assumptions reduce the problem to a situation in which a number of fractions can be distinguished being in "slow" or "fast" exchange or to a combination of both [11]. In biological systems these different fractions originate from water bound to various tissue types and macromolecules on one hand and free, unbound (bulk) water on the other hand. The correlation times of the bound water are longer than those of free water, resulting in different relaxation times for both types of water molecules as can be seen from Fig. 2.3.

We discuss now in somewhat more detail the consequences of the FETS model. Let us assume two water fractions in fast exchange: "free" (bulk) water, with a τ_c value in region A of Fig. 2.3 and a transverse and longitudinal relaxation time of T_{2f} and T_{1f} and "bound" water, with a τ_c value in region B of Fig. 2.3 with relaxation times T_{2b} and T_{1b} . Defining

$$1/T_2(\text{av}) = P_f/T_{2f} + P_b/T_{2b} \quad (2.19a)$$

and

$$1/T_1(\text{av}) = P_f/T_{1f} + P_b/T_{1b} \quad (2.19b)$$

it can be seen that:

- 1) The average spin-spin relaxation time ($T_2(\text{av})$) is shorter than that for bulk water, and decreases upon an increase of the bound water fraction P_b ;
- 2) $T_{1b} > T_{2b}$ thus leading to a longer value of $T_1(\text{av})$ than that of $T_2(\text{av})$. Also eq. (2.19b) predicts a decrease of $T_1(\text{av})$ upon an increase of P_b , unless τ_c of the bound water is so large that $T_{1b} > T_{1f}$.

Fig. 2.3 also shows that $T_1(\text{bound})$ and thus $T_1(\text{av})$ increases with ω_0 , as has been frequently observed [12].

It should be mentioned that for bound water the rotational and translational fluctuations may become non-isotropic, which means that eqs. (2.14a, b) and Fig. 2.3 do not apply anymore [14]. Therefore one needs to be care-

ful when calculating values of τ_C for bound water from observed relaxation rates. In case of doubt, eqs. (2.14a) and (2.14b) can be verified by measuring at different values of ω_0 .

Apart from intra- and intermolecular spin-relaxation as discussed before, cross-relaxation represents another important mechanism for spin relaxation in biological systems. Here, magnetization exchange takes place between spins in regions with different Larmor frequencies or magnetic moments. Usually these spins have also different magnetization values. These can be induced by selective excitation by rf fields, or may result from different relaxation times. The exchange model, described before, is frequently used for the description of this phenomenon [4,15-22], in which values of $1/\tau_b$ and $1/\tau_f$ should now be read as the rates of transfer (the cross-relaxation rates) of magnetization from phase b to f and vice versa.

In the theory described until now, multi-exponential behaviour was believed to result from the presence of distinguishable compartments and/or long correlation times. It has been demonstrated, however [23-26, Chapter 4], that in systems in which diffusion determines magnetization transfer, multi-exponential behaviour can also be observed, irrespective of the presence of multiple water fractions. In such a system the distance between a spin and a "relaxation sink" (e.g. a surface of a macromolecule or of a cell organelle) determines whether the spin reaches the sink or not. Systems in which this type of relaxation can be expected are those in which there are compartments with a size of the order of micrometers containing localized relaxation sinks such as cell walls. Most filled-pore systems will meet this criterium [26], provided that the pores are large enough, e.g. vacuoles of plants [8] or xylem vessels [Chapter 4].

2.5 Theory of NMR techniques

2.5.1 Flow measurements

For the NMR flow measurements described in this thesis we used the RP-method [27,28]. A series of equidistant, identical rf pulses is applied along the x' -axis of the rotating frame, in the presence of a static, linear magnetic field gradient (G) in the direction of flow (say: y), leading to $B_z(y) = B_0 + Gy$. The NMR signal, generated along the x' axis during

the interval between the pulses is sampled. Due to the fact that the sample (plant stem) extends through the rf coil there is a spatial distribution of the rf field B_1 in the direction of flow. The pulse angle is largest in the center of the rf coil and decreases in the directions $-y$ and $+y$. Provided that the rf coil is symmetrical, i.e. $B_1(y) = B_1(-y)$, and $B_z(y) = B_0 + Gy$

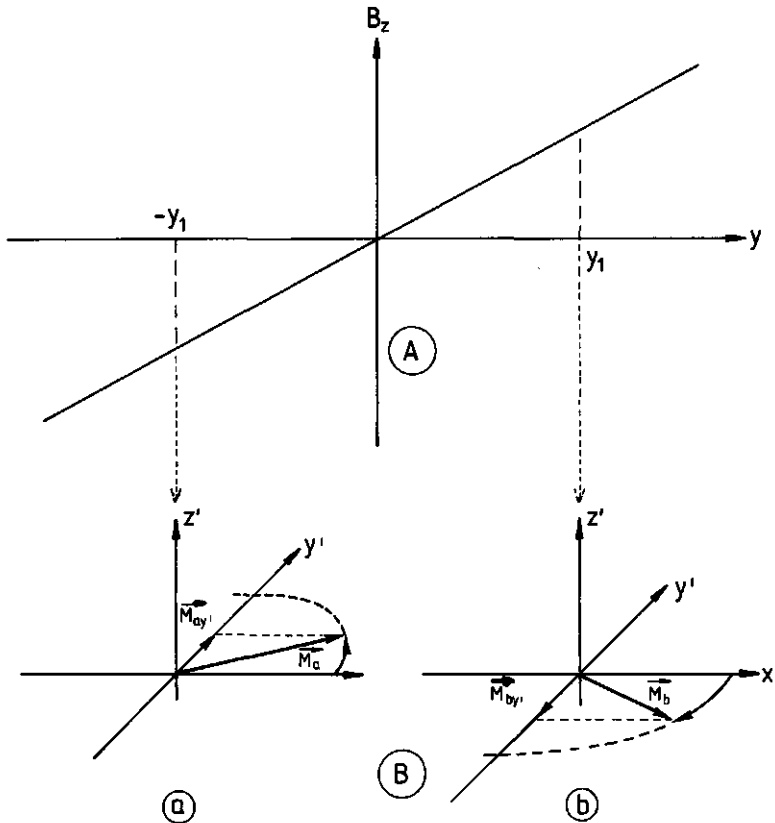


Figure 2.4

(A) Magnetic field strength as a function of the coordinate y in the flow direction. At the intersection of the y and B_z axes $B_z = B_0$.

(B) Rotating frames at positions $y = -y_1$ (a) and $y = y_1$ (b). \vec{M}_a and \vec{M}_b represent the magnetization vectors which have rotated around z' in the frames a) and b), respectively, during a time τ after the first $(\pi/2)$ pulse of a flow experiment. $\vec{M}_{ay'}$ and $\vec{M}_{by'}$ are the y' -components of \vec{M}_a and \vec{M}_b , respectively.

(see Fig. 2.4A), it can be seen from Fig. 2.4B that a signal will evolve for flowing water, whereas stationary water will generate no net signal. In Fig. 2.4B two rotating frames are shown at $y = -y_1$ (a) and $y = y_1$ (b), respectively. For clarity it has been assumed that at these positions $B_1(y)$ corresponds to a 90° pulse. Theory, however, applies for all pulse angles. After this pulse has been applied, \vec{M} is directed along the x' axis, and starts precessing around the z' axis leading to \vec{M}_a and \vec{M}_b after a period t for the frames a and b of Fig. 2.4B respectively. For stationary spins the measured components (\vec{M}_{ay}' and \vec{M}_{by}') are equal in amplitude, but opposite in sign, thus leading to a net zero vector component along y' . For moving spins (in the positive y direction) \vec{M}_{by}' will be larger than \vec{M}_{ay}' after a period t , and a net signal results [29]. Fig. 1 of section 7.2 shows typical curves for two different flow rates which can be expected from such an experiment. The observed signals cannot be described in a closed mathematical form, but approximations can be made [28,30], resulting in expressions which give quite good insight in the effect of changing the various experimental parameters. Computer simulations and experiments have shown that the main parameters affecting the flow curves are: value of G , time interval (τ) between the pulses, coil geometry, flow profile, and the relaxation times T_1 and T_2 of the flowing liquid [27,28,30,31]. From the observed signals the following parameters can be obtained:

1) linear flow rate (v , m/s):

$$v = K_v/t_m \quad (2.20)$$

in which t_m (s) = time at which the signal reaches an extremum; K_v is a calibration constant (see Chapter 6);

2) volumetric flow rate (Q , m³/s):

$$Q = K_q \dot{S}_0 \quad (2.21)$$

in which \dot{S}_0 is the (initial) slope at $t=0$. K_q is a calibration constant (see Chapter 6);

3) effective cross-sectional area available for flow (A , m²):

$$A = Q/v \quad (2.22)$$

2.5.2 T₂-measurements

The transverse relaxation rate ($R_2 = 1/T_2$) is measured using the Carr-Purcell-Meiboom-Gill (CPMG) pulse sequence [1]. This sequence consists of a single 90° pulse along the x'-axis and a train of 180° pulses along the y'-axis. The response signal along the y'-axis ("echo") occurs inbetween the 180° pulses and is sampled at $t = 2n\tau$ for the CPMG sequence:

$$90^\circ_{x'} - (\tau - 180^\circ_{y'} - \tau)_n \quad (2.23)$$

where the time between two 180° pulses = 2τ and n is the number of 180° pulses. The first 90° pulse aligns the magnetization vector \vec{M} along the y'-axis and the amplitude of $\vec{M}_{y'}$ at $t = 0$ (A_0) is a measure for the total amount of resonant spins in the sample. Subsequently $\vec{M}_{y'}$ decays in the x'y'-plane with a time constant defined as T_2^* . The response (i.e. of the y'-component) as a function of time is denoted as the Free Induction Decay (FID). For a perfectly homogeneous field $T_2^* = T_2$ of the sample. In practice, however, B_0 is not homogeneous, leading to a spread of Larmor frequencies of the various spins in the sample and thus an additional dephasing of the spins resulting in $T_2^* < T_2$. The 180° pulses compensate for this inhomogeneity, as a result of a rephasing of the spins at times $2n\tau$ ($n=1,2,\dots$), such that the envelope over the echoes, recorded at $t = 2n\tau$, represents the decay curve of the transverse (x'y') component of \vec{M} , characterized by T_2 of the sample only [1]. This rephasing will only be complete if each of the spins experiences the identical magnitude of the magnetic field during a time τ on both sides of the 180° pulse. The shorter τ the better the rephasing will be, since diffusion of molecules in the sample during a period 2τ will cause the spins to move from one region to another, with possibly a different magnitude of the magnetic field as a result of local inhomogeneities. On the other hand it is possible to calculate the diffusion constant from a T_2 -experiment by deliberately introducing an inhomogeneity (a linear magnetic field gradient) during the CPMG-experiment leading to an observed relaxation rate $1/T_2(\text{obs})$:

$$1/T_2(\text{obs}) = 1/T_2 + \gamma^2 G^2 D \tau^2 / 3 \quad (2.24)$$

in which D (m^2/s) = diffusion constant in the direction of G .

2.6 Water potential and (relative) water content

2.6.1 Water potential

The term water potential (Ψ) is frequently used in the study of plant-water and soil-water relationships. It is defined as follows:

$$\Psi = (\mu_w - \mu_0) / V_w \quad (2.25)$$

in which μ_w (J/mol) = the chemical potential of the water in the system; μ_0 (J/mol) = chemical potential of pure water at standard temperature and pressure (STP); and V_w (m³/mol) = partial molar volume of water. The water potential is expressed in units J·m⁻³. For practical purposes the equivalent units N·m⁻², Pa or bar are used: 1 J·m⁻³ = 1 N·m⁻² = 1 Pa = 10⁻⁵ bar. Between two systems separated by a semi-permeable membrane with a reflection coefficient of 1 which are in diffusive contact with each other, mass (water) transport will take place when their chemical (water) potentials are different.

The water potential is usually divided into four different components, the sum of which forms the total water potential:

$$\Psi = \Psi_p + \Psi_o + \Psi_z + \Psi_m \quad (2.26)$$

in which Ψ_p = pressure potential, Ψ_o = osmotic potential, Ψ_z = potential as a result of gravity and Ψ_m = matric potential.

1) Osmotic potential:

When a solution is separated from pure solvent by a membrane permeable only to the solvent, there is a net flux of solvent into the solution since the chemical potential of the solvent is higher in the pure phase than in the solution. This process is called osmosis and results from the osmotic potential:

$$\Psi_o = -\Pi \quad (2.27)$$

For an ideal solution the following applies for the osmotic pressure Π :

$$\Pi = RTc \quad (2.28)$$

in which R (J·K⁻¹·mol⁻¹) = gas constant; T (K) = absolute temperature; c (mol·m⁻³) = concentration of the solute. The minus sign in eq. (2.27)

refers to the fact that water flows from places with low to places with high concentrations of solute.

2) Matric potential:

Matric potential (Ψ_m) results from the binding forces between a solid (e.g. macromolecules or cell walls) and the water molecules, e.g. hydrogen bonds, electrostatic forces, London-Vanderwaals forces:

$$\Psi_m = -\tau_m \quad (2.29)$$

in which τ_m = matric suction [33] and the minus sign is included because water moves towards lower (more negative) potentials.

In the plant cells osmotic and matric potential are counteracted by:

3) Pressure potential (Ψ_p), due to hydrostatic pressure P:

$$\Psi_p = P \quad (2.30)$$

and

4) Gravitational potential (Ψ_z), resulting from the height of the water column above the roots in contact with soil water:

$$\Psi_z = -\rho g \Delta h \quad (2.31)$$

in which ρ ($\text{kg}\cdot\text{m}^{-3}$) = density of water, g ($\text{m}\cdot\text{s}^{-2}$) = gravitational constant and Δh (m) = height of the measuring point above the roots. Except in tall trees, Ψ_z can usually be ignored.

Substitution of eqs. (2.27), (2.29) and (2.30) in (2.26) and ignoring Ψ_z we find:

$$\Psi = P - \sigma\pi - \tau_m \quad (2.32)$$

in which a reflection coefficient (σ) has been included, which accounts for the porosity of the semi-permeable membrane for solute molecules. If the membrane is impermeable for the solute, $\sigma = 1$, and if the membrane is fully permeable for the solute, $\sigma = 0$. P is usually called turgor or turgor pressure and is to a large degree responsible for the stiffness of a plant. The relationship between turgor, osmotic pressure, water potential and the relative cell volume (or water content) of an idealized osmotic cell is given in a Höfler diagram [32]. This is shown in Fig. 2.5 for a cell with $\tau_m = 0$

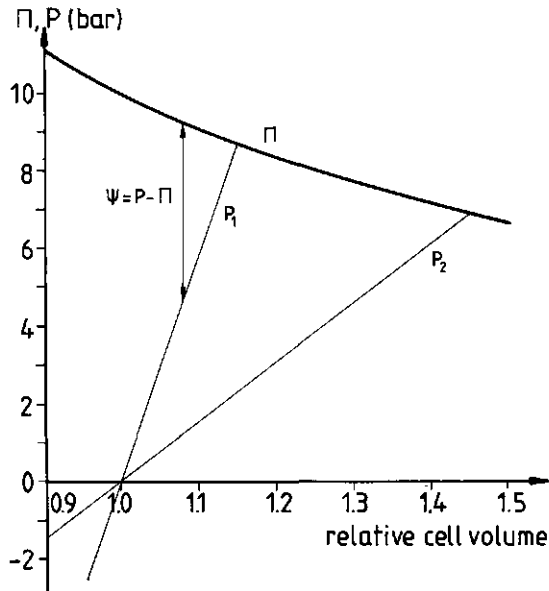


Figure 2.5

Model diagram, or Höfler diagram showing the relationship between osmotic pressure (Π), turgor pressure (P), plant water potential (Ψ) and the relative cell volume for an ideal osmotic cell. P_2 represents the turgor pressure curve for a cell with a more elastic wall than curve P_1 .

and $\sigma = 1$ in contact with pure water at standard temperature and pressure (for which $P = \Pi = \tau_m = 0$). In Fig 2.5 it can be seen that Π declines upon an increase of cell volume. This increase is due to dilution of the solution resulting from the influx of water. P (represented by P_1 or P_2) increases upon an increase of the cell volume because of the presence of a, more or less, rigid cell wall. Curve P_2 gives the turgor pressure for a cell with a more elastic cell wall than curve P_1 . $P = 0$ and $\Psi = -\Pi$ at a relative cell volume of 1. This is the point of incipient plasmolysis (loss of turgor). When the cell is at equilibrium with pure water in the external environment $P = \Pi$, $\Psi = 0$ and full turgor is reached.

Water flows towards sites with lower water potential. In plants Ψ is rarely above zero.

2.6.2 Water content

Apart from water potential a few other concepts are frequently used in the study of plant-water relationships [31]:

1) Water content (P_w), defined as:

$$P_w = (W_{fr} - W_d)/W_d \quad (2.33)$$

in which W_{fr} (kg) = fresh weight of the tissue sample and W_d (kg) = dry weight of the tissue sample obtained after drying the sample in an oven to constant weight at 80 - 90°C;

2) Relative water content (R_w) or relative turgidity, which expresses the water content as a percentage (R_w^*) or fraction (R_w) of the (maximum) water content under conditions of full turgor:

$$R_w^* = [(W_{fr} - W_d)/(W_t - W_d)] \cdot 100\% \quad (2.34a)$$

$$R_w = (W_{fr} - W_d)/(W_t - W_d) \quad (2.34b)$$

in which W_t (kg) = turgid weight, obtained by floating the tissue in water until the rate of water uptake has fallen below a predetermined value, and then weighing it;

3) water deficit R_d :

$$R_d = 1 - R_w \quad (2.35)$$

2.6.3 Relationship between water potential and water content

The relationship between (relative) water content and water potential depends on the relations between (relative) water content and the components of Ψ (Π , τ_m and P), as can be seen from eq. (2.32). The simplest one is Π . Rewriting eq. (2.28) and combining it with (2.33) or (2.34b) yields:

$$\Pi = RT\rho N_s/(W_{fr}-W_d) = RT\rho N_s/[R_w(W_t - W_d)] = RT\rho N_s/(P_w W_d) \quad (2.36)$$

in which ρ ($\text{kg}\cdot\text{m}^{-3}$) = density of the solution (\propto density of the solvent (water), since eqs. (2.36) and (2.28) only apply for very dilute solutions) and N_s = moles of solute. $W_{fr} - W_d$ = total weight of the water in the sam-

ple. It can be seen from eq. (2.36) that Π has a reciprocal relationship to R_w and P_w (see the dashed lines of Fig. 2.6). The relationship between R_w or P_w and P depends on the elasticity of the wall, frequently expressed in terms of an elastic modulus [34], which is the slope of the straight lines P_1 and P_2 in Fig. 2.5. In general P_1 and P_2 need not be straight lines; i.e. the slope and thus the elastic modulus is usually not constant but depends on the pressure exerted on the cell wall and varies strongly for different tissue types and age of the plant [34].

The matric potential (Ψ_m) decreases (i.e. it becomes more negative) upon a decrease of the water content. The less strongly bound water will be removed first. The thus reduced quantity of water will be bound stronger to surfaces. Of course this decrease of Ψ_m with P_w or R_w occurs only if water is removed from the region into which the matric forces extend. This is not likely to occur for the type of plants which we have studied until P_w and R_w have decreased to relatively low values.

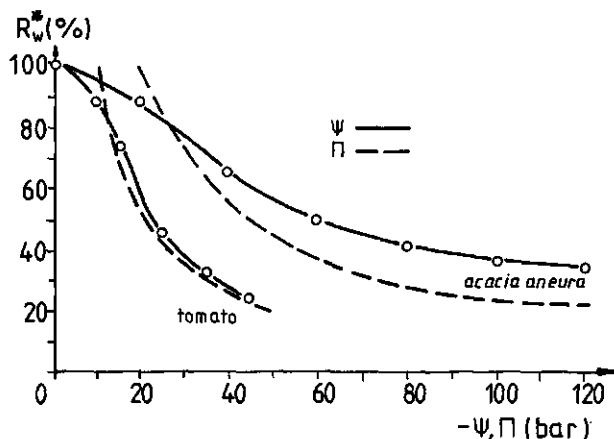


Figure 2.6

Relationship between osmotic pressure (Π), turgor pressure (P), plant water potential (Ψ) and the relative water content for tomato and acacia aneura plants (after [31]). The point of incipient plasmolysis (wilting) is the point of intersection of the curves of Ψ and Π .

A universal relationship between R_w (or P_w) and Ψ therefore does not exist for different types of plants and only empirical relationships can be used.

Typical relationships for R_w vs Ψ and Π are shown for tomato and acacia in Fig. 2.6 [31], and for tomato and cucumber in the most interesting region from a physiological point of view in Fig. 2.7 [35]. From Fig. 2.6 we may conclude that a reciprocal relationship exists between Π and P_w . As is clear from this figure, the tomato plant loses more water at high Ψ than does the acacia plant, and that wilting occurs at a less negative value of Ψ (potentials for incipient plasmolysis: tomato: ≈ -13 bar; acacia: ≈ -27 bar). Fig. 2.7 shows a linear relationship between R_w and Ψ for both tomato and cucumber plants for Ψ of -3 to -18 bar [35]. Equal changes in R_w lead to larger changes in Ψ for cucumber than for tomato.

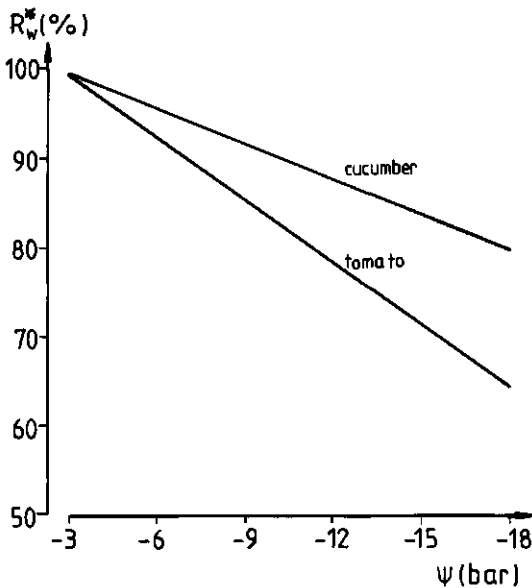


Figure 2.7

Relationship between relative water content (R_w^*) and leaf water potential (Ψ) for cucumber and tomato plants (after [35]).

2.7 Relationship between P_w , R_w , Ψ and proton spin relaxation times

To investigate the relationship between P_w , R_w , Ψ , and the relaxation times T_1 and T_2 , the separate relations between T_1 and T_2 and the three components of Ψ (P , Π and τ_m) are now discussed.

1) Effect of P .

Although P is a very important factor in determining the water potential it has hardly any effect on the relaxation times. In the range 0-3000 bar a decrease of T_1 upon an increase of pressure was found to be $< 0.01\%$ /bar at temperatures ranging from 0-60°C [36].

2) Effect of Π .

Ions in solution affect the "internal structure" of the bulk water and therefore affect the correlation time of the water near the ion. This effect, however, is only very small. In the first hydration layer of a Na^+ ion τ_c of a water molecule is about 3 times the value for bulk water [37], and very large concentrations of solute are necessary to appreciably affect the relaxation time [39]. The effect also depends on the type of solute. Raaphorst et al. [38] found that KCl had an increasing effect on T_1 , whereas LiCl, NaCl, CaCl, Na_2SO_4 and sucrose caused a decrease of T_1 . The effect was the largest with sucrose (a decrease of T_1 of $\approx 0.3\%$ /bar osmotic pressure) up till 0.1 M) and the effect increased with concentration. It was the weakest for NaCl (negligible until 1 M NaCl, which is equivalent to $\Pi \approx 50$ bar). The effect of the other ions was somewhat higher than for NaCl (about 0.03% /bar in the region 0 - 0.1 M). For electrolyte concentrations above ca. 0.1 M appreciable effects on T_1 were found [38].

If the solute molecules are paramagnetic a large decrease in T_1 occurs because the magnetogyric ratio of the electron spin of paramagnetic ions (γ_s) is much larger than for protons. In eqs. (2.14a,b) γ^4 is replaced by $\gamma_H^2 \cdot \gamma_s^2$, in which γ_H = magnetogyric ratio of the proton. It has been found that relaxation of water in plant material is not affected by the presence of paramagnetic ions in the tissue [41].

3) Effect of τ_m .

The correlation times of water bound to macromolecules or colloidal structures by matric forces can be several orders of magnitude higher than for free water. For example, the rotational correlation time of water molecules associated by hydrogen bonds to polar groups of macromolecules are of the order of 10^{-6} s [40] as opposed to correlation times for free water in the order of 10^{-12} s. From Fig. 2.3 it can be seen that this clearly influences the relaxation times, and the matric potential should be considered as the main factor relating water potential, water content and relaxation times.

Generally the sample contains regions with different relaxation times. We limit the following discussion to two regions (also denoted as "sites") consisting of free and bound water. For such a system eq. (2.15) is applicable. We distinguish the two limiting cases of fast exchange (FETS, eqs. (2.18) and (2.19a,b)) and slow exchange. From eqs. (2.15-2.17) it can be seen that the observed relaxation time ($T(av)$, in which T can be either T_1 or T_2) changes whenever a change in water potential results in a change of P_f , T_f , P_b and/or T_b . Within our model T_f and T_b are constants, independent of the water content. A decrease of the water content results in an increase of P_b and a decrease of P_f .

a) FETS model.

Because $P_f + P_b = 1$ we can derive from eqs. (2.18) and (2.19a,b):

$$1/T(av) = 1/T_f + P_b(1/T_b - 1/T_f) \quad (2.37)$$

Assuming equal densities for bound and free water the following applies:

$$P_b = W_b/(W_b + W_f) = W_b/(W_{fr} - W_d) = W_b/(P_w W_d) \quad (2.38)$$

where W_b and W_f are the weights of bound and free water, respectively. The sum of W_f and W_b is the total weight of water ($= W_{fr} - W_d$) in the tissue, which is proportional to $1/P_w$ as can be seen from eq. (2.33). Thus for high water contents (i.e. if the change in W_b can be neglected) P_b is linearly proportional to $1/P_w$, leading to a linear relationship between $1/T(av)$ and $1/P_w$, as can be seen from eqs. (2.37) and

(2.38). Indeed, a linear relationship between $1/T(av)$ and $1/P_w$ has often been found [11,40-43]. From Fig. 2.7 we can conclude that a decrease of Ψ results in a decrease of the nuclear spin relaxation time, if $T_f > T_b$.

b) Slow exchange.

Again assuming equal densities for free and bound water, for slow exchange eq. (2.15) leads to the result that the ratio of the amplitudes (P_f/P_b) obtained from the biexponential curve is proportional to P_w :

$$P_f/P_b = W_f/W_b = (P_w W_d/W_b) - 1 \quad (2.39)$$

For the latter equality eq. (2.38) has been used.

In practice, the two-site exchange model is too simple to explain the experimentally observed relaxation curves of plant tissue. The relationships between R_2 vs. Ψ and R_2 vs. P_w for stem segments of cucumber plants have been investigated by van As et al. [44,45]. The decay curve was found to be the sum of three exponents. These authors obtained relationships between R_2 and P_w as well as R_2 and Ψ as shown in Figs. 2.8a,b. They introduced the fast exchange limit artificially as follows:

$$R_2(av) = \sum_{i=1}^3 P_i/T_{2i} \quad (2.40)$$

in which P_i = relative amplitude of component i with transverse relaxation time T_{2i} .

Chapter 7 contains experimental data (Fig. 2 of §7.2 and Fig. 2A of §7.3) relating P_w and R_2 . These curves focus on the region of high relative water content (ca. 75% < R_w^* < 100%), since this is the region of physiological interest.

The previous concepts can also be applied to exchange of water between a bulk phase and the wall of a cylindrical vessel. Assuming that a layer of water molecules with thickness d is bound to the wall of a vessel with radius R the populations of both fractions are given by:

$$P_f = (1-d/R)^2 \quad (2.41a)$$

$$P_b = 2d/R - (d/R)^2 \quad (2.41b)$$

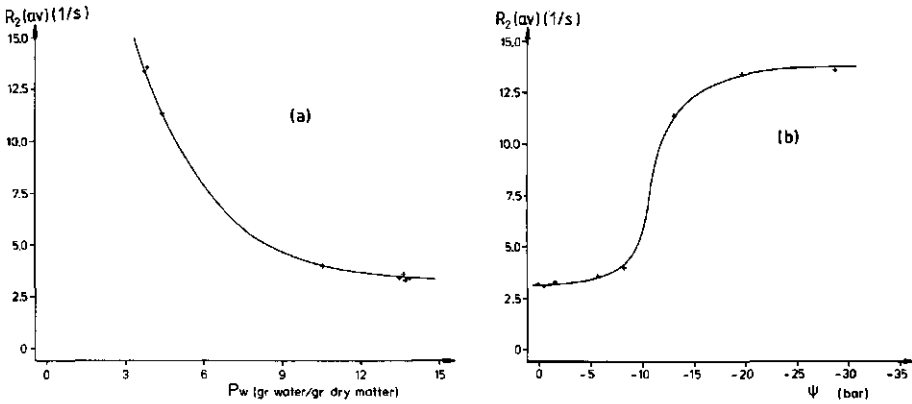


Figure 2.8

- a) Effective spin-spin relaxation rate ($R_2(av)$, defined by eq. (2.40)) vs. water content (P_w) for stem segments of Cucumber (after [45]).
 b) Effective spin-spin relaxation rate ($R_2(av)$, defined by eq. (2.40)) vs. water potential (Ψ) for stem segments of Cucumber (after [45]).

If $d \ll R$ the following results can be obtained:

- a) Fast exchange (eq. (2.19a))

$$1/T(av) = 1/T_f + 2d(1/T_b - 1/T_f)/R \quad (2.42)$$

A plot of $1/T(av)$ vs. $1/R$ has a slope $2d/(1/T_b - 1/T_f)$, from which in principle the layer thickness can be determined if T_f and T_b are known. This result corresponds to that obtained using the diffusion model of Chapter 4 when $Rh \ll 1$ in eq. (4.13). Combining eqs. (2.42) and (4.13) yields:

$$H = d/(1/T_b - 1/T_f) \quad (2.43)$$

with $h = H/D$, and H ($cm \cdot s^{-1}$) = sink strength parameter.

- b) Slow exchange

The ratio of the amplitudes of both exponents is given by:

$$P_f/P_b = R/2d \quad (2.44)$$

Note that for fast exchange the diffusion model and the exchange model yield very similar results.

The diffusion model also predicts a relation between the relaxation rate and Ψ of tissue. A decrease of Ψ and thus of R_w or P_w results in smaller cell volumes yielding larger relaxation rates (see Chapter 4).

2.8 Water flow through plants

Water flows towards sites with lower water potential. Roots take up water from the soil provided their water potential is lower than that of the soil, i.e. if the soil is not too dry (in which case Ψ_m of the soil is too low), or does not contain too many salts that cannot pass through the root membranes (in which case Ψ_o of the soil is too low). Sometimes root pressure (P_r) is present, which means that the osmotic potential of the xylem is lower than the water potential of the soil. From the root the water moves to the leaves and then transpiration takes place if the air water potential ($\Psi(\text{air})$) < the leaf water potential ($\Psi(\text{leaf})$). The latter situation is almost always true, as can be seen from the following argument: $\Psi(\text{air})$ is related to the relative humidity of the air (rh) as follows:

$$\Psi(\text{air}) = -(RT/V_w \ln(\text{rh}/100)) = -1373 \ln(\text{rh}/100) \quad (T=298 \text{ K}) \quad (2.45)$$

From this equation it can be calculated that $\Psi(\text{air})$ in general is lower than $\Psi(\text{leaf})$, even at high rh: e.g. a rh of 50% corresponds to $\Psi(\text{air}) = -950$ bar. Assuming $\Psi(\text{leaf}) = -20$ bar, transpiration takes place for rh up to 98.6%.

A difference in vapour pressure density (ΔV) and not a difference in water potential ($\Delta \Psi$) is the driving force for transpiration. The equation for the flow rate (Q , $\text{m}^3 \cdot \text{s}^{-1}$) is very often written in a form analogous to Ohms law [31,33,46-48]:

$$Q = \Delta \Psi / R = \kappa \Delta \Psi \quad (2.46)$$

in which R = hydraulic resistance to flow and $\kappa = 1/R$ = hydraulic conductance.

Eq. (2.46) does apply for the path of transport from soil to leaf, but is

incorrect when there is a phase change during transpiration from the leaf surface [33]. Then the rate of transport is given by [47]:

$$Q = \Delta V/R' \quad (2.47)$$

in which R' = resistance for transpiration.

The greatest resistance in the transpiration stream of a plant is normally in the gas phase, but the largest hydraulic resistance is usually in the root, where water must pass through living cells at least in the endodermis [46]. The resistance of the xylem is usually relatively small [46, 47], and is neglected in the model for the water balance in (*Cucumis*) plants presented in Chapter 7.

2.9 References

- [1] T.C. Farrar and E.D. Becker, 1971. "Pulse and Fourier transform NMR". Academic Press Inc., New York.
- [2] A. Abragam, 1961. "Principles of Nuclear Magnetism". Oxford at the Clarendon Press. Oxford.
- [3] C.P. Slichter, 1980. "Principles of Magnetic Resonance". Springer Verlag. Berlin.
- [4] L.J. Lynch, 1983. "Magnetic Resonance in Biology". Chapter 5. J.S. Cohen ed. John Wiley & Sons, Inc.
- [5] R. Mathur-de Vre, 1983. Ann. Ist. Super. Sanita, 19, 19-24.
- [6] R. Mathur-de Vre, 1979. Prog. Biophys. Mol. Biol. 35, 103-134.
- [7] K.J. Packer, 1977. Phil. Trans. Royal Soc. (London) B, 278, 59-87.
- [8] P.S. Belton and R.G. Rattcliffe, 1985. "Progress in NMR Spectroscopy", 17, 241-279.
- [9] P.T. Beall, 1983. Cryobiology, 20, 324-334.
- [10] C.F. Hazlewood, D.C. Chang, B.L. Nichols, D.E. Woesner, 1974. Biophys. J., 14, 583-606.
- [11] G.D. Fullerton, J.L. Potter and N.C. Dornbluth, 1982. Magn. Res. Imag., 1, 209-228.
- [12] P.A. Bottomley, T.H. Foster, R.E. Argersinger and L.M. Pfeifer, 1984. Med. Phys., 11, 425-448.
- [13] J.R. Zimmerman and W.E. Brittin, 1957. J. Phys. Chem. 6, 1328-1333.
- [14] J. Tabony and J.-P. Korb, 1985. Mol. Phys., 56, 1281-1305.
- [15] A. Kalk and H.J.C. Berendsen, 1976. J. Magn. Res., 24, 343-366.
- [16] E. Hsi, R. Hossfeld and R.G. Bryant, 1977. J. Coll. Interf. Sc., 62, 389-395.
- [17] H.T. Edzes and E.T. Samulski, 1977. J. Magn. Res., 31, 207-229.

- [18] B.D.Sykes, W.E. Hull and G.H. Snyder, 1978. *Bioph. J.*, 21, 137-146.
- [19] S.H. Koenig, R.G. Bryant, K.Hallenga and G.S. Jacob, 1978. *Biochemistry*, 17, 4348-4358.
- [20] E. Hsi, J. Vogt and R.G. Bryant, 1979. *J. Coll. Interf. Sci.*, 20, 338-345.
- [21] J.M. Escanye, D. Canet and J. Robert, 1984. *J. Magn. Res.*, 58, 118-131.
- [22] B.M. Fung and T.W. McGaughy, 1980. *J. Magn. Res.*, 39, 413-420.
- [23] K.R. Brownstein and C.E. Tarr, 1977. *J. Magn. Res.*, 26, 17-24.
- [24] K.R. Brownstein and C.E. Tarr, 1979. *Phys. Rev. A.*, 19, 2446-2453.
- [25] K.R. Brownstein, 1980. *J. Magn. Res.*, 40, 505-510.
- [26] S.D. Senturia and J.D. Robinson, 1970. *Soc. Petrol. Eng. J.*, 237-244.
- [27] M.A. Hemminga and P.A. de Jager, 1980. *J. Magn. Res.*, 37, 1-16.
- [28] H. Van As and T.J. Schaafsma, 1987. *J. Magn. Res.*, 74, in press.
- [29] H. Van As and T.J. Schaafsma, 1984. *Biophys. J.*, 45, 469-472.
- [30] H. Van As, 1982. Thesis. Agric. Univ. Wageningen.
- [31] R.O. Slatyer, 1967. "Plant-Water relationships". Academic Press, London, New York.
- [32] K. Höfler, 1920. *Ber. Dtsch. Bot. Ges.*, 38, 288-298.
- [33] J.B. Passioura, 1982. "Physiological Plant Ecology II. Encyclopedia of Plant Physiology", Vol. 12B. Chapter 1. O.L. Lange et al. eds. Springer Verlag, Berlin.
- [34] M.T. Tyree and P.G. Jarvis, 1982. "Physiological Plant Ecology II. Encyclopedia of Plant Physiology", Vol. 12B. Chapter 2. O.L. Lange et al. eds. Springer Verlag, Berlin.
- [35] M.H. Behboudian, 1977. Thesis, Agric. Univ. Wageningen.
- [36] J.A. Glasel, 1972. "Water: a comprehensive treatise". Chapter 7. F. Franks, ed. Plenum Press, New York.
- [37] H. Pfeifer and W. Grunder, 1978. *Proc. XXth Congress Ampere*, Tallin, 135-136.
- [38] G.P. Raaphorst, P. Law and J. Kruuv, 1978. *Physiol. Chem. & Physics*, 10, 177-191.
- [39] G. Basic, B. Bozovic and S. Ratkovic, 1978. *Stud. Biophys.*, 70, 31-43.
- [40] B.M. Fung, 1977. *Biophys. J.*, 18, 235-239.
- [41] H. Van As, W.P.A. van Vliet and T.J. Schaafsma, 1980. *Biophys. J.*, 32, 1043-1050.
- [42] T. Seiler, L. Trahms and J. Wollensak, 1982. *Graefe's Arch. Clin. Exp. Ophthalmol.*, 219, 287-289.
- [43] B.R. Masters, V.H. Subramanian and B. Chance, 1982/83. *Current Eye Res.*, 2, 317-321.
- [44] H. Van As, T.J. Schaafsma and J. Blaakmeer, 1986. *Bruker Report*, 1, 33-36.

- [45] H. Van As, T.J. Schaafsma and J. Blaakmeer, 1986. *Acta Horticulturae*, 174, 491-495.
- [46] P.E. Weatherley, 1982. "Physiological Plant Ecology II. Encyclopedia of Plant Physiology", Vol 12B. Chapter 3. O.L. Lange et al. eds. Springer Verlag, Berlin.
- [47] J.A. Milburn, 1979. "Water flow in plants". Longman Group, London.
- [48] P.S. Nobel, 1970. "Introduction to Biophysical Plant Physiology". Freeman and Co. San Francisco.

CHAPTER III

=====

3. MATERIALS AND METHODS3.1. Introduction

This chapter presents a schematic outline of the equipment and experimental procedures used in the plant experiments. Particular attention is given to a number of essential parts of the used equipment: a lock system compensating for long term magnetic field drift (§ 3.3.1), the radiofrequency (rf) probe (§ 3.3.2), and the linear variable differential transformer (LVDT) (§ 3.3.3). In addition some details of the plant material are discussed (§ 3.4).

3.2 Computer-controlled experiments

Figure 3.1 presents scheme of the automated set-up for conducting unattended flow- and T_2 -measurements. In this figure the NMR equipment, plant, climate control equipment and data handling instrumentation are shown.

A computer-controlled NMR flow experiment is conducted as follows. First the desired environmental conditions are chosen (i.e. air temperature, root temperature, relative humidity and light intensity). Subsequently, a computer program, that alternately conducts a lock-, flow-, and T_2 -experiment, is read from hard disk by a dedicated computer (Bruker ASPECT 2000). This program conducts the following steps. First the pulse program for the lock procedure is loaded into the pulse programmer, controlling the lock experiment. The y-gradient (G) is switched off and a 90° pulse is given by the the rf transmitter along the y'-axis of the rotating frame. Then the signal detected along the x'-axis is passed through an electronic device, named 'lock', which uses this signal to generate a voltage in the flux stabilizer by which the B_0 field is adjusted to the resonance value. The lock procedure is repeated

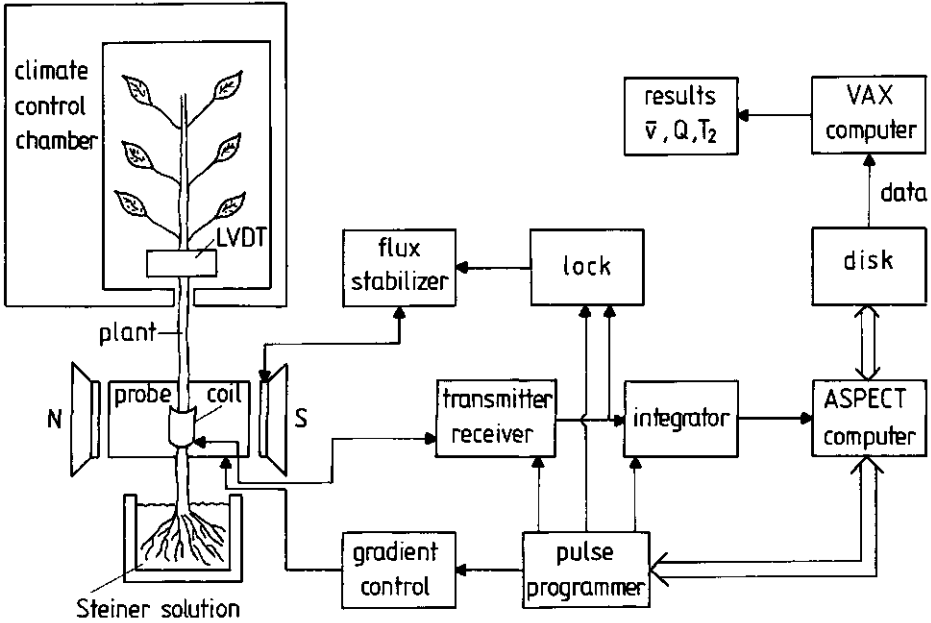


Figure 3.1
Scheme of equipment.

a few times to ensure the correct resonance condition. After completion of the lock-procedure, the pulse program for the flow measurements is loaded into the pulse programmer. G is turned on and a train of 8192 rf pulses is given. The resulting NMR signal is integrated and stored on disk.

After each flow measurement the lock procedure is repeated again, followed by the T_2 measurement, for which the appropriate pulse program is loaded into the pulse programmer. For this measurement G is turned off and a CPMG pulse sequence is given. The echoes are integrated again and after a lock procedure and subtraction of a second T_2 curve, which has been obtained with an inverted 90° pulse stored on disk [1]. The whole procedure can be repeated a large number of times. Computer-controlled experiments have been conducted for periods as long as several days, as can be seen from the figures in Chapter 7. For data processing the data are transferred to a DEC MICROVAX computer, for

which computer programs are available to calculate relaxation times and flow rates.

The LVDT measurements are conducted parallel with the NMR measurements and the output is monitored on a y-t recorder. The actual temperature and relative humidity (rh) in the climate chamber are also registered on y-t recorders.

3.3 Outline of equipment

For computer controlled experiments, using the scheme of Fig. 3.1, we used the following components:

- Newport 7" electromagnet operating at 0.47T;
- transmitter/receiver consisting of modified Bruker Minispec electronics operating at 20 MHz;
- Bruker ASPECT 2000 computer;
- Control Data Corporation (CDC) cartridge module disk drive CMD;
- Bruker Z17C pulse programmer;
- Home built flux stabilizer;
- Home built gradient control unit;
- Home built lock system (§ 3.3.1);
- Home built rf probe (§ 3.3.2);
- Home built integrator (§ 7.2);
- Tamson TK20 thermostatically controlled water bath to control the temperature of the Steiner solution;
- Greenco GPGK climate control chamber (§7.2);
- Höttinger Baldwin Messtechnik type HBM W1/E5 LVDT (§ 3.3.3);
- DEC MICROVAX II computer;
- Siemens infra red gas analyser (NDIR) to monitor CO₂ concentration;
- BBC Goertz Metrawatt illuminance meter. (Photon) irradiance was calculated from illuminance using the spectrum of the lights.

(A detailed description of each component is found in the paragraph between parentheses).

3.3.1 Lock system

To conduct NMR experiments over long periods of time a stable B_0 field is required. This cannot be achieved by a flux-stabilizer alone, since it can only compensate for relatively fast field fluctuations. For a slowly drifting magnetic field the flux stabilizer will not react properly. Therefore a lock system was developed, using the plant proton magnetic resonance signal itself as a monitor [2]. The principle is as follows. A 90° pulse is given along the y' -axis of the rotating frame which rotates the magnetization \vec{M} to the x' -axis. When the system is on resonance \vec{M} remains along the x' -axis and no magnetization can be detected along the y' -axis. When off-resonance, however, a signal is detected along the y' -axis, because \vec{M} rotates in the rotating frame. The lock system uses this y' -component to control the magnetic field. The y' -component of \vec{M} is integrated during 1 ms following the 90° pulse. The amplitude of the resulting error signal is proportional to the off-resonance frequency shift and is used to correct the B_0 field. For an integration time of 1 ms the lock system corrects for resonance offsets up to 1000 Hz in either direction. Since local inhomogeneities in the sample [Chapter 5 and 6] cause a small y' -component when the system is on resonance, an additional circuit is included with which a specific "off-resonance" frequency can be created to compensate for the effects of inhomogeneities on the flow signal (see Chapter 6).

3.3.2 NMR probe

For the plant experiments an NMR-probe was designed with criteria I-VIII, mentioned below, in mind.

- I The probe should be easily accessible for intact plants.
- II The rf coil should allow short values of τ , the interval between the rf pulses and
- III it should be possible to apply large values of the field gradient G , in the direction of flow [Chapter 6].

To increase the reproducibility from plant to plant:

- IV The rf field (B_1) amplitude and

- V G should be homogeneous throughout a cross-section of the plant stem, i.e. over a ca. 1 cm^2 area in the xz-plane (see Fig. 3.2A), since the xylem vessels are spread out over this area (Fig. 3.3A).
- VI The rf coil and gradient coils should have a fixed (or at least reproducible) orientation with respect to each other.

Additionally one should attempt to obtain:

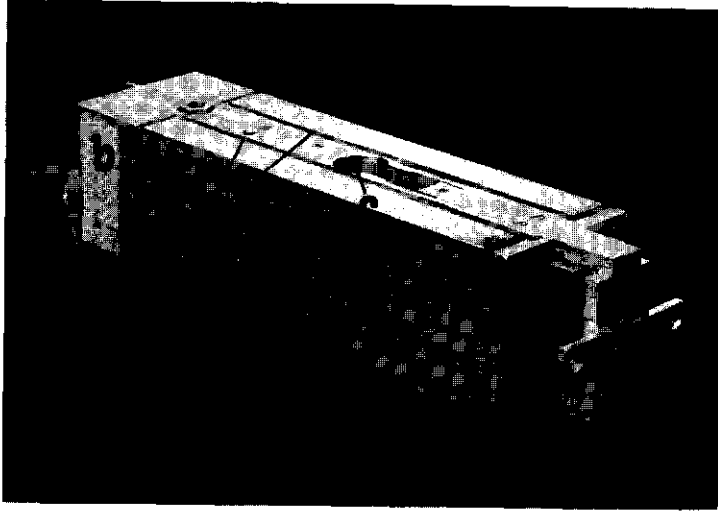
- VII A high quality factor (Q_p) as well as
- VIII A high signal to noise ratio (S/N).

The probe constructed along these lines is shown in Fig. 3.2. In the following text constructional details are related to the design-criteria (between parentheses). The rf coil in the probe is of the Helmholtz type, with a length and diameter of 12 mm [4]. One half of the coil pair has a fixed position in the probe, whereas the other half can be rotated over 90° to allow easy access of the intact plant stem in the opened coil (I) (part a in Fig. 3.2B). By sliding in a separate part (part a in Fig. 3.2A), the rf coil can be closed to form a proper Helmholtz pair (VII) and has a fixed position in the probe (VI). The coil is wound in grooves cut into the outside of a holder consisting of 99.8% perdeuterated polymethylmethacrylate (Zentral Institut für Isotopen und Strahlenforschung, Leipzig) with a thickness of 2 mm, ensuring a rigid construction and no physical contact between coil and plant. Moreover the plant is confined to the most homogeneous region (in

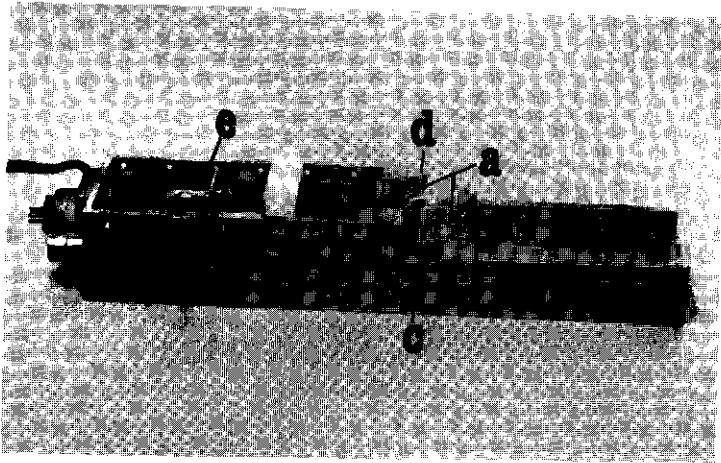
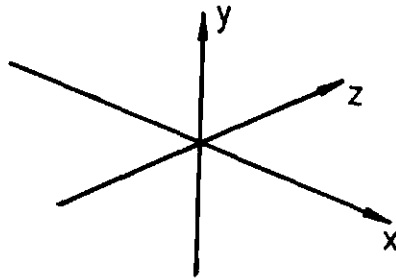
Figure 3.2 (page 39)

NMR probe and rf coil.

- A. Side view of the probe; (xyz) refers to the laboratory coordinate system: flow is in the y-direction, B_0 is along z. The aluminium housing (b) is firmly connected between the magnet poles, whereas part (a) can be removed to insert an intact plant into the opening (c) around which the rf coil is positioned. (d) indicates 4 of the total of 8 magnetic field gradient wire-bundles.
- B. Top view of the opened probe: (a) represents the rf coil, wound around the opening (c); (d) indicates the aluminium rings for additional shielding; (b) indicates the aluminium housing and (e) the tuning capacitor.



A



B

the radial direction of the coil (IV) and a good filling factor is obtained (VII). To enable opening and closing of the coil (I), the rf coil consists of ~ 10 windings of thin, isolated and flexible, Litz wire with a relatively low effective resistance at the operating frequency (VII). The high filling factor and high Q_p (VII) result in high S/N (VIII) and enables us to use short pulses [5]. When the probe is closed the rf coil is well shielded against external signals due to radiofrequency interference (VIII) by the large and thick aluminium housing of the probe (part b in Fig. 3.2A,B), in the center of which the rf coil is symmetrically positioned. Only a narrow opening remains at both sides through which the plant stem extends (part c in Fig. 3.2 A,B). Two aluminium rings positioned under and above the rf coil provide additional shielding (part d in Fig. 3.2B). The coil is symmetrically coupled to the tuning circuit [6], i.e. both sides of the coil are connected to equal capacitors (type ATC100, American Technical Ceramics, New York, and Bruker variable air capacitor (part e in Fig. 3.2.B)) leading to approximately zero electrical potential halfway the coil, thus reducing dielectrical losses in the sample (VII) and detuning effects of the coil. Furthermore the 'hot' sides of both coil halves are located at the outside and the 'cold' sides at the sample position, leading to further reduction of electric losses in the sample (VII). A balance-matched probe reduces the 'antenna' effect of the probe, i.e. the tendency of a long sample to radiate electromagnetic energy (and thereby reducing the Q_p) and to pick up rf signals e.g. from the computer or nearby radio transmitters [7] (VII). Also the breakdown voltage of the capacitor is high allowing for high power pulses and high duty cycles (II). A constant air stream along the rf coil supplies additional cooling (II). The dimensions of the aluminium probe housing are (in cm): 18(x) \times 5(y) \times 5(z). The linear field gradient coils are wound in grooves on the outside of the housing. They consist of 4 rectangular loops positioned symmetrically around the center of the probe, which is also the center of the rf coil. The produced magnetic field gradient can be described by a system of 8 infinitely long straight wires at different positions in the yz plane and extending in the x direction (d in Fig. 3.2A). Choosing the center of the rf coil as the origin (y,z)=(0,0) then a linear field gra-

gradient in the y direction is obtained with the zero point in (0,0) when the angle of a line connecting the coordinates of the 8 wires with (0,0) is 22.5° with respect to the z or y axis [8], which is the case for the coordinates (y,z) chosen (mm): (10,25), (25,10), (25,-10), (10,-25), (-25,-10), (-10,-25), (-25,10) and (-10,25). This construction of the gradient coil on the probe housing enables high reproducibility (the gradient coils always have the same position with respect to the rf coil (VI)), high values of G (the aluminium housing serves also as a cooling body (III)) and a homogeneous G (V): computer simulations showed less than 5% deviations from the value of G at (0,0) within a cylinder of 1 cm diameter and 2 cm length, symmetrically positioned around (0,0).

3.3.3 The Linear Variable Differential Transformer (LVDT)

The LVDT is a dendrometer, with which it is possible to measure the thickness of the plant stem, which has been shown to be related to the water content [9] and potential [10] of the plant. The heart of the LVDT consists of an iron core that serves as an amplifier between a set of primary and secondary windings, whose magnitude is determined by the absolute position of the iron core between the windings. The LVDT is connected to the plant in such a way that the part containing the windings has a fixed position with respect to the stem. The iron core is in contact with the stem surface, using an extension [11]. Variation of stem thickness leads to a different position of the core within the windings, thus resulting in a different induction voltage, which is monitored after conversion into a DC voltage. It is obvious that growth also causes a change in the LVDT output, without necessarily changing the water content.

3.4. Plant Material

The plant used in the experiments described in this thesis are mostly water cultures of Cucumbers (Cucumis sativus L. cv. Farona) and sometimes Gherkins (Cucumis sativus L. cv. Hokus). The length of the intact plants was usually 2-3 m. The age varied with season. Plants

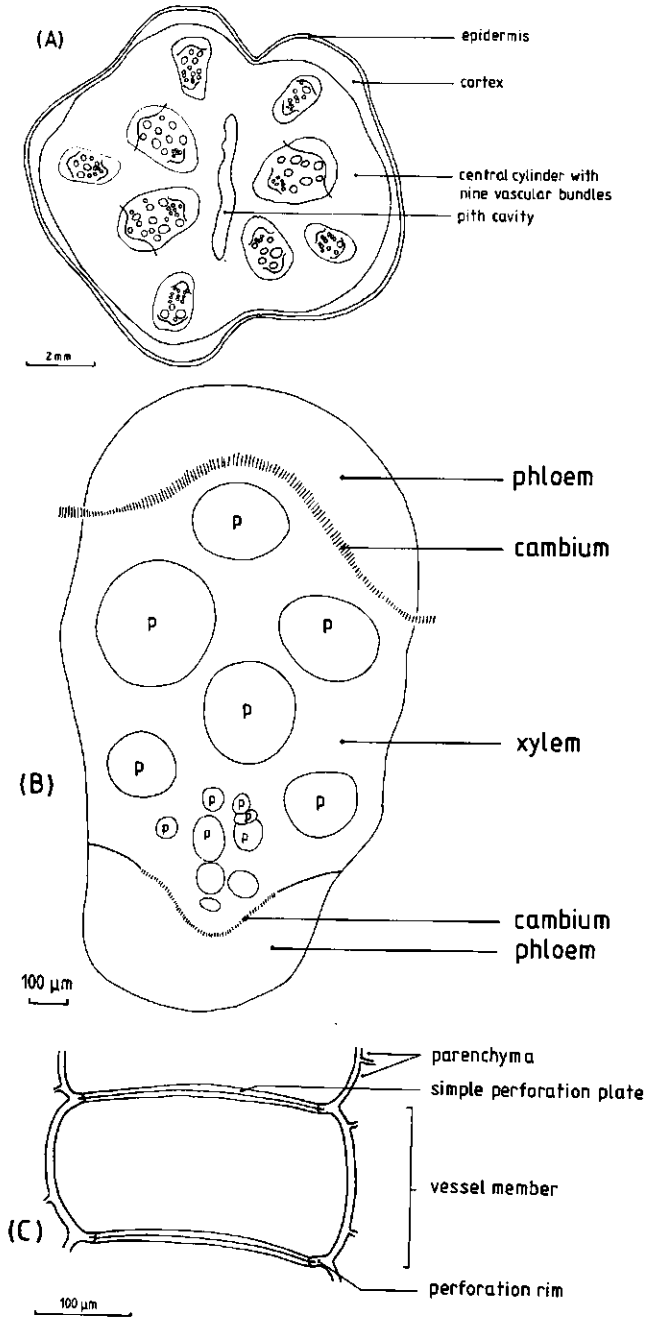


Figure 3.3 (page 42)

Transverse and longitudinal sections of a cucumber plant (Cucumis sativus L.).

- A. Transverse section of a complete stem showing epidermis, cortex, central cylinder with nine vascular bundles and pith cavity. (WILD M4A with drawing mirror).
- B. Transverse section of bicollateral vascular bundle with pitted vessel (p). Annular and helical vessels (not marked). (WILD M20 with drawing tube).
- C. Longitudinal section of a part of a pitted vessel with two simple perforation plates. The vessel is surrounded by parenchyma. Bordered and half-bordered pit-pairs in surface and side view are not shown. (WILD M20 with drawing tube).

grown during the summer were younger and had usually a thicker stem than 'autumn' or 'spring' plants, which were younger than 'winter' plants again.

Figure 3.3 shows some transverse and longitudinal sections of a 4 months old cucumber plant. All cucumber and gherkin plants have 9 bicollateral vascular bundles (Fig. 3.3A) and a pith cavity. The dimensions and geometry of the pith cavity vary strongly, and are often larger than shown in Fig. 3.3A. The vascular bundles contain a varying number of vessels. The larger ones, which are by far the most important for water flow, are always pitted vessels (p). Some small annular and helical vessels are present as well (Fig. 3.3B). Figure 3.3C shows a longitudinal section of a part of a pitted vessel, with two simple perforation plates. It can be seen that the xylem vessels of cucumbers are not smooth cylinders, but are composed of many vessel members joined by perforation plates. The length of the vessel members varies strongly, even within one plant. The protrusions formed by the perforation rims are generally of the order of 10% of the diameter, although occasionally they may reduce the diameter of the opening of the perforation plate by a factor 2.

3.7. Acknowledgements

I am indebted to Mr. A.J. Munting of the Department of Plant Cytology and Morphology for the drawing of the Figs. 3.3A-C.

3.8. References

- [1] M.A. Hemminga, P.A. de Jager and A. Sonneveld, 1977. *J. Magn. Res.*, 27, 359-370.
- [2] P.A. de Jager, J.E.A. Reinders and H. Van As, 1986. *Proceedings of the 8th European Experimental NMR Conference (EENC)*, 53-54, Spa, Belgium.
- [3] M.A. Hemminga and P.A. de Jager, 1980. *J. Magn. Res.*, 37, 1-16.
- [4] D.M. Ginsberg and M.J. Melchner, 1969. *Rev. Sci. Instr.*, 41, 122-123.
- [5] D.I. Hoult, 1978. "Progress in NMR spectroscopy", 12, 41-77.
- [6] J. Murphy-Boesch and A.A. Koretsky, 1983. *J. Magn. Res.*, 54, 526-532.
- [7] J. Murphy-Boesch, 1984. in "Biomedical Magnetic Resonance", 47-61. T.L. James and A.R. Margulis eds. *Radiology Research and Education Foundation*, San Francisco.
- [8] P. Mansfield and P.G. Morris, 1982. "NMR Imaging in Biomedicine". Chapter 8. *Academic Press*, New York.
- [9] B. Klepper, D. Browning and H.M. Taylor, 1971. *Plant Physiol.*, 53, 565-568.
- [10] G.M. Huck, B. Klepper, 1977. *Agron.J.*, 69, 593-597.
- [11] W.G. Gensler, 1986. "Advanced Agricultural Instrumentation Design and Use". W.G. Gensler ed., *Martinus Nijhof Publishers*, Dordrecht.

CHAPTER IV

=====

4 PROTON SPIN RELAXATION AND DIFFUSION OF WATER IN TRANSPORT VESSELS OF PLANTS4.1 Introduction

It is possible to measure the sapstream velocity in the stem of cucumber plants using the NMR RP method when it is applied to plants with not too small xylem vessel diameters [1,2,3, Chapter 6]. This can be understood by invoking a reduction of the transverse relaxation time T_2 in narrow vessels [4] resulting in a decrease of the NMR flow signal amplitude [3, Chapter 6]. There are two models, i.e. the "two site exchange model" [5] and the "diffusion model" both predicting a dependence of T_2 on the vessel diameter [4, Chapter 2].

The "two site exchange model" has been used in biological systems frequently [6-13, Chapter 2]. For water in transport vessels of plants the model involves two sites, one being the bulk water within the xylem-vessel, the other being a fraction bound at the vessel wall [4]. Such a model yields a biexponential decay of the nuclear spin magnetization unless $\tau \ll T_1, T_2$. Then a single exponential curve is found (fast exchange) as outlined in chapter 2.

An alternative way to describe relaxation in heterogeneous systems (e.g. cells) was introduced by Brownstein & Tarr [14,15]. A very similar model including bulk relaxation was previously applied to nuclear spin relaxation of fluids in porcelain [16] and glass [17]. This "diffusion model" assumes the spins to be confined in a volume with known geometry. Within this volume the transverse nuclear spin magnetization decays with a rate constant T_2^{-1} . In addition to this bulk-relaxation, the nuclear spin magnetization can also relax at the surface of the vessel wall, containing relaxation sinks. The probability of a nuclear spin to reach the surface of the vessel wall is determined by diffusion (Fick's laws). The model yields a multi-exponential decay of spin magnetization with in principle an infinite number of relaxation times. The distribution of

amplitudes and the rate constants for decay of these exponential curves depend on the geometry, the diffusion coefficient and the effectiveness of the relaxation sinks at the surface.

In this chapter the "diffusion model" is used as an explanation for transverse nuclear spin relaxation in xylem vessels of cucumber plants. Frequently, these xylem vessels are rigid, approximately cylindrical pipes with diameters up to a few hundreds of microns. These vessels therefore meet the criteria suggested by Belton and Ratcliffe [18] for the validity of the "diffusion model". A second argument favouring the use of the "diffusion model" is its simplicity: there is only a single adjustable parameter. By contrast, the "two site exchange model" contains several adjustable parameters. The formalism of our model (applied to biological systems) is similar to that developed by Senturia et al. [16] for inorganic material. The bulk spin relaxation rate (T_2^{-1}) can be measured for a water sample collected from the vessels, the distribution of vessel diameters is measured microscopically, and the diffusion constant is accessible for measurements [19].

The goal of this chapter is to test the validity of the diffusion model for the transverse nuclear spin relaxation of water in a well-defined system of plant transport vessels, i.e. the xylem vessels of cucumber. From this study a hitherto unknown value is obtained for the parameter (H) describing the effectiveness of nuclear spin relaxation at the wall of a plant vessel. These results can be generalized to include the effect of wall- and bulk relaxation on nuclear spin magnetization decay of water in plant cells and vessels.

4.2 Theory

Defining \mathbf{m} as the magnetization density, the transverse magnetization $m_{x'}$ or $m_{y'}$ parallel to the x' - or y' -axis of the rotating frame following a 90° pulse is measured. Then the Bloch equation for $m_{x'}, y'$ is:

$$\frac{dm}{dt} = D \frac{v^2}{\omega} m - T_2^{-1} m \quad (4.1)$$

\underline{D} = diffusion tensor; $m = m_x, m_y$.

T_2 = transverse relaxation time of protons in the bulk water within the plant vessel.

For cylindrical geometry there is only a spin-density gradient in radial direction and eq. (4.1) becomes:

$$\frac{dm}{dt} = -\frac{m}{T_2} + D \left(\frac{d^2 m}{dr^2} + \frac{1}{r} \frac{dm}{dr} \right) \quad (4.2)$$

For eq. (4.2) diffusion is assumed to be isotropic and homogeneous. The loss of magnetization M per unit wall area (A) is introduced by

$$-\frac{dM}{dt} / A = Hm \quad (H > 0) \quad (4.3)$$

Combining eq. (4.3) with Fick's first law which states:

$$-\frac{dM}{dt} / A = -D \frac{dm}{dr} \quad (4.4)$$

yields the first boundary condition:

$$\frac{dm}{dr} + hm = 0 \quad \text{at } r = R \quad (4.5)$$

in which $h = H/D$, H = sink strength parameter (in m/s) and R is the vessel radius. At $t = 0$, a uniform equilibrium magnetization density distribution is assumed, resulting in the second boundary condition:

$$m(r,t) = m_0 \quad \text{at } t = 0 \quad (4.6)$$

The solution of eq. (4.2) subject to the boundary conditions (4.5) and (4.6) yields for the total transverse magnetization M after integration over the cylindrical volume [16,20]:

$$M(t) = M(0) \sum_{n=1}^{\infty} I_n \exp(-t/T_{2,n}) \quad (4.7)$$

with:

$$I_n = 4 / [k_n^2 (1 + (k_n/Rh)^2)] \quad (4.8)$$

$$1/T_{2,n} = Dk_n^2/R^2 + 1/T_2 \quad (4.9)$$

and $k_n (n = 1, 2, \dots)$ are the roots of

$$k_n J_1(k_n) - Rh J_0(k_n) = 0 \quad (4.10)$$

J_0 and J_1 are Bessel functions of the first kind and of order zero and one, respectively.

For $Rh \ll 1$:

$$k_1^2 \approx 2Rh \quad (4.11)$$

Combining eq. (4.11) with eqs. (4.8) and (4.9) leads to:

$$I_1 = 1, I_n (n \neq 1) = 0 \quad (4.12)$$

and the effective rate constant for decay of transverse magnetization is given by:

$$1/T_{2,1} = 2H/R + 1/T_2 \quad (4.13)$$

Thus, for $Rh \ll 1$, the decay of magnetization will be single-exponential with the decay rate given by eq. (4.13).

For:

$$(i) 2HT_2/R \ll 1 \text{ or } R^2 \gg 2DT_2: T_{2,1} \approx T_2 \quad (4.14)$$

and

$$(ii) 2HT_2/R \gg 1 \text{ or } R^2 \ll 2DT_2: T_{2,1} < T_2 \quad (4.15)$$

these conditions correspond to situations where the vessel radius is larger (i) or much smaller (ii) as compared to the pathlength of diffusion during the transverse relaxation time T_2 .

For higher values of Rh the higher modes of I_n become more and more important. For the extreme case $Rh \rightarrow \infty$ it takes 40 modes to describe 99% of the amplitude of the decay curve. For large values of R however each of the decay rates $1/T_{2,n}$ of the lower modes equal the bulk relaxation rate $1/T_2$, since for this case

$$DK_n^2 / R^2 \ll 1/T_2 \quad (4.16)$$

and thus

$$1/T_{2,n} = 1/T_2 \quad (4.17)$$

Therefore, for $R \rightarrow \infty$ (or $D = 0$) the decay again will be single exponential with a relaxation time T_2 . In practice, however, R is finite so that the decay always contains fast components.

The initial decay rate $1/T_{in}$ can be obtained, given by [14]:

$$\frac{1}{T_{in}} = \frac{2H}{R} + \frac{1}{T_2} \quad (4.18)$$

in which

$$-\frac{1}{T_{in}} = \left[\frac{d(M(t)/M(0))}{dt} \right]_{t=0} \quad (4.19)$$

T_{in}^{-1} equals the single exponential decay rate for $Rh \ll 1$ (cf. eq. (4.13)). Although eq. (4.2) was solved for the conditions (4.5) and (4.6) and $H > 0$, it can be shown that for $H = 0$ the solution is given by [20]:

$$M(t) = M(0) \exp(-t/T_2) \quad (4.20)$$

4.3 Materials and methods

Plant material. To test the predictions of the model, we used a stem segment (± 20 cm length) of a 3 months old cucumber plant (Cucumis sativus L.) cut from the lowest quarter of the plant. It contained one node to shutt off the pith cavity. A thin slice was cut off from the end of this section for microscopic measurement. The stem segment was oven dried, washed with tap water a few times and dried again so that a dead, woody, and rigid stem segment was left. One end of the segment was firmly connected to a plastic tube using Bayer Xantopren kit. Water or gas was pumped through the xylem vessels of the segment. The other end was positioned inside the r.f. coil of the spectrometer.

Xylem vessel diameters. Radii of xylem vessels were determined before

and after drying by microscopy of a thin segment slice assuming the vessels to have a cylindrical shape.

T₂ measurements. The T₂ measurements were carried out using a modified CPMG method [2, Chapter 2] and the signal was recorded using a DEC PDP 11 minicomputer. For all experiments the time 2 τ between successive 180° pulses was 0.64 msec. To determine T₂ of water inside the xylem vessels, we used the following procedure. A stem segment was tightly connected to a plastic tube and put into the spectrometer rf coil. After filling the tube with water, and allowing the stem segment to saturate with water, its open end was connected to a cylinder containing N₂-gas and pressurized. The xylem vessels were loaded with water using ca. 1.5 atm. N₂ and a decay curve was recorded. Immediately afterwards the xylem vessels were freed from water, which was collected, by repressuring with N₂ and a second decay curve was recorded. By far the largest part of the water which is responsible for this latter decay curve is comprised by stem cells outside the xylem and a minor part arises from water in the xylem, after the vessels were emptied. The difference between both decay curves represents the relaxation behaviour of the water inside the xylem vessels. The relaxation time T₂ of the collected, water was also determined. For the relaxation time measurements of the stem segments we used a train of 3840 180° pulses. Each data point represents the integrated signal over a period of 1.28 msec (2 pulses). For the collected water fraction the signal was integrated over 8 successive pulses to cover a sufficiently long time-interval.

4.4 Results and discussion

The relaxation curve for the water inside the xylem vessels is shown in Fig. 4.1 and on a semilog scale in Fig. 4.2. From both figures it is obvious that the decay is not a single exponential. Fig. 4.3 represents the semilog T₂ curve for the water collected from the xylem vessels, yielding T₂ = 2.45 s. In order to estimate the sink strength parameter H a computer program was written simulating the curves given by eqs. (4.7-4.10) with the single free parameter H. The various values of R are obtained from the measured distribution of vessel radii (Fig.

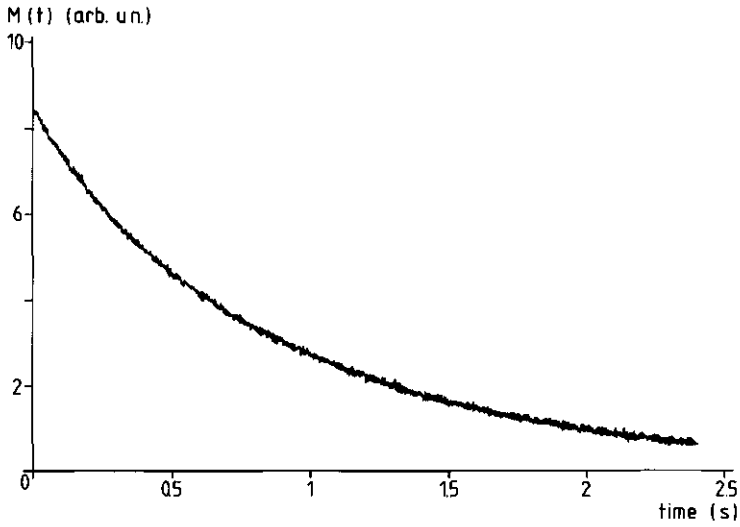


Figure 4.1

Measured transverse relaxation decay curve for water in xylem vessels of a cucumber stem segment, after applying the subtraction procedure, described in the text.

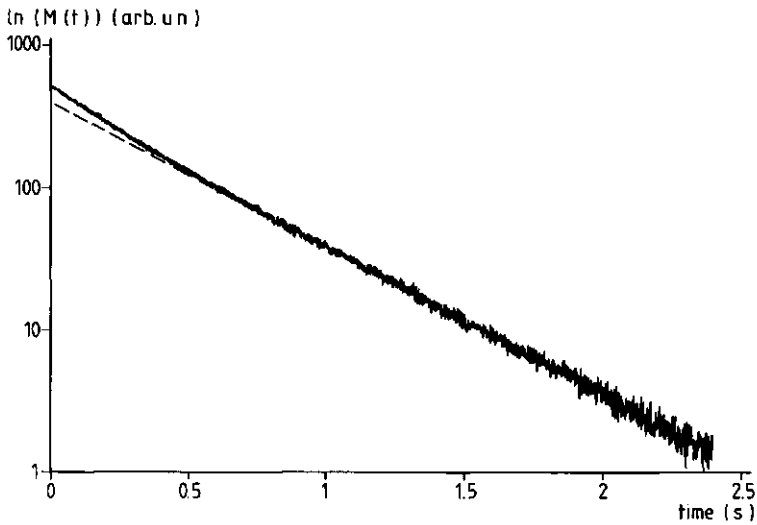


Figure 4.2

Semilog plot of Fig. 4.1.

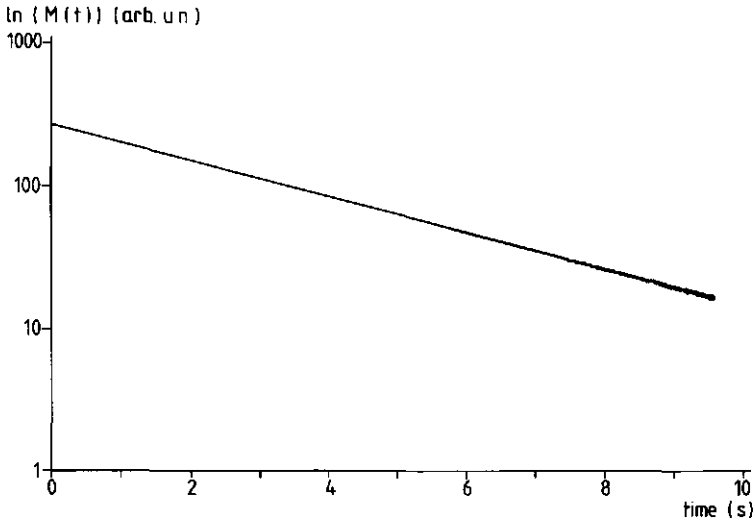


Figure 4.3

Experimental transverse relaxation decay curve for water, collected from the xylem vessels of the cucumber stem segment.

4.4). The vessel diameters did not change at all by the drying process, justifying the assumption that the xylem vessels can be considered as rigid pipes. For T_2 we used the measured bulk relaxation time of 2.45 s. The value of the self-diffusion constant of water at room temperature $D = 2.5 \cdot 10^{-9} \text{ m}^2/\text{s}$. The values of k_n obeying eq. (4.10) were read from the table given in [20]. Values not present in this table were obtained by linear interpolation from the nearest two tabulated values. Although theory requires summation until infinity we could not discriminate between calculated decay curves obtained with $n \geq 10$, therefore summation was limited to $n = 1$ to 10. For values of $n > 6$ k_n was calculated using: $k_{n+1} \approx k_n + \pi$.

The computer simulation for the observed relaxation curve using the full distribution of Fig. 4.4 and $H = 6 \cdot 10^{-3} \text{ cm/s}$ (Fig. 4.5, curve a) was found to be coincident with the experimental curve of Fig. 4.1.

We attempted to ascertain whether all xylem vessels contributed to the observed decay curve. For the larger vessels visual observation was sufficient as a check. We simulated the decay using the largest vessels

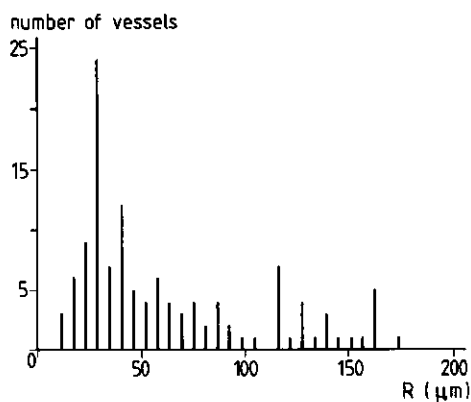


Figure 4.4

Distribution of xylem vessel radii in the stem segment at the position of the rf coil. The diameters were rounded off to 1 unit of the graduation scale of the microscope, i.e. the accuracy is $\pm 6 \mu\text{m}$.

only. In order to make an estimate of the accuracy of the calculated H value, taking into account the effects of partial filling of the vessels on the shape of the decay curve, we simulated the decay using only vessels with $R > 100 \mu\text{m}$ and H as an adjustable parameter. Note that the contribution of a vessel with radius R depends on R^2 (eq. 4.8), favouring vessels with large R . Fig. 4.5 curve b represents the calculated curve including all vessels with $R > 100 \mu\text{m}$ of the distribution. Other parameters are the same as in Fig. 4.5 curve a. Curve b clearly deviates from the observed decay (Fig. 4.1). As an illustration, curve c represents the decay curve using all vessels from the distribution of Fig. 4.4 with $R < 100 \mu\text{m}$. This curve shows that for plants with smaller vessels the measured decay is faster.

A satisfactory fit to the experimental data could be obtained with $H = 1.2 \cdot 10^{-2} \text{ cm/s}$, using all vessels of the distribution of Fig. 4.4 with $R > 100 \mu\text{m}$. Using a smaller top fraction of the distribution of Fig. 4.4 no satisfactory fit could be obtained. Curve D of Fig. 4.5 is the calculated curve using the same parameters as in curve A except for T_2 which has been chosen infinitely long. The difference between the two curves illustrates the importance of the value of T_2 of bulk water for the dimensions considered.

Although the bulk T_2 value of water can be determined with high precision (see Fig. 4.3) and better than 2% reproducibility, the hetero-

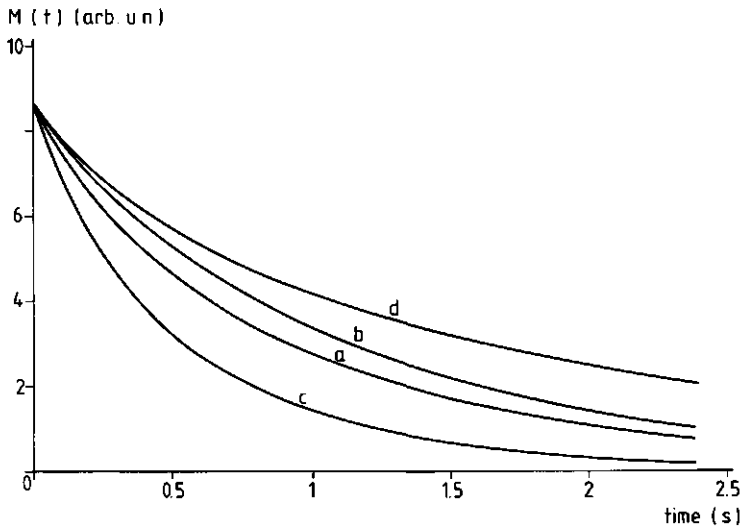


Figure 4.5

Calculated decay curves.:

- a) $T_2 = 2.45$ s; $H = 6 \cdot 10^{-3}$ cm/s; the vessel distribution of Fig. 4.4 is used for R.
- b) $T_2 = 2.45$ s; $H = 6 \cdot 10^{-3}$ cm/s; only vessels with $R > 100$ μm of Fig. 4.4 are used.
- c) $T_2 = 2.45$ s; $H = 6 \cdot 10^{-3}$ cm/s; only vessels with $R < 100$ μm of Fig. 4.4 are used.
- d) $T_2 = \infty$; other parameters as in a).

Curve a coincides with experimental curve of Fig. 4.1.

geneous structure of the stem segment may cause the bulk relaxation rate in the vessels to be higher due to diffusion of spins through local field gradients. By choosing τ as small as possible (0.32 ms for our instrument) this effect has been minimized [21]. By choosing dead material the T_2 value of water contained by it could not be influenced by physiological processes.

Finally we note that the calculated value of H may be influenced by the experimental procedure. The xylem vessel walls have a finite thickness and contain bound (see note at end of this section) water and macromolecular protons. All of these nuclear spins are excited in addition to those of bulk protons when the xylem vessels are filled with

Table 1. Values of the sink strength parameter H for various materials.

Material	H(cm/s)	Remarks
rat gastrectonemius muscle	$8 \cdot 10^{-2}$	a)
Northern White Cedar wood chips	$< 2.6 \cdot 10^{-2}$	b)
selas porcelain	$8.7 \pm 0.7 \cdot 10^{-5}$	c)
glass (Pyrex)	$< 3 \cdot 10^{-5}$	d)
cucumber xylem vessel walls	$> 0.6 - 1.2 \cdot 10^{-2}$	

Remarks:

- a) calculated from ref. [15] by Van As [4]
- b) calculated from ref. [32] by Van As [4]
- c) from ref. [16], derived from T_1 -measurements
- d) J.E.A. Reinders: unpublished results.

water. Under those conditions there is exchange of magnetization between the bulk water and the vessel wall due to proton exchange with the bound water inside the vessel wall and cross relaxation with the protons in the wall [6-13, 22-30, Chapter 2] i.e. magnetization transfer may take place from the vessel wall into the bulk in addition to the reverse process, the latter of which contributes to H. Assuming equal spin densities in the bulk and the wall the net effect will be a transfer of magnetization from the bulk into the vessel wall, because T_2 of the protons in the bulk is longer than that of protons residing in the vessel wall. The relaxation time of the protons in the vessel wall is longer when the vessels are filled with water as compared to a situation in which the vessels contain no water. We recall the subtraction procedure: the curves obtained from the stem segment when the vessels are freed from water is subtracted from the curve obtained when the vessels are filled with water. This does not completely compensate for the magnetization present in the wall. Effectively, the difference curve has a too small decay rate, resulting in a too low value of H. Therefore the value of H of the curve of Fig. 4.1 (or Fig. 4.2) represents a lower limit. In view of the results (see Table 1) for Northern White Cedar wood chips (which, like xylem, consists of cellulose-like material) the actual value of H for xylem is likely to be close to the quoted lower

limit of $0.6-1.2 \cdot 10^{-2}$ cm/s. From Table 1 it can be safely concluded, that the value of H is 2 to 3 orders of magnitude larger for biological material than for glass and porcelain.

Modern NMR imaging techniques allowing a spatial resolution of a few tens of μm [33] may be used to obtain more accurate values of H. By making a spatially resolved T_2 image or by selective excitation [34] of the water in a xylem vessel this can be achieved without the uncertainties mentioned above.

The relation between the effective relaxation rate and R for various values of H is presented in Fig. 4.6.

This study also shows that a diffusion model adequately describes the proton spin relaxation in xylem vessels of plants. In Chapter 6 the information obtained with this model is used to calculate a lower limit of the diameter of biological transport vessels for which an NMR flow signal can be obtained, using the RP method.

Note:

The definition of the amount of bound water is strongly dependent on the experimental techniques and on the procedures determining its magnitude [31]. In this discussion bound water refers to the amount of water which is left in the plant xylem after ca. 1.5 bar gas pressure has been applied to free the conducting xylem vessels from liquid water.

4.5 Diffusion in a spherical geometry.

For cells the model described before should be adapted for spherical dimensions. This also leads to a multi exponential behaviour as given by eq. (4.7), with a decay rate given by eq. (4.9). Similar conclusions can be drawn for the case of spherical dimensions as for cylindrical dimensions, by replacing the previous equations by [16,20]:

$$I_n = 6/[k_n^2 (1-(1/Rh) + (k_n/Rh)^2)] \quad (4.8s)$$

$$k_n \cot(k_n) + Rh - 1 = 0 \quad (4.10s)$$

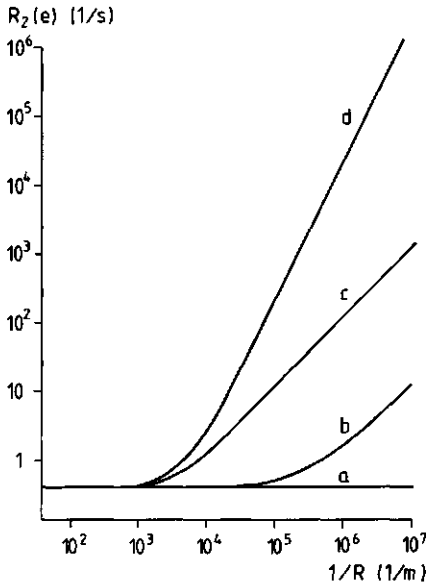


Figure 4.6

Relation between the effective relaxation rate $R_2(e)$ and the reciprocal of the radius ($1/R$) on a logarithmic scale for 4 values of H and for $T_2 = 2.5$ s:

- a) $H = 0$ cm/s;
- b) $H = 6 \cdot 10^{-5}$ cm/s;
- c) $H = 6 \cdot 10^{-3}$ cm/s;
- d) $H = \infty$.

$R_2(e)$ is the reciprocal of the time at which the magnetization has decayed to $1/e$ times its initial value.

$$k_1^2 = 3Rh \quad (4.11s)$$

$$1/T_{2,1} = 3H/R + 1/T_2 \quad (4.13s)$$

$$(i) \quad 3HT_2/R \ll 1 \text{ or } R^2 \gg 3DT_2 : T_{2,1} \approx T_2 \quad (4.14s)$$

$$(ii) \quad 3HT_2/R \gg 1 \text{ or } R^2 \ll 3DT_2 : T_{2,1} < T_2 \quad (4.15s)$$

$$1/T_{in} = 3H/R + 1/T_2 \quad (4.18s)$$

4.6 References

- [1] H. Van As and T.J. Schaafsma. 1984. *Biophys. J.*, 45, 469-472.
- [2] M.A. Hemminga, P.A. de Jager and A. Sonneveld, 1977. *J. Magn. Res.*, 27, 359-370.
- [3] M.A. Hemminga and P.A. de Jager, 1980. *J. Magn. Res.*, 37, 1-16.
- [4] H. Van As, 1982. *NMR, Water and Plants*. Ph.D. dissertation. Agricultural University, Wageningen, The Netherlands.
- [5] J.R. Zimmerman and W.E. Brittin, 1957. *J. Phys. Chem.*, 61, 1328-1333.

- [6] C.F. Hazlewood, D.C. Chang, B.L. Nichols and D.E. Woesner, 1974. *Biophys. J.*, 14, 583-606.
- [7] R. Cook and R. Wien, 1971. *Biophys. J.*, 11, 1002-1016.
- [8] B.M. Fung and T.W. McCaughy, 1981. *J. Magn. Res.*, 43, 316-323.
- [9] B.M. Fung and P.S. Puon, 1981. *Biophys. J.*, 33, 27-38.
- [10] G.D. Fullerton, J.L. Potter and N.C. Dornbluth, 1982. *Magn. Res. Imag.*, 1, 209-228.
- [11] B.M. Fung, D.A. Wassil, D.L. Durham, R.W. Chesnut, N.N. Durham and K.D. Berlin, 1975. *Bioch. Biophys. Acta*, 385, 180-187.
- [12] R.T. Pearson, I.D. Duff, W. Derbyshire and J.M.V. Blanshard, 1974. *Bioch. Biophys. Acta*, 326, 188-200.
- [13] F. Hanus and P. Gillis, 1984. *J. Magn. Res.*, 59, 437-445.
- [14] K.R. Brownstein and C.E. Tarr, 1977. *J. Magn. Res.*, 26, 17-24.
- [15] K.R. Brownstein and C.E. Tarr, 1979. *Phys. Rev. A*, 19, 2446-2453.
- [16] S.D. Senturia and J.D. Robinson, 1970. *Soc. Petrol. Eng. J.*, 249, 237-244.
- [17] D. Michel and H. Pfeiffer, 1965. *Z. Naturforschg.*, 20a, 220-226.
- [18] P.S. Belton and R.G. Ratcliffe, 1985. *Progress in NMR Spectroscopy*, 17, 241-279.
- [19] G.E. Wesbey, M.E. Moseley and R.L. Ehman, 1984. *Invest. Radiol.*, 19, 491-498.
- [20] H.S. Carslaw and J.C. Jaeger, 1959. "Conduction of heat in solids". Oxford University Press, London.
- [21] A. Abragam, 1961. "Principles of Nuclear Magnetism". Oxford University Press, Oxford.
- [22] L.J. Lynch, 1983. "Magnetic Resonance in Biology". Chapter 5. J.S. Cohen ed., John Wiley and Sons.
- [23] A. Kalk and H.J.C. Berendsen, 1976. *J. Magn. Res.*, 24, 343-66.
- [24] E. Hsi, R. Hossfeld, R.G. Bryant, 1977. *J. Coll. Interf. Sc.*, 62, 389-385.
- [25] H.T. Edzes and E.T. Samulski, 1977. *J. Magn. Res.*, 31, 207-229.
- [26] B.D. Sykes, W.E. Hull, and G.H. Snyder, 1978. *Biophys. J.*, 21, 137-146.
- [27] S.H. Koenig, R.G. Bryant, K. Hallenga, and G.S. Jacob, 1978. *Biochemistry*, 17, 4348-4358.
- [28] E. Hsi, J. Vogt and R.G. Bryant, 1979. *J. Coll. Interf. Sc.*, 20, 338-345.
- [29] J.M. Escanye, D. Canet, and J. Robert, 1984. *J. Magn. Res.*, 58, 118-131.
- [30] B.M. Fung and T.W. McCaughy, 1980. *J. Magn. Res.*, 39, 413-420.
- [31] H.J.C. Berendsen, 1975. "Water; a comprehensive treatise". Chapter 6. F. Franks ed., Plenum Press, New York.
- [32] K.R. Brownstein, 1980. *J. Magn. Res.*, 40, 505-510.
- [33] C.D. Eccles and P.T. Callaghan, 1986. *J. Magn. Res.*, 68, 393-398.
- [34] P. Mansfield and P.G. Morris, 1982. "NMR Imaging in Biomedicine". Academic Press, New-York.

CHAPTER V

=====

5 ANGULAR AND FIELD STRENGTH DEPENDENCE OF ^1H NMR SPECTRA OF THE CUCUMBER STEM5.1 Introduction

Although cucumber stems consist for more than 90% of water, the proton NMR spectrum of a stem segment is essentially different from that of bulk water. This is already evident from inspection of the FID in a pulse experiment. T_2^* (see Chapter 2) was typically 4-7 ms (i.e. considerably shorter than for bulk water) after optimal shimming. In addition, the FID was not exponential. When the receiver phase was shifted 90° (ie. when not the x' -component but the y' -component of the magnetization decay was monitored, see Chapter 2), a small signal could be observed, starting at zero, reaching a maximum after a few milliseconds, and then decaying to zero. These observations suggest the presence of local field gradients, due to differences in susceptibility (χ) within the sample. Since

- 1) in NMR flow measurements local field gradients cause a contribution of stationary water to the flow signal [Chapter 6],
- 2) the value of the field gradient does not reproduce from plant to plant when inhomogeneities are present, and
- 3) diffusion through field gradients shortens the T_2 value of the flowing water, thus reducing the range of flow velocities accessible for measurement [Chapters 2 and 6],

more information on the magnetic properties of the cucumber stem was required. The magnetic field dependence of the NMR-spectrum of a cucumber stem segment was therefore studied at proton resonance frequencies of 60 MHz and 90 MHz. By rotating the stem around its axis with respect to the direction of the static magnetic field B_0 , oriented perpendicular to the stem-axis, the angular dependence of the NMR-spectra was studied as well.

5.2 Theory

Susceptibility (χ) differences result in chemical shifts of resonance transitions [1,2]. Differences in bulk sample susceptibility [1], or anisotropic magnetic susceptibilities [2] lead to an angular (θ) dependence of the resonance field when the sample is rotated in the magnetic field, given by $\cos^2\theta$, i.e. every rotation over 90° inverses the spectrum (high and low field resonances are interchanged) whereas every rotation over 180° leads to an identical spectrum.

As will be shown below, it can be derived from the theory developed by Zimmerman and Foster [1] that the resonance field strength B inside a planar sample with finite thickness and uniform susceptibility is given by [3]:

$$B = B_0 (1 - \Delta\delta \cos^2\theta) \quad (5.1)$$

in which B_0 = the external static magnetic field, θ = angle between B_0 and a vector normal to the plane surface, and $\Delta\delta = (\chi_s - \chi_m)$ where χ_s and χ_m represent the magnetic susceptibilities of the sample and the medium respectively [1]. By rotating the planar sample, the value of B_0 , at which the resonance is observed varies between B and $B/(1 - \Delta\delta)$, where $B = \omega_0/\gamma$; ω_0 is the angular frequency at which the NMR-experiment is carried out and γ = proton magnetogyric ratio. The magnetic field difference ΔB_0 for the extreme resonance positions is thus given by

$$\Delta B_0 = (\omega_0/\gamma)[1/(1-\Delta\delta) - 1] \quad (5.2)$$

Since $\omega_0/\gamma \approx B_0$, this results in $\Delta B_0/B_0 \approx \Delta\delta$ for $\Delta\delta \approx 10^{-6}$.

For an annular tissue cylinder at the inside and outside surrounded with air, with an internal radius R_1 , the magnetic field strength at $r \geq R_1$ can be derived from [1] to be

$$B(r, \theta) = B_0 \left[1 - \frac{1}{2} \Delta\delta \left(1 + \frac{R_1^2}{r^2} \cos 2\theta \right) \right] \quad (5.3)$$

If the cylinder is infinitely thin (i.e. $r = R_1$) eq. (5.3) yields eq. (5.1) again. The number of molecules in an annular element with an angle between θ and $\theta+d\theta$ is proportional to:

$$N(\theta) = d\theta = m \frac{dB}{dB} dB \quad (5.4)$$

where the constant m represent the spin density in the annulus. Using eq. (5.1) one finds that:

$$\frac{dB}{d\theta} = 2 B_0 \Delta\delta \sin\theta \cos\theta \quad (5.5)$$

Therefore $N(\theta)$ has two maxima at $\theta=0$ and $\pi/2$, respectively, corresponding to $B_0 = B$ and $B_0 = B/(1-\Delta\delta)$, just as was found for a flat sample [4]. Increasing the thickness of the annulus decreases the distance between both maxima [1]. The presence of internal structure in the stem (e.g. a central pith) can be accounted for by introducing an angular dependence of R_1 , similar to the treatment in [1].

The susceptibility effect on the shape of the NMR spectrum, in particular its width, is predicted to be linearly dependent on the applied magnetic field strength B_0 , and therefore the observed line widths are expected to be independent of the measuring frequency when expressed in units parts per million (ppm).

5.3 Materials and methods

For the measurements a fresh, ca. 3 cm long stem segment of a cucumber plant was used with an outer diameter of ca. 5 mm, which fitted into a standard NMR tube with an inner diameter of 5 mm. NMR spectra were recorded on CW spectrometers at 90 MHz (Varian EM 390) and 60 MHz (Hitachi Perkin Elmer R 24B) at eight different angles (θ). θ is the angle between B_0 and an arbitrarily chosen radial vector in the plant stem. For each spectrum, shown in Fig. 5.1 the NMR tube was rotated around the cylinder axis over ca. 45° . The resonance line of water was obtained with an identical NMR tube as used for the stem segments.

5.4 Results

Fig. 5.1 shows the NMR spectra of the cucumber stem segment at 90 MHz and 8 angles θ . The angular accuracy is estimated to $\pm 10\%$. The shape

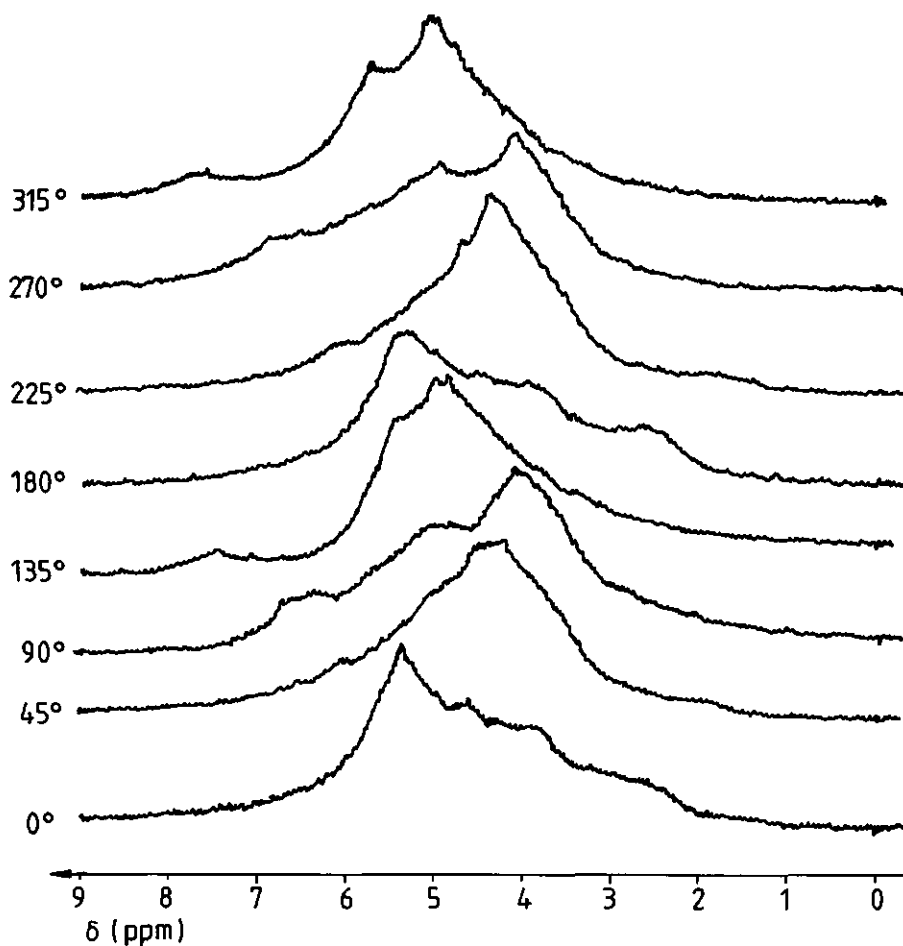


Figure 5.1

NMR spectra of a cucumber stem segment at 90 MHz proton resonance frequency and at 8 different angles (θ) with respect to the magnetic field direction B_0 . θ is the angle between B_0 and an arbitrarily chosen radial vector in the stem segment. No reference was used for the ppm scale, which has an arbitrary starting position.

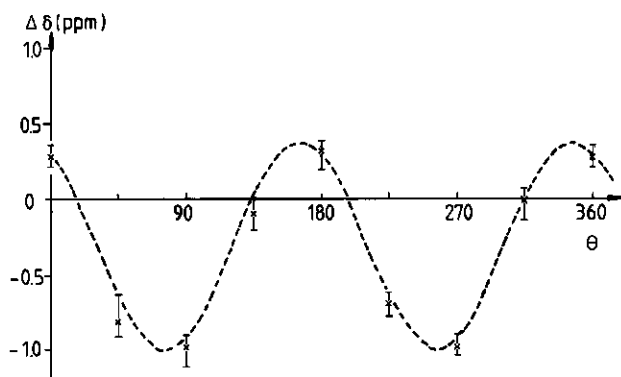


Figure 5.2

Chemical shift difference ($\Delta\delta$) between the maxima of Fig. 5.1 and the resonance position of water ($\delta = 5$ ppm in Fig. 5.1) as a function of θ .

of the spectra clearly varies with θ , and the symmetry of the spectrum upon a rotation of 90° suggests a $\cos^2\theta$ dependence. This is confirmed by Fig. 5.2 where the chemical shift of the signal maximum with respect to the resonance position of water ($\delta = 5$ ppm, on the scale of Fig. 5.1) is shown as a function of θ . In this figure the starting position of θ was chosen arbitrarily, but it was equal for the spectra recorded at 90 MHz and 60 MHz. The spectra recorded at 60 MHz (not shown) showed the same angular dependence; their shape was essentially the same as the 90 MHz spectra. As can be seen from Fig. 5.3, however, the line width (Δw), measured as the width at half height on a ppm scale, was larger for the 90 MHz spectra than for the 60 MHz spectra. When comparing line widths at 90 MHz ($\Delta w(90)$) and 60 MHz ($\Delta w(60)$), obtained at the same value of θ at eight values of θ it was found that: $\Delta w(90)/\Delta w(60) = 1.46 \pm 0.21$.

5.5 Discussion

The angular dependence as shown in Fig 5.1 is in agreement with results found for a number of leaf tissues [3,5], cellulose acetate membranes [6] and Red Osier Dogwood stem segments [4]. In first approximation a cucumber stem segment can be seen as an annular cylinder, the

central part of which is formed by the pith cavity (see Fig. 3.3A) and the ring is formed by the tissue. Both regions have different magnetic susceptibility (χ). This would lead to a broad spectrum with two equally intense maxima, as outlined before, and no angular dependence would be observed due to the cylindrical geometry. A broad spectrum is indeed observed, but its irregular shape and angular dependence indicate that the stem is not a smooth annular cylinder. The observed spectra can be explained by assuming that the cylinder contains (mainly inward) protrusions at certain places on the ring. From Fig. 3.3A it can be seen that this is a reasonable assumption, since neither the pith cavity nor the overall shape of the cucumber stem are smooth cylinders. The observed spectrum can be considered to be originating from a combination of spectra of an annular cylinder and those of a number of flat shaped volume elements at various fixed orientations with respect to one another and to the ring.

Thus the observed spectra can be explained by assuming a noncylindrical sample geometry, corresponding to non-cylindrical distribution of the magnetic susceptibility.

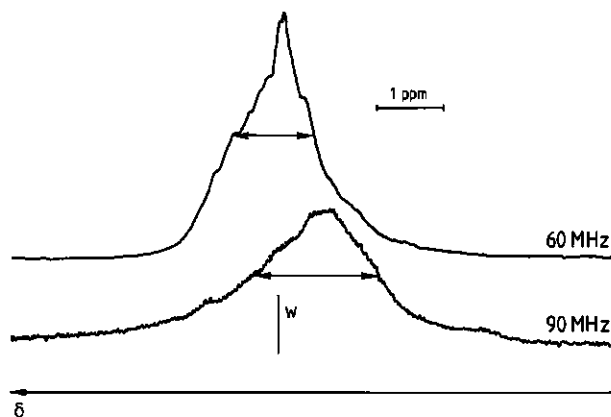


Figure 5.3

NMR spectra of cucumber stem segment at 60 MHz and 90 MHz proton resonance frequency at identical values of θ . The spectra were oriented in such a way that the resonance positions of a sample of tap water (indicated with the vertical bar marked 'w') were identical.

A $\cos^2\theta$ dependence also is observed if χ is anisotropic, i.e. if there are molecules in the sample with a value of χ which depends on their orientation in the B_0 field. Oriented molecules present in a complex system like a plant stem can give rise to similar broadening of the NMR spectra as described before.

The spectra of Fig. 5.1 do not show much resemblance to those observed by McCain and Markley [5] for leaves with a high concentration of reserve Mn^{2+} ions. These ions are bound near the outer surface of the thylakoid in the leaf-chloroplasts. NMR spectra of such leaves contain three peaks, two of which result from dipolar interactions of water-molecules with Mn^{2+} inside the chloroplasts which were either aligned parallel or perpendicular to the leaf surface. These two orientations occur preferentially due to the leaf structure. For such a distribution the dipolar interactions of water with Mn^{2+} are not averaged out. A third peak was believed to originate from the water in the spongy layer of the leaf. When the leaf surface was rotated with respect to B_0 a $\cos^2\theta$ dependence was predicted and observed. The line widths were independent of the value of B_0 , when expressed in units ppm. Spectra of leaves with low concentrations of reserve Mn^{2+} ions only showed one broad peak.

Although the cucumber stem contains chloroplasts, and a preferential orientation of these chloroplasts cannot be excluded, the shape of the spectra observed by McCain and Markley is quite different from that in Fig. 5.1. We therefore conclude that the spectra of Fig. 5.1 cannot be explained by magnetic dipolar interaction between Mn^{2+} and water in oriented chloroplasts.

The observed magnetic field dependence (Fig. 5.3) is in disagreement with the experimental results cited in literature [3-5]. Experiments with a large number of different leaves at 470 Mhz and 200 MHz [3,5] as well as experiments with Red Osier Dogwood stem samples [4] conducted at 100 Mhz and 60 MHz yielded equal and frequency-independent line widths when expressed in units ppm. From Fig. 5.3 it is concluded that the line width in ppm is linearly proportional to the magnetic field strength, (i.e. proportional to B_0^2 , if expressed in units Gauss or Tesla). This is not yet understood.

5.6 Conclusions

The observed angular dependence of the NMR spectra of cucumber stem segments agrees with earlier observations on similar systems. The observed $\cos^2\theta$ dependence is most likely the result of the internal structure of the cucumber stem, giving rise to a spatial distribution of the magnetic susceptibility which lacks cylindrical symmetry.

Although the magnetic field effect is not understood some consequences are noteworthy.

As outlined in the introduction it is important for NMR flow measurements that local field gradients, and thus line widths, are minimized. It is obvious from the present experiments that a low value of B_0 must be chosen to achieve this goal. This is an important criterium for the choice of the operating frequency for NMR instruments designed to measure NMR flow. In addition, the observed magnetic field dependence has consequences for NMR imaging experiments. To overcome the inhomogeneity effect, which causes blurring of the image, progressively higher field gradient strengths must be chosen when increasing the operating frequency, to avoid loss of resolution.

5.7 Acknowledgements

I am indebted to Mr. A. van Veldhuizen of the Department of Organic Chemistry for making available the CW NMR spectrometers.

5.8 References

- [1] J.R. Zimmerman and M.R. Foster, 1957. J. Phys. Chem., 61, 282-289.
- [2] A. Carrington and A.D. McLachlan, 1967. "Introduction to Magnetic Resonance". Harper and Row, New York.
- [3] D.C. McCain, T.C. Selig, Govindjee and J.L. Markley, 1984. Proc. Natl. Acad. Sci. USA, 81, 748-752.
- [4] M.J. Burke, R.G. Bryant and C.J. Weiser, 1974. Plant Physiol., 54, 392-398.
- [5] D.C. McCain and J.L. Markley, 1985. Biophys. J., 48, 687-694.
- [6] V.V. Mank and N.I. Lebovka, 1983. Chem. Phys. Lett., 96, 626-630.

CHAPTER VI

=====

6 EVALUATION OF THE NMR METHODS AND CALIBRATION6.1 Introduction

This chapter discusses the practical aspects of measuring flow and water content making up the water balance of intact plants, in particular calibration procedures, required for quantitative measurements, error sources, reproducibility, and validity ranges for flow (§ 6.2) as well as relaxation time measurements (§ 6.3). The methods as well as the biological material determine to which the degree quantitative and qualitative information with respect to the plant water balance can be obtained.

6.2 Flow measurements

Important factors which affect the flow curves obtained by the NMR RP method are: magnetic field gradient strength (G), flow velocity profile ($P(v)$), rf coil geometry and dimensions, pulse spacing (τ), pulse angle and the relaxation times T_1 and T_2 of the flowing fluid [1,2,3, Chapter 2]. Therefore calibration should be carried out in a system in which each of these parameters has the same value as in the plant of interest. In practice calibration is carried out by measuring water flow in a glass capillary using the same experimental set-up and the same instrumental values of G , τ and pulse angle as in the experiments with plants [3] (see also Chapter 7). A number of parameters, however, is different in plants than in the calibration system. In the following paragraphs we use computer simulations to investigate the errors in v , Q and A which may arise from this calibration (see Chapter 7). The relevant parameters are: $P(v)$ (§ 6.2.1.) and the relaxation times T_1 and T_2 (§ 6.2.2.), all of which are plant dependent. The influence of local field gradients in plants [Chapter 5] on the flow curves and its implications for the choice of G and τ are discussed in § 6.2.3. Experimental

calibration curves are presented in § 6.2.5. Finally we discuss the importance of the values of Q , v , \hat{S}_0 and $1/t_m$, with regards to the plant experiments (described in Chapter 7) in § 6.2.6.

6.2.1 Flow profiles

A linear relationship exists between v and $1/t_m$ for plug and laminar flow, given by eq. (2.20) [1-3]. For laminar flow the flow velocity v for plug flow is replaced by the average flow velocity \bar{v} . The calibration factor K_v , relating v to $1/t_m$ is different for plug and laminar flow and, in general, depends on the flow profile $P(v)$ [1,2,3, Chapter 2]. The linear relationship which has been found for \hat{S}_0 and Q was shown to be independent of the flow profile [2]. The influence of the shape of $P(v)$ on the relationship between \bar{v} and $1/t_m$ is discussed in this paragraph. Since $A=Q/v$, $P(v)$ affects the calculated value of A as well.

First we discuss the theory on flow velocity profiles in plants in some detail. If $P(v)$ represents the probability density to find a flow velocity v , or the fraction of the total area available for flow with a linear flow velocity v , the volume flow rate Q is given by:

$$Q = A \int_{v=0}^{v=v_{\max}} P(v) v dv \quad (6.1)$$

in which v_{\max} represents the maximum value of v present in the system. The average flow velocity \bar{v} is defined as:

$$\bar{v} = Q/A = \int_{v=0}^{v=v_{\max}} P(v) v dv \quad (6.2)$$

For plug flow, v is constant (v_0) for the total area available for flow. The velocity flow profile then becomes:

$$P(v) = \delta(v-v_0) \quad (6.3)$$

For flow in a cylinder with radius R this leads to:

$$Q = v_0 \pi R^2 \quad (6.4)$$

$$\bar{v} = v_0 \quad (6.5)$$

For "laminar flow", or, as it is sometimes called, "viscous flow" or "Poiseuille flow" (see e.g. [4]) in a cylinder with radius R the velocity depends on the radial coordinate (r):

$$v(r) = - \left(\frac{dP}{dy} \right) (R^2 - r^2) / 4\eta = D_p (R^2 - r^2) = v_{\max} (1 - (r/R)^2) \quad (6.6)$$

in which $v_{\max} = D_p R^2$, η = viscosity of the fluid and dP/dy = pressure gradient along the direction of flow (y). The minus sign indicates that water flows in the direction of decreasing pressure. It can be shown that the flow profile for laminar flow is given by [18]:

$$P(v) = 1/v_{\max} = 1/(2\bar{v}) \quad 0 \leq v \leq v_{\max} \quad (6.7)$$

This is shown in Fig. 6.1. Combining eqs. (6.1) and (6.2) with (6.7) leads to:

$$Q = 0.5 v_{\max} \pi R^2 \quad (6.8)$$

$$\bar{v} = 0.5 v_{\max} = 0.5 D_p R^2 \quad (6.9)$$

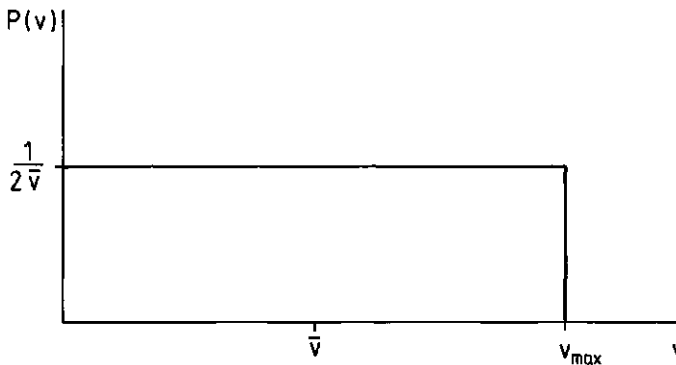


Figure 6.1

Flow velocity profile for laminar flow. $P(v)$ = probability density to find a flow velocity v in the distribution of velocities. Maximum and average flow velocities are denoted by v_{\max} and \bar{v} , respectively.

Laminar flow occurs whenever the Reynolds number (Re) $<$ ca. 2000 [4]. Re is a dimensionless quantity defined as:

$$Re = 2 \rho v R / \eta \quad (6.10)$$

in which ρ = density of the fluid. For flow velocities $<$ 40 mm/s and a maximum radius of the plant xylem vessels of 0.5 mm, representing the ranges for \bar{v} and R that may be expected for water flow in plant systems [5,6], $Re <$ ca. 40. Also within a capillary with a diameter of a few millimeters, used for calibration, $Re \ll 2000$. Eq. (6.10) only applies for smooth conductors. In general, cucumber xylem vessels are not smooth, but contain many perforation rims, as can be seen in Fig. 3.3C. In general the protrusions formed by the perforation rims are not so large that disturbances of the laminar flow profile can be expected [3], although resistances to flow are often found to be somewhat higher than calculated from Poiseuille flow [7-9]. Therefore, water flow in individual plant vessels is considered to be laminar.

The water conducting system of the plant consists of many xylem vessels with different diameters. The total flow profile of the plant is the summation of the (laminar) flow profiles of the individual vessels. Since in most cases the distribution of xylem vessel radii is a priori unknown, the flow velocity flow profile $P(v)$ in a plant stem, and thus K_v is unknown. To investigate the effect of a distribution $P(v)$ different from that for laminar flow on the calibration constant K_v , we introduce a "model plant" that is used in the computer simulations. For such a model plant the following assumptions are made:

- 1) There is a discrete distribution $P(R)$ of 20 vessel radii, all of which are equally abundant, i.e. $P(R)$ is constant up to a maximum value R_{max} . For $R > R_{max}$, $P(R) = 0$ (Fig. 6.2).
- 2) In each vessel flow is laminar.
- 3) The pressure gradient (dP/dy) is independent of R ; i.e. all vessels experience the same value of D_p [10].

The flow velocity profile for such a system is the result of the summation of the flow profiles of the individual vessels, each weighed with its relative area:

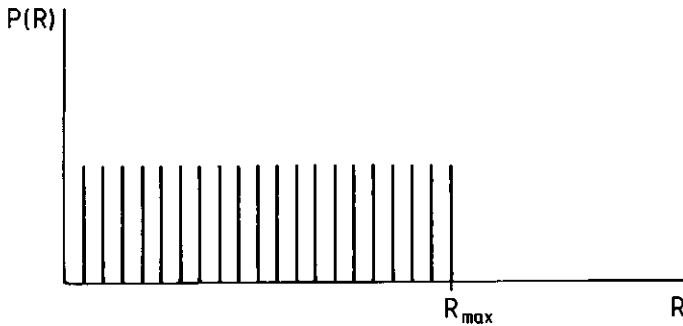


Figure 6.2

Distribution of the vessel radii for a con-flow profile.

$$P(v) = \sum_{i=1}^{20} P_i(v) A_i/A \quad (6.11)$$

in which $P_i(v)$ and A_i are the flow velocity profile and area of the i 'th vessel, respectively:

$$P_i(v) = 1/v_{\max,i} = 1/(Dp R_i^2) \quad 0 \leq v_i \leq v_{\max,i} \quad (6.12)$$

$$A_i = \pi R_i^2 \quad (6.13)$$

and

$$A = \sum_{i=1}^{20} \pi R_i^2 \quad (6.14)$$

The flow profile of eq. (6.11) is shown in Fig. 6.3. Each step represents the flow profile of a single vessel. Effectively, a reduction in R_{\max} only results in a loss of the corresponding high velocities in the $P(v)$ distribution. It is found numerically that for the limiting case of an infinite number of vessels with equal abundance:

$$\bar{v} = 0.3 v_{\max} \quad (6.15)$$

$$Q = 0.3 v_{\max} A \quad (6.16)$$

In Fig. 6.4 the relationship between \bar{v} and $1/t_m$ is represented for two types of flow: laminar flow (referred to as lam-flow) and the flow profile as shown in Fig. 6.3 (referred to as con-flow). Fig. 6.4 has been obtained from RP flow curves which were calculated using the computer program based on the formalism developed by Hemminga and de Jager [1]. From Fig. 6.4 it can be concluded that for both lam-flow and con-flow a linear relationship is found between the linear flow velocity and $1/t_m$, given by:

$$\text{lam-flow: } \bar{v} = (0.5)v_{\max} = 5.3/t_m \quad (6.17a)$$

$$\text{con-flow: } \bar{v} = (0.3)v_{\max} = 4.1/t_m \quad (6.17b)$$

These equations are represented by the solid lines in Fig. 6.4, obtained for $T_1=T_2$. For values of $v_{\max} < \text{ca. } 75 \text{ mm/s}$, (i.e. $\bar{v}(\text{con}) < \text{ca. } 25 \text{ mm/s}$ en $\bar{v}(\text{lam}) < \text{ca. } 40 \text{ mm/s}$), a range including the majority of velocities occurring in plants, the value of \bar{v} calculated from eqs. (6.17a) and (6.17b) is within 5% of its actual value. At higher values of \bar{v} , \bar{v}

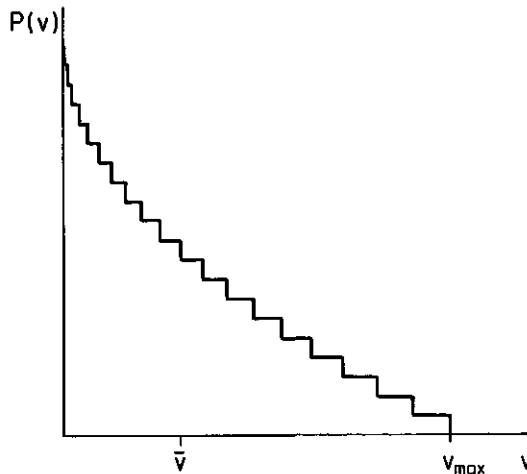


Figure 6.3

Flow velocity profile (con-flow profile) distribution of vessel radii as shown in Fig. 6.2, with a laminar flow profile in each individual vessel.

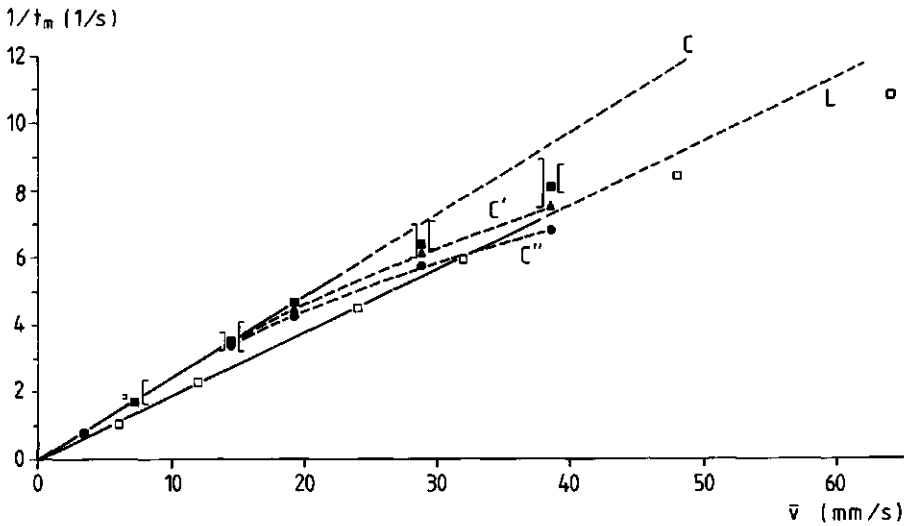


Figure 6.4

Relationship between $1/t_m$ and \bar{v} for various experimental conditions and $T_1 = 1$ s and $T_2 = 0.5$ s. The datapoints apply for $T_1 \leq 2 T_2$.

1) \square : Lam-flow profile; on resonance:

2) Con-flow profile (curves C, C', C''):

a) \blacksquare : on resonance: (Curve C).

b) on resonance + 'non-equilibrium effect':

\blacktriangle : $d/T_1 = 80$ mm/s (curve C');

\bullet : $d/T_1 = 40$ mm/s (curve C'').

c)] : margins for the shift of $1/t_m$ due to the off-resonance effect on the flow curves for off-resonance frequencies between -200 Hz and +200 Hz.

d) [: margins for the shift of $1/t_m$ due to the off-resonance signal from a 25 fold excess of stationary water at off-resonance frequency shifts between -200 Hz and +200 Hz.

For clarity the symbols] and [are drawn to the left and right of the data points.

vs $1/t_m$ is no longer linear, and K_V increases. It is obvious from Fig. 6.4 that K_V depends on the flow profile. The value of K_V , obtained from calibration with a single capillary system with a lam-flow profile, is too large to be used in plant experiments. For a model plant with a distribution of vessel radii as given in Fig. 6.2, the value of K_V is

77% of that obtained from an experiment with a single capillary. Although the actual shape of $P(R)$ for plants is not a priori known, it can always be considered to be between the two distributions, corresponding to con-flow and lam-flow. This implies that for the actual value k_v in a plant: $K_v(\text{con}) < K_v < K_v(\text{lam})$. This is based on a logical argument, but we did not verify this by detailed computer calculations.

We conclude that as long as $P(v)$ is not known, this uncertainty causes an inaccuracy in the value of \bar{v} , and thus in the value of A calculated from Q/\bar{v} . The error is expected to be in the order of ten percent.

6.2.2 Effect on the flow-curves of relaxation times T_1 and T_2 of ----- flowing water -----

In general T_1 and T_2 of water flowing in the plant xylem are expected to be shorter than the values for distilled water, and, in addition $T_1 > T_2$ [Chapter 2]. T_2 and probably T_1 strongly depend on the xylem vessel diameter [Chapter 4]. The effect of the relaxation times T_1 and T_2 on the flow curves is shown in Fig. 6.5 for a number of simulated con-flow curves. Simulations were carried out again with the computer program mentioned in the previous paragraph.

All the results of Fig. 6.5 are in agreement with those previously found for lam-flow [2,3]. The effect of decreasing T_2 is to shift t_m to lower values and to decrease the amplitude of the signal maximum ($S(t_m)$) (Fig. 6.5A). The effect of decreasing T_1 is to shift t_m to higher values and to increase $S(t_m)$ slightly. For $t > \text{ca. } t_m$, however, a decreasing value of T_1 leads to a much more pronounced increase of $S(t)$. This is shown in Fig. 6.5B. Whenever $T_1=T_2$ a decrease of the relaxation times does not affect t_m , but leads to a decrease of the signal amplitude around $t=t_m$ and an increase of the signal amplitude for $t > \text{ca. } t_m$, i.e. the signal maximum becomes less sharp (Fig. 6.5C). The initial slope, however, is not changed by the relaxation times since at $t=0$ relaxation effects have not yet had time to take place.

Therefore the decreasing effect of T_2 relaxation on $S(t)$ becomes more pronounced with increasing time. This is illustrated in Figs. 6.5D

and 6.5E. If the values of $S(t_m)$ of Fig. 6.5D ($S(t_{mD})$) are compared with those of Fig. 6.5E ($S(t_{mE})$) for the same flow velocities, it can be seen that the ratio $S(t_{mE})/S(t_{mD})$ decreases upon decreasing flow velocity. Eventually, for low velocities and short T_2 values this leads to signal

Figure 6.5

Effect of relaxation times T_1 and T_2 on the NMR flow curves for a con-flow profile.

fig. 6.5A: Effect of T_2 ; $\bar{v}=14.4$ mm/s; $T_1=2.4$:

a) $T_2=2.4$; b) $T_2=1.2$; c) $T_2=0.5$; d) $T_2=0.2$.

fig. 6.5B: Effect of T_1 ; $\bar{v}=14.4$ mm/s; $T_2=0.2$;

a) $T_1=0.2$; b) $T_1=1.0$; c) $T_1=2.4$.

fig. 6.5C: Effect of T_1 and T_2 ; $\bar{v}=14.4$ mm/s; $T_1=T_2=$

a) 2.4; b) 0.5; c) 0.2; d) 0.1.

fig. 6.5D+E: Effect of T_2 on various flow rates for $T_2=0.5$ (Fig. 6.5D) and $T_2=0.2$ (Fig. 6.5E); $T_1=1.0$; values of \bar{v} (mm/s):

a) 38.4; b) 28.8; c) 14.4; d) 7.2; e) 3.6.

Values of T_1 and T_2 are in seconds. The scaling factor is the same in Figs. 6.5A-E.

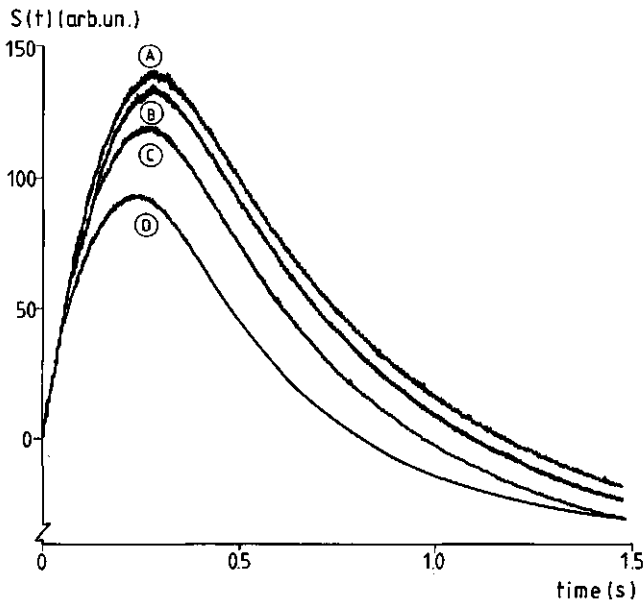


Fig. 6.5A

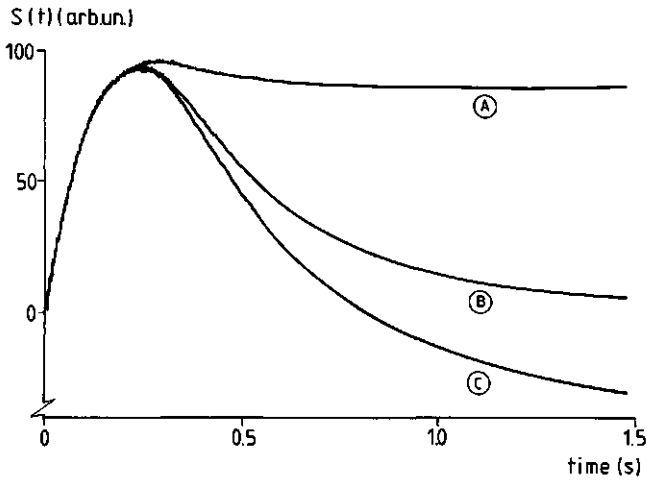


Fig. 6.5B

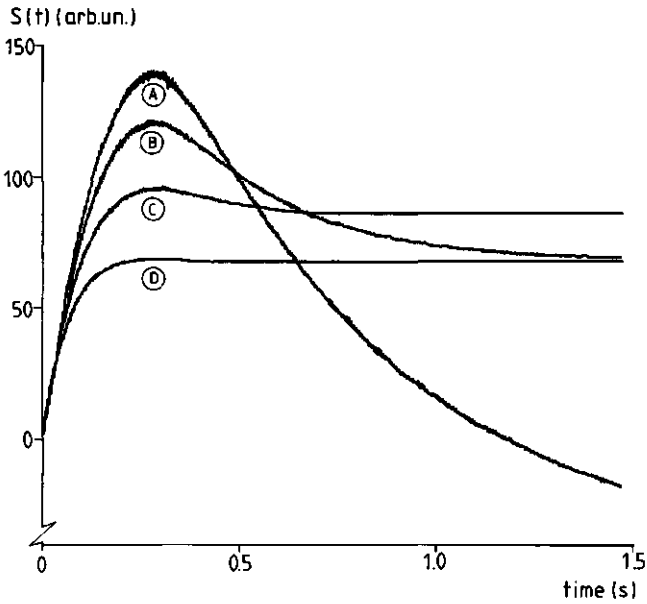


Fig. 6.5C

amplitudes which are too small to be observed, i.e. the signal becomes too small to be distinguished from error signals due to stationary water (§ 6.2.3.3.). Shortening of T_2 leads to a higher value of \bar{v} below which no flow signals can be observed anymore. For flow velocities leading to

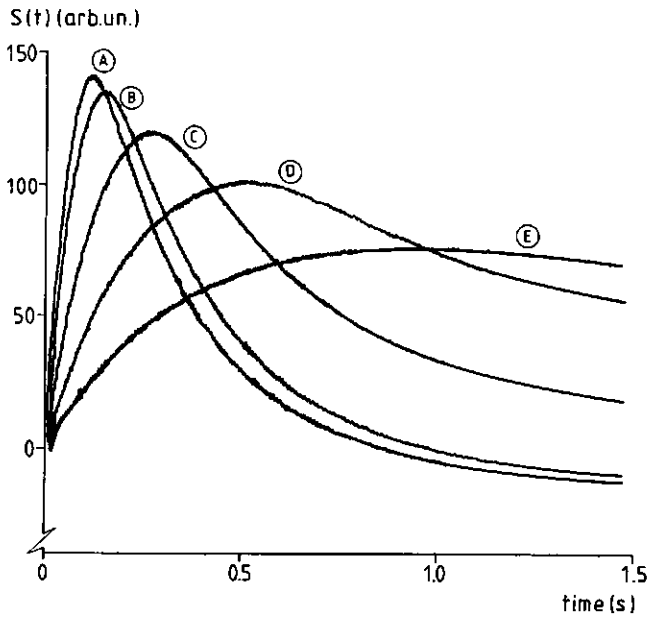


Fig. 6.5D

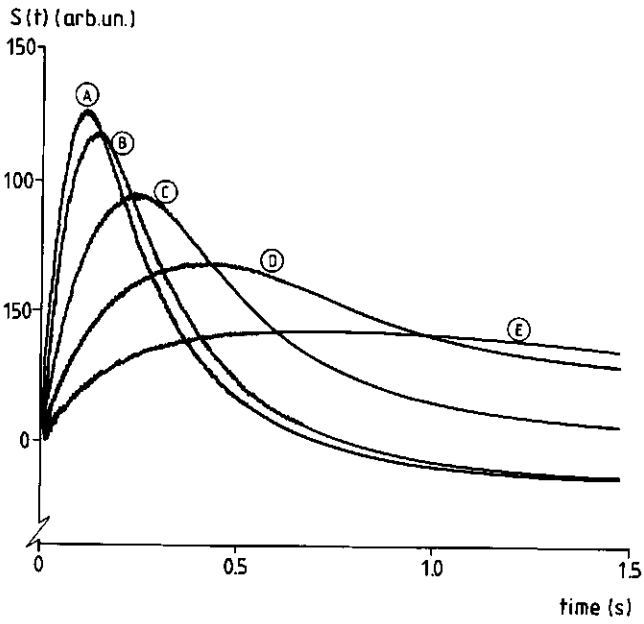


Fig. 6.5E

values of $t_m > \text{ca. } 3T_2$ no maximum is observed anymore. Since a) T_2 decreases upon a decrease of the xylem vessel diameter (see Chapter 4) and b) \bar{v} is proportional to the square of the vessel radius, small vessels provide only a little contribution to the flow signal. Assuming a maximum value of \bar{v} of ca. 40 mm/s (which is approximately the maximum value which has been observed in cucumber plants, and for which $1/t_m \approx 8-9 \text{ 1/s}$ under the chosen experimental conditions) computer simulations showed that the flow curve has only a maximum as long as T_1 and $T_2 > \text{ca. } 50 \text{ ms}$, i.e. for cucumber plants with xylem vessel diameters $> 12 \mu\text{m}$ (see Fig. 4.6). These high velocities, however, are only encountered in the largest vessels. Assuming a value of \bar{v} of 40 mm/s in a vessel with a diameter of $300 \mu\text{m}$, \bar{v} for a $12 \mu\text{m}$ vessel will be ca. 0.06 mm/s, resulting in $t_m \approx 1 \text{ min}$. Clearly this gives no significant contribution to the flow signal. For the values of G , τ and L , used in this experiment and under optimal transpiration conditions, the lower boundary for the diameter of vessels leading to an extremum in the flow curves is found to be $\approx 90 \mu\text{m}$, resulting in a lower boundary of $\bar{v} = 3.6 \text{ mm/s}$, corresponding to $t_m = 1 \text{ s} \approx 3T_2$ at this vessel radius (see Fig. 4.6). Actually, the boundary for \bar{v} is too pessimistic, because it is not necessary that all velocities, present in the distribution, give rise to an extremum in $S(t)$. Therefore, the xylem vessel diameter for which a flow signal still can be observed is expected to be somewhat lower than $90 \mu\text{m}$.

In principle, there would be several ways to lower the detection limit of $90 \mu\text{m}$ of the vessel diameter:

- a) Reduction of t_m by increasing Gr . This, however, results in a reduction of signal amplitude [1] and does not necessarily improve the performance of the method.
- b) Signal averaging. Of course, averaging of signals lengthens the period, needed to record the $S(t)$ curve. Without averaging, a full curve usually develops in a few seconds.

In practice however, the intensity of the error signal from stationary water (see section 6.2.3.3) determines the lower limit of the vessel diameter from which flow curves can be obtained. Unlike the signal to noise ratio, this effect cannot be reduced by signal

averaging.

If we "weigh" the flow profile (Fig. 6.3) with the T_2 effect, the relative contribution of low velocities to $P(v)$ decreases at lower values of v in Fig. 6.3, since the effect of T_2 increases with decreasing vessel radius, and therefore, with decreasing values of v . This means that the deviation of the con-flow velocity profile $P(v)$ from that for lam-flow becomes smaller, and the actual value for K_v shifts towards $K_v(\text{lam})$.

It has been shown for lam-flow that the relationship between $1/t_m$ and v starts to deviate from the solid lines in Fig. 6.4 when $T_2 < \text{ca. } 0.5 T_1$ [3]. For the con-flow curves we found identical results (not shown). Although the relaxation times decrease upon a decrease of the vessel radius it has been shown that the ratio T_1/T_2 for the flowing water is not likely to become larger than 2 [3].

All effects discussed above only influence K_v , the calibration constant relating \bar{v} to $1/t_m$. They have no effect on K_Q , which relates Q to \dot{S}_0 . Both \dot{S}_0 and $1/t_m$, however, are affected whenever the nuclei of the flowing fluid have not experienced the static magnetic field B_0 long enough to have attained Boltzmann equilibrium before entering the rf coil. This effect, referred to as the 'non-equilibrium effect', affects $S(t)$ and $dS(t)/dt$ in the following way [3]:

$$S(t) = S_0(t)(1 - \exp(-d/vT_1)) \quad (6.18a)$$

$$dS(t)/dt = (dS_0(t)/dt)(1 - \exp(-d/vT_1)) \quad (6.18b)$$

in which $S_0(t)$ =signal intensity when Boltzmann equilibrium has been attained; d =distance between the center and the rim of the magnet poles. For simplicity, it is assumed, that the static field vanishes outside the region between the magnet poles. It can be seen from eqs. (6.18a) and (6.18b) that the signal amplitude and \dot{S}_0 are mostly affected by large values of v and T_1 . This means that:

- a) The flow profile of each individual xylem vessel as observed with NMR ($P(v)$ NMR) will be different from the actual lam-flow profile as is shown in Fig. 6.6, in which $d=8$ cm, approximately the experi-

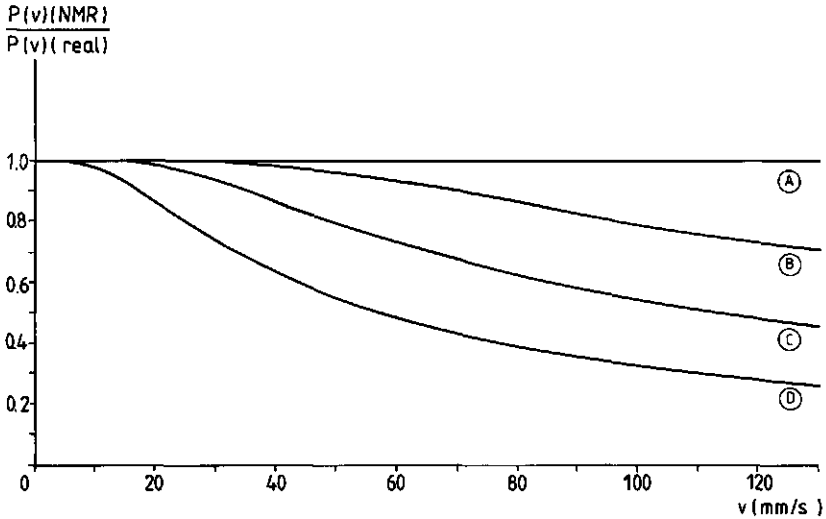


Figure 6.6

Relationship between v and the ratio $P(v)(\text{nmr})/P(v)(\text{real})$
 $(=1-\exp(-d/vT_1))$ for $d=8$ cm and 4 values of T_1 (s):
 a) 0.0; b) 0.5; c) 1.0; d) 2.0.

mental value; this, of course, will affect the total flow velocity profile of the collection of vessels.

- b) Since v (and probably) T_1 increase upon an increase of the xylem vessel diameter this effect will be most pronounced in large xylem vessels.

This can also be seen in Fig. 6.4 in which the nonequilibrium effect has been included for two values of d/T_1 (80 and 40 mm/s) for the con-flow curves. Since the maximum value of $T_1 \sim 2$ s, the nonequilibrium effect can be neglected for values of $\bar{v} < 15 - 20$ mm/s. For larger values of \bar{v} the effect will become increasingly important resulting in an increase of K_v .

The nonequilibrium effect on \dot{S}_0 is shown in Fig. 6.7. Similar to what has been found for \bar{v} , the calculated value of Q , using the calibration constant (K_Q) obtained from an experiment in which Boltzmann equilibrium was attained, is lower than the actual value. Since the effect is more pronounced on \dot{S}_0 (from which Q is calculated) than on

$1/t_m$ (from which \bar{v} is calculated) the effective cross-sectional area $A(=Q/\bar{v})$ available for flow, calculated from the NMR experiment, is also affected. The calculated value of A is expected to be smaller than its actual value. Since the ratio of calculated and actual values of A decreases upon an increase of v , A should preferably be calculated from curves obtained for low values of v (<ca. 15 mm/s.)

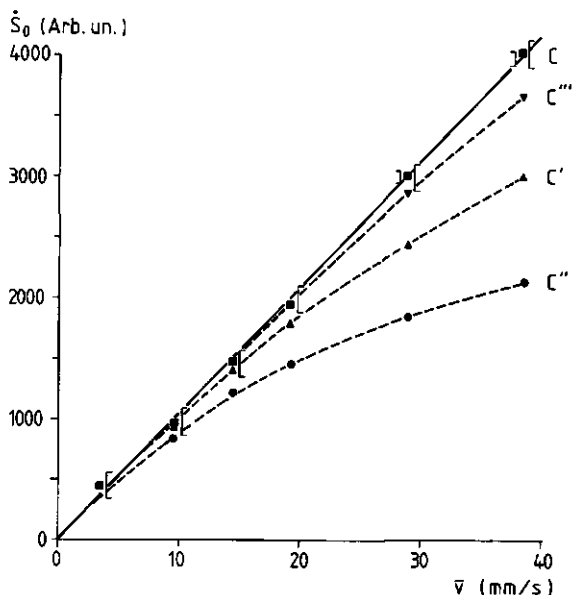


Figure 6.7

Relationship between \dot{S}_0 and \bar{v} for various experimental conditions for a con-flow profile; $T_1=1.0$ s. The data apply for $T_1 \ll 2 T_2$.

a) non-equilibrium effect:

- : $d/T_1 = \infty$ (curve C);
- ▼ : $d/T_1 = 160$ mm/s (curve C''');
- ▲ : $d/T_1 = 80$ mm/s (curve C');
- : $d/T_1 = 40$ mm/s (curve C'').

c)] : margins for the shift of \dot{S}_0 due to the off-resonance effect on the flow curves for off-resonance frequencies between -200 Hz and $+200$ Hz.

d) [: margins for the shift of \dot{S}_0 due to the off-resonance signal from a 25 fold excess of stationary water at off-resonance frequencies between -200 Hz and $+200$ Hz.

For clarity the symbols] and [are drawn to the left and right of the data points.

6.2.3 Local field inhomogeneity, off-resonance effects and stationary water signals

Local field inhomogeneities, field gradients [Chapter 5] and off-resonance effects affect the observed flow curves in two ways:

- 1) by affecting the NMR flow signal itself and
 - 2) by creating an additional signal originating from stationary water.
- These effects will be separately discussed in the following paragraphs.

6.2.3.1 Effect of local field gradients on NMR flow signal

It has been shown [1,2] that both $1/t_m$ and \dot{S}_0 of the NMR flow signal depend on the value of the product $G \tau$. Due to the inhomogeneous structure of the plant, local field gradients exist [Chapter 5]. Whenever these gradients have components in the direction of flow, they affect the NMR flow signal.

The length of the NMR free induction decay (FID) gives an impression about the r.m.s. value of these local field gradients. Typically, the $t_{\frac{1}{2}}$ value (i.e. the time at which the FID has reached half its initial height) of the FID in our set-up is ca. 4 ms for cucumber plants. For the rf coil used in the experiments the value of a linear field gradient in the direction of flow (G) can be calculated from $t_{\frac{1}{2}}$ as follows [1]:

$$G = 6.67 / t_{\frac{1}{2}} \quad (6.19)$$

in which G is in units G/m and $t_{\frac{1}{2}}$ in ms. For $t_{\frac{1}{2}} = 4$ ms this leads to $G = 2$ G/m. However, locally, the field gradient may very well exceed this value. To minimize the local field effect the value of G should be chosen as high as feasible. Large values of G , however, lead to a decrease in signal amplitude. This can be overcome by reducing the pulse spacing τ , and in practice, the upper limit for G is determined by the minimum value that can be chosen for τ (corresponding to the maximum attainable duty cycle) without causing damage to the rf coil or the plant. The higher the duty cycle, the higher the heat production. This can lead to

burning of the rf coil or the plant.

An additional effect of short values of τ may be an increase of the observed T_2 of the flowing water. The NMR flow experiment highly resembles a CPMG pulse sequence, used for T_2 measurements, without applying the first 90° pulse. Therefore it can be expected that the NMR flow curves contain the same values of T_2 as measured using the CPMG pulse sequence. For the CPMG sequence it is known that the measured transverse relaxation time increases with τ if magnetic field gradients are present [Chapter 2], or magnetization exchange exists between different sites [11,12], both of which are present in the plant tissue. Thus we conclude that it is advantageous to choose high values of G and low values of τ for a given value of Gr .

6.2.3.2 Effect of off-resonance on NMR flow curves

Off-resonance effects on the flow curves can most clearly be seen from a shift of the signal amplitude at $t=0$ ($S(0)$) with respect to the on-resonance situation. The effect can be approximated by adding a term ($S_{\text{off}}(t)$) to the flow signal obtained under on-resonance conditions, given by:

$$S_{\text{off}}(t) \approx K_0 + K_1 \cdot \exp(-t/T_e) \quad (6.20)$$

K_0 , K_1 and T_e depend on the flow velocity and the sign and magnitude of the off-resonance frequency-shift. K_0 only affects the base line or "zero level" of the flow curve and does not affect $1/t_m$ and \dot{S}_0 . The second term of eq. (6.20), however, affects both $1/t_m$ and \dot{S}_0 . Computer simulations show that a decrease of v results in a decrease of K_0 and K_1 and an increase in T_e . T_e can be approximated by:

$$1/T_e \approx 1/T_2 + v/L \quad (6.21)$$

representing the effect of a flow of magnetization out of the rf coil (with length L) on T_2 of the flowing water [13]. Computer simulations have shown that for $\bar{v} = 38.4$ mm/s $T_e \approx 0.2$ s, and for $\bar{v} = 7.2$ mm/s $T_e \approx$

0.55 s. This means that the off-resonance effect on $1/t_m$ and \dot{S}_0 decreases upon a decrease of v as predicted by eq. (6.21). This can also be seen in Fig. 6.4, in which the calculated off-resonance effect has been indicated for 4 values of \bar{v} and for off-resonance frequency-shifts of -200 Hz and +200 Hz (for the rationale behind this see next paragraph) and for $T_2=0.5$ s and $T_1=1$ s. The errors in $1/t_m$ resulting from these off-resonance effects are typically in the range 5-10%. Errors in \dot{S}_0 are smaller and again increase with increasing flow rate. They are maximally in the order of a few percent (for $\bar{v} > 30\text{mm/s}$) as can be seen in Fig. 6.7. The error in A as a result of the off-resonance effect is therefore in the order of 5-10%. The shift in $S(0)$ ($= K_0+K_1$) with respect to the on-resonance situation was found to be in the order of 10% of $S(t_m)$ for off-resonance frequencies of + 200 Hz and -200 Hz.

6.2.3.3 Contributions of stationary water to the flow signal

In Chapter 2 and [1, 2] it was stated that in an NMR flow experiment stationary water does not give rise to a signal. The reason for this is that the magnetization of the stationary spins in one half of the rf coil yielding a positive NMR signal is exactly counterbalanced by a negative signal arising from the spins in the other half of the coil. (see Fig. 2.4.) Whenever this balance is perturbed, a net signal due to stationary water will occur as is usually found for plants [17]. The abovementioned balance can be perturbed by:

- 1) an excess of spins (water) in either half of the coil, resulting in unequal lengths of \vec{M}_a and \vec{M}_b and thus M_{ay} and M_{by} in Fig. 2.4;
- 2) differences in Larmor frequency at positions symmetrically located around the center of the rf coil. Different Larmor frequencies may result from:

2a) local field inhomogeneities

2b) off-resonance value of B_0 .

In this case \vec{M}_a and \vec{M}_b have rotated through different angles during a time period t , which also results in unequal lengths of \vec{M}_{ay} and \vec{M}_{by} (Fig. 2.4).

These perturbing effects cause additional exponential terms ($S_{\text{stat}}(t)$)

in the signal observed from flow experiments:

$$S_{\text{stat}}(t) = B \sum_{i=1}^3 [K_2(i) + K_3(i) \exp(-t/T_2)] \quad (6.22)$$

in which $K_2(i)$ and $K_3(i)$ depend on the value and type ($i=1$: excess of spins, $i=2$: local field inhomogeneities, $i=3$: off-resonance) of the perturbation; B =(number of stationary spins)/(number of flowing spins) and T_2 = spin-spin relaxation time of the stationary water. In eq. (6.22) it is assumed that B and T_2 are equal for the different types of perturbations. Only the exponential term in eq. (6.22) affects \dot{S}_0 and $1/t_m$. By choosing the frequency at which the flow measurements are carried out in such a way that $(B \sum K_3(i) = 0)$, the error in \dot{S}_0 and $1/t_m$ due to stationary water is minimized. Thus perturbations due to local field inhomogeneities and excess of spins in either coil half can effectively be reduced by adjusting the measuring frequency. The off-resonance effect on the flow curves, introduced in this way, can be reduced by taking the exponent of eq. (6.20) into account. Since T_e is of the same order of magnitude as T_2 this means that at the optimal measuring frequency:

$$B \cdot \sum_i K_3(i) + K_1 = 0 \quad (6.23)$$

If $T_2 = T_e$ this results in a straight horizontal baseline. This situation is usually not found because T_e depends on v , $S_{\text{off}}(t)$ is only approximately described by eq. (6.20) and transverse relaxation in a plant cannot be described with a single T_2 : [Chapters 2 and 4]. Another problem arises from the fact that the stationary water balance in both coil halves changes in the course of the experiments due to physiological processes, thus requiring a resetting of the measuring frequency to reduce the error signal. Experiments on plants have shown that under experimental conditions frequency shifts necessary to (re-)establish condition (6.23) are typically within ± 200 Hz, i.e. the errors in \dot{S}_0 and $1/t_m$ due to an unbalance in stationary water typically equal those caused by stationary water at + 200 Hz or -200 Hz off-resonance. The errors indicated in Figs. 6.4 and 6.7 due to this effect on $1/t_m$ and \dot{S}_0 have been calculated, using the previously mentioned computer program

and taking $v=0$, $B=25$, $T_1=1$ s, $T_2=0.5$ s, off-resonance frequency shifts: +200 Hz and -200 Hz, and the same (arbitrary) units as in Fig. 6.5. It was found that $K_2(3)=8.4$ and $K_3(3)=2.3$. Due to the large value of B in cucumber plants it can be seen by comparing with Fig. 6.5, that the variation in $S(0)$ (given by eq. (6.23)), due to stationary water, is of the same order of magnitude as $S(t_m)$. The effect on $1/t_m$ (Fig. 6.4) is comparable to the off-resonance effect in the flow signal itself. The relative effect on \bar{S}_0 (Fig. 6.7) and thus on Q becomes increasingly important at a decrease of the flow rate, because the error is a constant value ($\sum K_3(i) \cdot B/T_2$), independent of the flow rate. In practice this turns out to be the largest error source in determining Q for low flow rates.

In practice, the baseline is adjusted at the beginning of an experiment by comparing flow curves while scanning through a frequency range. This leads to variations in the signal amplitude $S(t)$. Due to the presence of the exponents in eqs. (6.20) and (6.22) the variation of the amplitude at $t=0$ ($S(0)$) is larger than at $t>0$, e.g. at the end level of the $S(t)$ curve. Eventually, the measuring frequency is chosen in such a way that a change in frequency results in an equal change of amplitude of $S(0)$ and end level, implying that eq. (6.23) applies. (Note, that $S(0)$ need not be adjusted to the zero level, in order to do reliable flow measurements). Typically, this frequency was found to be within ± 200 Hz from the resonance frequency.

6.2.4 The accuracy of NMR flow measurements, a summary

In this paragraph the total error involved in NMR measurement of linear and volumetric flow is estimated by combining the effects discussed in the previous paragraphs.

6.2.4.1 Relationship \bar{v} vs. $1/t_m$; the calibration constant K_v

The main error in \bar{v} is arising from K_v in the expression $\bar{v} = K_v/t_m$. The value of \bar{v} for a plant can be calculated with an accuracy of $\pm 20\%$ from $\bar{v} = K_v/t_m$, using a calibration system with a lam-flow profile as

long as $5 \leq \bar{v} \leq 20$ mm/s, for the plant, under the following conditions: $T_1/T_2 \approx 0.5-1$; $B=25$; $d=8$ cm (for definitions of B and d , see §6.2.3.3 and §6.2.2, respectively).

In an actual experiment, K_V is first determined by calibration using a capillary with a lam-flow profile. For a plant with a con-flow profile $K_V(\text{con}) = 0.77 K_V(\text{lam})$. For a real plant the value of K_V is expected to be between $K_V(\text{lam})$ and $K_V(\text{con})$.

For $\bar{v} \geq 20$ mm/s, K_V increases. The upper limit of \bar{v} (20 mm/s) decreases on increasing T_1 and decreasing d . K_V increases upon an increase of the relative abundance of high velocities (large vessels). An increase in the value of B leads to a decrease of the upper limit (20 mm/s) of \bar{v} and to an increase of its lower limit (5 mm/s). This lower limit can be reduced by resetting the (off-resonance) measuring frequency so that condition (6.23) is fulfilled.

6.2.4.2 Relationship Q vs. \dot{S}_0 ; the calibration constant K_Q

Q can be calculated for a con-flow profile from $Q = K_Q \dot{S}_0$ with an accuracy of $\pm 20\%$ under the same conditions as quoted for \bar{v} , and $T_1 = \text{ca. } 1\text{ s}$.

For $\bar{v} > \text{ca. } 20$ mm/s, K_Q increases. For $\bar{v} < \text{ca. } 5$ mm/s the error in Q increases. The lower limit of \bar{v} can be reduced by resetting the (off-resonance) measuring frequency so that condition (6.23) is fulfilled. The upper limit (20 mm/s) decreases upon increasing T_1 , upon decreasing d , upon increasing the relative abundance of large vessels and upon increasing B . An increase of B also results in an increase of the lower detection limit for \bar{v} (5 mm/s).

6.2.5 Calibration procedures

The experimentally obtained calibration curves \bar{v} vs. $1/t_m$ and Q vs. \dot{S}_0 , obtained for a lam-flow profile in a glass capillary in the absence of stationary water, are shown in Figs. 6.8 and 6.9 respectively. The experimental conditions were: $G = 98$ G/m, $\tau = 180$ μs , $T_2 \approx 0.5$ s, $T_1 \approx 1$ s, pulse angle = 0.24π rad. A Helmholtz type rf coil was used with a

length and diameter of 12 mm. The deviation from the linear relationship of \dot{S}_0 vs. Q in Fig. 6.9 is entirely due to the nonequilibrium effect. The linear relationship between \bar{v} and $1/t_m$ is not affected until $\bar{v} > \text{ca. } 40 \text{ mm/s}$. It should be emphasized that deviation from a linear relationship between \bar{v} and $1/t_m$ for flow curves obtained from plants starts at a lower flow rate, since for a con-flow profile larger vessels are required to obtain a particular value of \bar{v} than for lam-flow profiles. This can also be seen in Fig. 6.4. From Fig. 6.8 the following relationship can be obtained:

$$\bar{v}(\text{lam}) = 3.45/t_m \quad (6.24)$$

For the con-flow profile this results in:

$$\bar{v}(\text{con}) = 2.76/t_m \quad (6.25)$$

with the restrictions:

$$5 \text{ mm/s} \leq \bar{v} \leq 20 \text{ mm/s}.$$

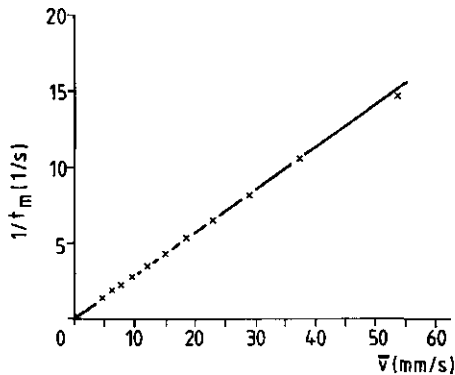


Figure 6.8

Experimentally obtained relationship between $1/t_m$ and \bar{v} for a laminar flow profile. Experimental conditions:

$G = 98 \text{ G/m}$; $T_1 \approx 1.0 \text{ s}$; $T_2 \approx 0.5 \text{ s}$; pulse angle = $0.24\pi \text{ rad.}$; $\tau = 180 \mu\text{s}$; no stationary water; Helmholtz type rf coil with length and diameter of 12 mm.

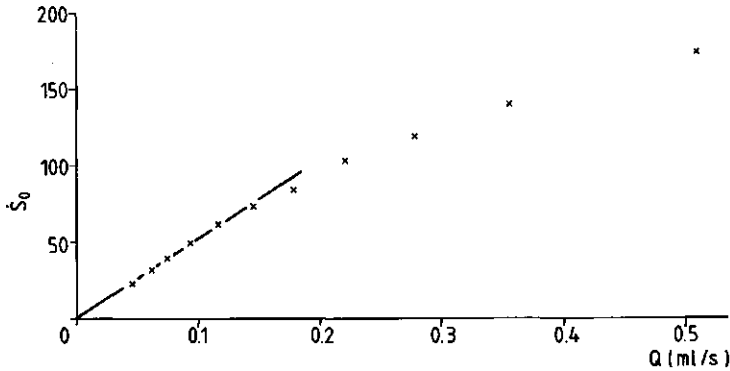


Figure 6.9

Experimentally obtained relationship between \dot{S}_0 and Q for a laminar flow profile. Experimental conditions are the same as in Fig. 6.8. Data are calculated from the same flow curves as those used in Fig. 6.8.

Using eq. (6.25) this corresponds to:

$$1.85 \text{ s}^{-1} \leq 1/t_m \leq 7.2 \text{ s}^{-1}.$$

In eqs. (6.24) and (6.25) t_m is expressed in seconds and \bar{v} is in mm/s.

From Fig. 6.9 the following relationship can be obtained:

$$Q = 2.10^{-3} \dot{S}_0 \quad (6.26)$$

in which Q is in ml/s and \dot{S}_0 is expressed in the same units as used in the plant experiments described in Chapter 7.

6.2.6 Discussion of the accuracy and limitations of NMR flow measurements

The reproducibility of the NMR flow curves is very high, as deduced from repeated measurements on a capillary system. \dot{S}_0 and $1/t_m$ are obtained using a computer algorithm described in Chapter 7. This algorithm (a third order polynome) closely approximates the shape of the

flow curves, but the calculated values of $1/t_m$ and \dot{S}_0 may deviate slightly from the actual ones. The resulting errors depend on the shape of the flow curve and the signal to noise ratio (S/N). The errors were estimated to be a few percent for $1/t_m$ and about 10% for \dot{S}_0 , by visual inspection. For values of $t_m > \text{ca. } 1.2\text{-}1.5$ s accurate calculations of t_m are often impossible, and in these cases $1/t_m$ is set to be zero.

Hitherto we have only discussed the accuracy with which \bar{v} and Q can be obtained from a plant. In many cases the absolute value of the flow rate is of minor importance and changes in \bar{v} and Q , resulting from changes in environmental conditions, contain the desired information [Chapter 7]. Therefore the accuracy to which a change in the observed values of $1/t_m$ and \dot{S}_0 in an experiment with a particular plant predicts a change in \bar{v} and Q is of importance. Since $P(v)$ and the relaxation times of flowing water within a plant are constant during the experiment, they will not affect $1/t_m$ or \dot{S}_0 for one and the same plant in a particular experiment, as is done in Chapter 7. The contribution of stationary water to the flow signal may change during an experiment due to growth and/or redistribution of water between different stem parts, and may therefore cause changes in $1/t_m$ and \dot{S}_0 , even if \bar{v} and Q remain unchanged. These effects, however, are only noticeable in the flow curves at a time scale of several tens of minutes, rather than over a period of tens of seconds needed for an NMR flow experiment. Taking into account that S/N of flow curves obtained from plants is usually less than that of the calibration curves, we remain on the safe side by concluding that if changes in \dot{S}_0 larger than 10-20% and changes in $1/t_m$ larger than 5-10% are observed, these are due to changes in flow rate. These percentages should be increased when flow curves are compared which are measured at longer time intervals (e.g. several hours). For a demonstration, see Fig. 4 of § 7.4.

6.3 Measurements of water content and water potential

Water content and water potential can be determined by NMR by measuring the transverse relaxation rate $R_2(e)$ or $R_2(av)$ or the amplitude at $t=0$ (A_0). The accuracy with which the water content or potential

(differences) can be obtained from these parameters will be discussed below.

6.3.1 Transverse relaxation time

It was shown in Chapter 2 that transverse relaxation in plants (and in general: in biological systems) is influenced by various parameters which are strongly dependent on the tissue type and age of the plant. Even within one (geno)type of tissue appreciable differences occur. These differences are related to the size and structure of the plant tissue, and all factors affecting these parameters (such as growing conditions of the plants) therefore affect the measured value of the transverse relaxation rate.

For cucumber plants, grown under summer conditions (high light intensity during long day periods, temperature > ca. 25-30°C), $T_2(e)$ values were found of ca. 800 ms, whereas cucumber plants of approximately the same size (ca. 2.5 m length), but generally older, grown during autumn (less light, shorter day periods, air temperature ca. 20°C) yielded relaxation times of ca. 400 ms. Average values of $T_2(e)$ for gherkin and pumpkin plants, grown under "autumn" conditions, again with a length of ca. 2.5 m, were 300 ms and 600 ms respectively. Additionally, within each of the individual groups of (approximately equally old) plants, deviations from the above mentioned (average) values were found of $\pm 25\%$. Typical variations in transverse relaxation time, due to short term variations of external conditions, (light, relative humidity, etc.; see Chapter 7) are about 5%, and wilting of a plant already occurred when T_2 had decreased with about 10%, which is less than the variation within one genotype of plants, grown under (as far as possible) identical conditions. Therefore it is not possible to calculate the numerical value of the water content or potential from T_2 measurements alone without additional information on the plant. The relaxation rates can only be used in a comparative way, by monitoring a decrease or increase of the water content/potential. Thus, as was done for flow measurements, the accuracy with which a change in the observed relaxation time in an experiment with a particular plant can predict a change in its water

content/potential is discussed below.

The magnetization decay curve is obtained using a modified (PAPS) CPMG-method [13-16, Chapter 2]. Relaxation times i.e. inverse relaxation rates obtained with this method are known to be dependent on

- 1) setting of the phase of the 90° and 180° pulses,
- 2) the length of the "180°" pulses [14, 15],
- 3) the presence of local field gradients in combination with the pulse spacing τ [18, Chapter 2],
- 4) exchange between different sites, again in combination with τ [12,13], or
- 5) a change of cell dimensions or geometry during the experiment [Chapter 4].

Field gradient effects on T_2 [Chapter 2] are minimized by choosing a low value of τ (520 μ s).

Due to the inhomogeneous nature of the plant tissue there are local differences in the high frequency magnetic susceptibility within the plant, affecting the pulse width and -angle. In addition, local differences in the static magnetic susceptibility result in field gradients within the sample. The presence of a distribution and/or change of the magnetic susceptibility within the sample affects the measured relaxation time. Changes of the susceptibility may be caused by:

- a) a change of position of the plant within the rf coil,
- b) expansion or shrinking of the plant, or
- c) a redistribution of water between spatially separated sites within the rf coil.

The effect of (a) can be overcome by ensuring a fixed position of the plant in the probe; (b) may result from growth or a change of the water content, or both. Although (c) results from local differences in water potential (due to e.g physiological changes) inside the rf coil giving rise to different values of T_2 , the water content and average water potential within the rf coil volume may remain unchanged.

Additionally, the exchange rate for water between different compartments (and thus the relaxation rate) is influenced by the temperature (see also Chapter 7). By passing an airstream with a constant temperature through the rf coil along the plant stem during the plant

experiments, this effect is minimized.

Finally, measuring off-resonance also turns out to have some effect on the relaxation time. T_2 curves, recorded at +200 Hz and -200 Hz off-resonance at extreme positions in the rf coil (close to either half of the Helmholtz pair), thus simulating susceptibility changes, yielded fluctuations in $R_2(e)$ and $R_2(av)$ of typically 3%. These conditions, however, are extreme and it is very likely that redistribution of water (c) is the most important parameter causing relaxation rate changes during longer periods of time without changing the average waterpotential. This redistribution of water also affects exchange rates between different sites and cell geometry (resulting in a change of relaxation rate) again without affecting the total water content inside the rf coil.

Changes in water content cause variations in $R_2(e)$ and $R_2(av)$ in the order of percents (see § 6.3.3.). This is comparable to variations in the relaxation rates due to the error sources mentioned above. Therefore rather large changes in environmental conditions are required to cause changes in the relaxation rates that can reliably be attributed to changes in P_w or Ψ .

6.3.2 Initial height (A_0)

The initial height of the relaxation curve is determined by the length of the "90°" pulse, i.e. the transverse magnetization immediately following the first pulse or the height of the FID at $t=0$. Therefore, all factors influencing the pulse length, as described in the previous paragraph, affect A_0 . Again, only changes in A_0 , measured in one and the same plant are relevant. From the experiment described in § 6.3.1 it was also possible to conclude that off-resonance and a varying position of the stem in the rf coil lead to errors in A_0 of about 5%. This, however, represents an extreme situation and in general the error is estimated to be a few percent. As in flow measurements, the error in A_0 increases when decay curves are compared which are measured a longer time apart. In practice, the first data point in T_2 measurements is not obtained at $t = 0$ and A_0 has to be obtained by extrapolation of the transverse

relaxation curve to $t=0$. Thus water with short relaxation times is not seen. For the experiments described in Chapter 7 the first data point is at 6.5 ms. This means that protons with relaxation times shorter than a few milliseconds are not reflected in A_0 . These short relaxation times are only observed for bound water, which plays no role in the variation of P_w or Ψ [Chapter 2]. Therefore this effect can be neglected for the high water contents considered. A_0 is also affected by growth. This, however, can only be observed in A_0 over periods of days and can be neglected in most of the experiments of Chapter 7.

Summarizing, we conclude that, like for $R_2(e)$ and $R_2(av)$ the errors in changes in A_0 are in the order of a few percent, again leading to the conclusion that rather large environmental changes are required to induce relevant variations in A_0 .

6.3.3 Experimental calibration curves and conclusions.

In Fig. 2 of § 7.2 and Fig. 2 of § 7.4 three calibration curves are shown relating A_0 to P_w , $R_2(av)$ to $1/P_w$ and $R_2(e)$ to $1/P_w$. The relaxation data were obtained during a dehydration experiment. This may cause physiological conditions in the plant stem that differ from the ones that occur during any of the other experiments, in which e.g. relative humidity or light intensity were changed, thus leading to different relaxation times. It will be obvious from the above that these curves do not represent universal relationships between the relaxation parameters and P_w . The exact position and slope of the calibration curves are strongly dependent on the type and age of the plant and the experimental conditions. They only show that a change in water content, and thus water potential, within a physiological relevant region results in an observable change in A_0 and relaxation time of the same sign.

As an approximate guideline for quantitative evaluation of the data the following can be used.

A wilting point for cucumber was suggested of about -11 bar [19,20]. From Fig. 2.7 it can be seen that this is equal to a relative water content of about 89%, i.e. a decrease of ca. 11% with respect to a situation of 100% relative water content. From experiments with cucum-

bers we learn that a decrease in A_0 and an increase in $R_2(av)$ and $R_2(e)$ of about 10% resulted in wilting of the plant. Therefore it can be concluded, that a change in A_0 , $R_2(av)$ and $R_2(e)$ of 1% is approximately equal to a change in the relative water content of about 1% and to a change in water potential of about 1 bar. The accuracy of calculated changes in the relative water content and water potential is therefore estimated to a few percent and a few bar respectively.

6.4 References

- [1] M.A. Hemminga and P.A. de Jager, 1980. *J. Magn. Res.* 37, 1-16.
- [2] H. Van As and T.J. Schaafsma, 1987. *J. Magn. Res.*, 74. in press.
- [3] H. Van As, 1982. Thesis. Agric. Univ., Wageningen.
- [4] F.W. Sears and M.W. Zemansky. 1972. "University Physics". 4th edition. Chapter 14. Addison-Wesley Publishing Company, Reading, Mass.
- [5] B. Slavik, 1974. "Methods of studying plant water relations". Chapter 4. Springer-Verlag, Berlin.
- [6] P.S. Nobel, 1974. "Introduction to biophysical plant physiology". Chapter 8. W.H. Freeman and Company, San Francisco.
- [7] A.A. Jeje and M.H. Zimmermann, 1979. *J. Exp. Bot.* 30, 817-827.
- [8] H.W. Calkin, A.C. Gibson and P.C. Nobel, 1984. *Can. J. Bot.* 63, 632-637.
- [9] J.A. Petty, 1978. *J. Exp. Bot.*, 29, 1463-1469.
- [10] M.H. Zimmermann and C.L. Brown, 1971. "Trees, structure and function". p. 200. Springer-Verlag, Berlin.
- [11] P.S. Belton and R.G. Rattcliffe, 1985. *Progr. in NMR Spect.*, 17, 241-279.
- [12] A. Allerhand and H.S. Gutowsky, 1965. *J. of Chem. Phys.*, 42, 1587-1599.
- [13] M.A. Hemminga, P.A. de Jager and A. Sonneveld. 1977. *J. Magn. Res.*, 27, 359-370.
- [14] D.G. Hughes and G. Lindblom, 1974. *J. Magn. Res.*, 13, 142-147.
- [15] R.L. Vold, R.R. Vold and H.E. Simon, 1971. *J. Magn. Res.*, 11, 283-298.
- [16] T.C. Farrar and E.D. Becker, 1971. "Pulse and Fourier Transform NMR. Introduction to Theory and Methods". Academic Press, New York.
- [17] H. Van As and T.J. Schaafsma, 1984. *Bioph. J.*, 45, 469-472.
- [18] K. Fukuda and A. Hirai, 1979. *J. Phys. Soc. Japan*, 47, 1999-2006.
- [19] H. Van As, T.J. Schaafsma and J. Blaakmeer, 1986. *Bruker Report*, 1, 33-36.
- [20] H. Van As, T.J. Schaafsma and J. Blaakmeer, 1986. *Acta Horticulturae*, 174, 491-495.

CHAPTER VII

=====

7 Experiments on intact plants7.1 Introduction

The measurement of the influence of a number of environmental parameters on the plant water status by NMR, are reported in this Chapter. Its main purpose is to establish the scope and degree of reliability of the NMR-method by comparing the results with those obtained by another, known method and to verify whether the NMR results are reasonable from a plant physiological point of view. The NMR results are compared with those obtained with a dendrometer (LVDT). A model for the plant water status is presented as well (§7.2). The parameters that have been considered are:

- relative humidity (rh) (§7.2);
- day-night cycle (§7.2, §7.4);
- root temperature (§7.3);
- changes of root area in contact with root medium (§7.3);
- effect of transport of the plant (§7.4);
- effect of CO₂ concentration on root and shoot (§7.4);
- influence of infestation of the plant with white flies (§7.4).

7.2 WATER BALANCE IN CUCUMUS PLANTS, MEASURED BY NUCLEAR MAGNETIC RESONANCE, I

J.E.A. REINDERS, H. VAN AS, T.J. SCHAAFSMA, P.A. de JAGER

Dept. of Molecular Physics, Agricultural University,
De Dreijen 11, 6703 BC Wageningen, The Netherlands.

Abstract

This paper describes a highly automated experimental set-up to measure non-invasively, non-destructively, and unattended volumetric and linear rates of water flow in plant xylem as well as tissue water content by proton nuclear magnetic resonance (NMR). Using this set-up the effects of changes in a few environmental conditions on these parameters have been investigated for cucumus plants. The results of the measurements are explained by use of a simple model, based on water potential, flow rate and (stomatal) resistance. The presented NMR method allows discrimination between root- and shoot responses.

Introduction

Nuclear Magnetic Resonance (NMR) can be used to measure, noninvasively and in the presence of an excess of stationary water, water flow through capillaries (Hemminga, de Jager and Sonneveld, 1977; Hemminga and de Jager, 1980) and plant xylem (Van As, 1982; Van As and Schaafsma, 1984; Van As and Schaafsma, 1985). In addition, NMR has been used to obtain information on water content and water potential, using transverse relaxation time (T_2) measurements (Van As, Schaafsma and Blaakmeer, 1986a,b). Both types of measurement detect the protons of the water molecules themselves and take place on a time scale of a few seconds. The method does not affect the flow in any way and is able to monitor fast changes (ca. 5 sec.) in flow rate or water content or both. The potential of the method has been demonstrated previously (Van As, 1982; Van As et al., 1986a,b). Recently, a high degree of automation has

been applied, allowing unattended data acquisition for several days (de Jager, Reinders and Van As, 1986) and fast computer data analysis. By use of a custom-made climate chamber a number of important environmental conditions can be controlled and programmed. This paper reports the measurement of the effect of variations in some external conditions on changes in tissue water content (or water potential) and linear as well as volumetric flow rate, measured virtually simultaneously.

Theory

FLOW MEASUREMENTS

The NMR flow experiment (for detailed description see: Hemminga and de Jager, 1980; Van As and Schaafsma, 1987) gives rise to signals $S(t)$ as shown in Fig. 1. From these signals both the (mean) linear flow velocity (v , in $m \cdot s^{-1}$) and the volume flow rate (Q , in $m^3 \cdot s^{-1}$) can be determined. For the linear flow rate the following equation holds:

$$v = K_v / t_m \quad (1)$$

where t_m is the time at which the signal reaches its maximum amplitude. K_v is a calibration constant which depends on the following parameters: the magnetic field gradient (G), the time interval (τ) between two radio frequency (rf) pulses, rf coil geometry, flow profile (laminar, plug, turbulent) and, to a less degree, the relaxation times T_1 and T_2 (Hemminga and De Jager, 1980; Van As, 1982). For volumetric flow the following equation holds:

$$Q = K_Q [dS(t)/dt]_{t=0} = K_Q \dot{S}_0 \quad (2)$$

K_Q is a calibration constant depending on G , τ and rf coil geometry. The sign of $dS(t)/dt$ is determined by the flow direction and the sign of G (Van As and Schaafsma, 1984). Q and v are related by:

$$Q = v A \quad (3)$$

where A is the effective cross-sectional area available for flow. The amplitude of a signal representing a certain flow velocity is determined by both A and the relaxation times T_1 and T_2 of the flowing fluid i.e. a shorter relaxation time results in a smaller signal amplitude. It has been shown (Reinders, Schaafsma and Van As, 1987) that T_2 decreases upon a decrease of the xylem vessel diameter. It is predicted that for xylem vessel diameters $< \text{ca. } 50 \mu\text{m}$ no flow signals can be observed.

WATER CONTENT/WATER POTENTIAL MEASUREMENTS

Measurement of the transverse relaxation of the magnetization (Farrar and Becker, 1971) of water protons in plant tissue was carried out

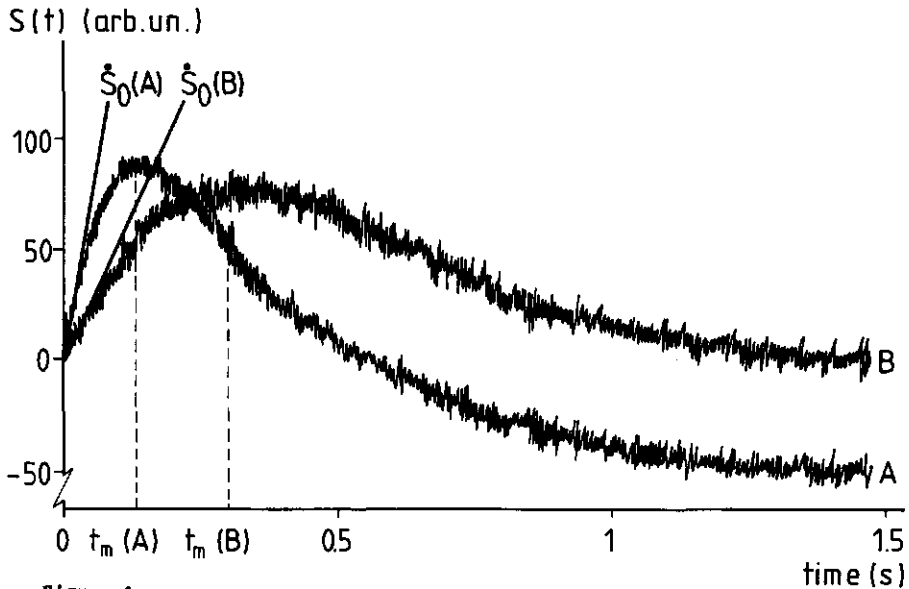


Figure 1

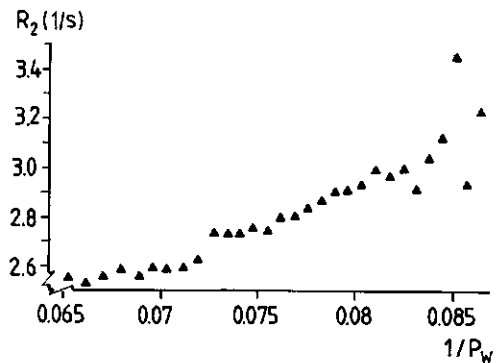
Two typical signal response curves $S(t)$ from one and the same plant, as obtained in a flow experiment. Curve A represents a higher flow velocity than curve B. $\dot{S}_0(A)$ and $\dot{S}_0(B)$ indicate the initial slopes of the curves A and B respectively. The time at which the curves A and B reach their maximum amplitude is indicated by $t_m(A)$ and $t_m(B)$ respectively. Each recorded datum is a signal integrated over 8 successive pulses.

to obtain information about the water content of the plants. For various biological tissues it has been reported that a reduction of the water content results in a shorter transverse relaxation time of the magnetization, conventionally denoted by T_2 (Belton and Packer, 1974; Van As, van Vliet and Schaafsma, 1980; Fullerton, Potter and Dornbluth, 1982; Seiler, Trahms and Wollensack, 1983; Ghambir, Panda and Puri, 1983; Ghambir and Agarwala, 1985). As often occurs in complex biological systems (see e.g. Belton and Rattcliffe, 1985), we observed multi-exponential decay in cucumber and gherkin stems. Van As, et al. (1986a,b) found the decay curve to be composed of three exponents and they obtained an empirical relationship between the inverse of the water content ($1/P_w = \text{dry weight}/(\text{fresh weight}-\text{dry weight})$) and the average transverse relaxation rate:

$$R_2 = \sum_{i=1}^3 A_i / T_{2i} \quad (4)$$

in which A_i = amplitude of component i of the three components solution divided by the total amplitude and T_{2i} = decay time of component i . The exact relationship between R_2 and $1/P_w$ depends on the type and age of the plant, but invariably it was found that a reduction of the water content of a stem segment resulted in an increase in R_2 . The relationship between R_2 and $1/P_w$ for a cucumber stem segment was linear when

Figure 2
Relationship between R_2 and $1/P_w$ obtained for a cucumber stem segment during dehydration in the rf coil.



P_w was within a physiological range (i.e. a relative water content in the range 100% - ~ 75%). A typical result is shown in Fig. 2. Because the slope and intercepts depend on the type and age of the plant only qualitatively, but nevertheless striking conclusions can be drawn from the T_2 experiments presented in this paper. Since a change of P_w results from a change in water potential (Ψ) of the same sign (Slatyer, 1967; Milburn, 1979) R_2 is also related to Ψ (Van As et al., 1986a,b). A decrease (i.e. a more negative value) in Ψ is associated with an increase in R_2 .

Materials and methods

PLANTS: MATERIAL AND CLIMATOLOGICAL CONDITIONS

The plants used in the experiments were greenhouse hydro cultures of cucumber and gherkin plants (Cucumis sativus L.), grown at the Institute of Horticultural Plant Breeding in Wageningen during August and September 1986. The root medium was a Steiner solution (Steiner, 1961) adapted for tap water and was kept at 20°C. Electric conductivity and pH were 1.8 - 2.5 mS and 5.5 - 6.8 respectively. Light/dark periods and light intensity were determined by natural illumination. Air temperature was 18°C at night and 20 - 25°C (depending on irradiance level) during the day. Relative humidity was 50-70 %.

For the NMR measurements a six week old plant was transferred to the NMR spectrometer described below. A part of the experimental set-up is shown in Fig. 3. The first 0.5 m of the plant above the root were positioned between the poles of the magnet and surrounded by the rf coil of the NMR spectrometer. The remaining top part of the plant, including all leaves, was mounted inside a controlled climate chamber, and its roots were placed in a Steiner solution. Then the plant was allowed to acclimatize at least overnight. During all experiments the plants were exposed to a 12 h light period (07.00 to 19.00 h) and a 12 h dark period. Root medium and air were maintained at 20°C.

The climate control chamber is a modified version of the type GPGK (Grenco Testtechniek, Den Bosch, The Netherlands). The inside dimensions

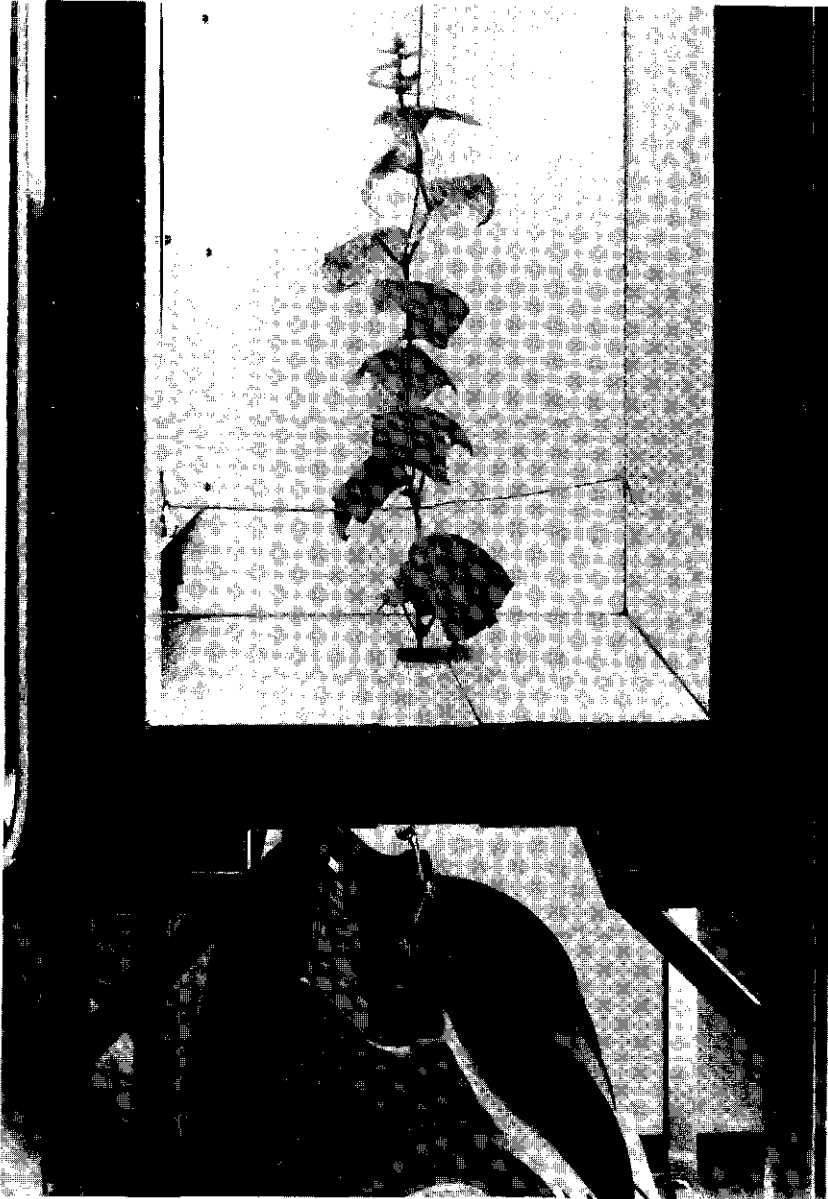


Figure 3

Part of the experimental set up showing plant, climate chamber and magnet.

of this chamber are: 0.5 m wide, 0.5 m deep and 1.3 m high. The floor of this chamber contains a wedge that extends from the middle of the chamber front to the center of the floor. This wedge can be removed and replaced to allow insertion of the top of a plant into the chamber, while the lower part of the plant remains outside for the NMR measurements. With the wedge in place there is a hole in the center of the floor large enough to accommodate the plant stem. The controlled climate chamber is mounted on a mobile frame so that it can be positioned above the magnet. The chamber is of stainless steel to prevent distortion of the magnetic field, and contains circuitry to suppress rf interference. For illumination we used 16 quartz halogen dichroic mirror lamps (type 13117, Philips). Light input was continuously variable from 0 - 50 klux (= power per area of 0 - 215 $\text{W}\cdot\text{m}^{-2}$ = photon irradiance (PI) of 0 - 1050 $\mu\text{mol}\cdot\text{s}^{-1}\cdot\text{m}^{-2}$), measured at the bottom of an empty chamber. A 20 mm deep, circulating layer of water below the lights is used to reduce thermal radiation at the plant level. This layer absorbs about one fourth of the total radiant energy. Temperature and relative humidity (rh) were continuously variable from 5 - 40 °C and 40 - 95% (at 20 °C), respectively.

NMR: EQUIPMENT AND EXPERIMENTAL CONDITIONS

For NMR flow and T_2 measurements we made use of a pulse NMR spectrometer, consisting of a Newport 7" electromagnet (0.47 T), modified Bruker Minispec electronics operating at 20 MHz, a Bruker Aspect 2000 computer and a Z17C pulse programmer. A home built, hinged, Helmholtz type rf coil with a length and diameter of 12 mm, allowing measurements on intact plants, was used. The magnetic field gradient coils were mounted on the housing of the rf coil in order to obtain a reproducible, linear field gradient (G). Signals from the rf receiver were fed into a home-built integrator, which integrates the signals between rf pulses and resulting data were stored on disk (Control Data Corporation). A lock system compensates for long-term magnetic field drift thus making possible automatic measurements alternately of flow and of water content or potential (T_2). For the measurement of a flow curve we applied a

linear magnetic field gradient of $9.8 \pm 0.7 \text{ mT}\cdot\text{m}^{-1}$ and a series of 8192 equidistant pulses at intervals of $180 \mu\text{s}$, which gives rise to a time dependent NMR signal $S(t)$ (Fig. 1). Immediately after a flow measurement the linear field gradient was turned off automatically and a T_2 -curve was measured using a modified CPMG method (Farrar and Becker, 1971; Hughes and Lindblom, 1974, Hemminga *et al.*, 1977), with a total of 8192 180° pulses at intervals of $520 \mu\text{s}$. Eight successive echoes were integrated, resulting in a time of 4.16 ms between data points. The values of R_2 , used to obtain the relationship $R_2 \sim 1/P_w$, were calculated from NMR relaxation curves obtained at regular time intervals for a stem segment while it was dehydrated in the rf coil. Immediately after this, values of P_w were obtained by periodically weighing a stem segment from a region adjacent to the first, which also dehydrated in the rf coil. Combination of both experiments thus yielded R_2 as a function of $1/P_w$.

For analysis of the measured curves the data were transferred to a DEC MICROVAX computer. The first part of the flow curves, extending from 0 to about 1.3 times t_m (see eq. (1)) was fitted to a third order polynomial function (Savitzky and Golay, 1964) from which the initial slope and the value of t_m were derived. Multi exponential analysis of the T_2 curves was carried out using a computer program performing a non-linear least-square fit on the data (Provencher and Vogel, 1983).

Calibration constants K_v and K_q of eqs. (1) and (2) for the experiments described here are: $K_v = 2.8 \text{ mm}$ and $K_q = 2.0 \mu\text{l}\cdot\text{s}^{-1}\cdot\text{Au}^{-1}$, in which Au = arbitrary units as used in Figs. 4B and 5B. The reproducibility of $1/t_m$ is estimated to $\pm 10\%$. When translating this into a value of v , using eq. (1), or when comparing it to values obtained from other plants, the inaccuracy is somewhat higher. This is mainly due to the uncertainty about the plant flow profile (Van As, *et al.*, 1984) and the very large excess of stationary water, which, in combination with the inhomogeneous nature of the plant tissue, causes some signal distortion. The latter also applies to values of \dot{S}_0 where reproducibility is estimated to $\pm 20\%$. The inaccuracy in the values of R_2 is of the order of a few percent.

Results and discussion

Fig. 4 shows the effects of a day/night cycle and rh on v ($1/t_m$), Q (\dot{S}_0) and water content or potential (R_2). For comparison, Fig. 5 presents the behaviour of these parameters during one day when rh was unchanged. Day/night rhythm was maintained, however. Parallel effects of light/dark and rh on v and Q (Figs. 4A,B and 5A,B) are found, as predicted by eq. (3), provided A does not show large variations.

It is possible to explain the observed effects using the following model:

The rate of transpiration (E , in $\text{kg}\cdot\text{s}^{-1}$) from a leaf is proportional to the difference (ΔV , in $\text{kg}\cdot\text{m}^{-3}$) between the water vapour concentration of air in leaf air spaces and that of the bulk air (Milburn, 1979; Hall, A.E., 1982):

$$E = A_1 \Delta V/R \quad (5)$$

in which A_1 = total leaf area (m^2) and R = total resistance to water transport per unit leaf area ($\text{s}\cdot\text{m}^{-1}$). R is the series resistance of the boundary layer resistance (r_b , in $\text{s}\cdot\text{m}^{-1}$) and the leaf resistance. The latter can be thought of as a parallel circuit containing the resistances of the stomata (r_s) and the cuticle (r_c). By varying the stomatal aperture, r_s and thus R can be regulated by the plant. This leads to:

$$R = \frac{r_c r_s}{r_c + r_s} + r_b \quad (6)$$

It has been suggested that r_s depends on the water potential of the leaf (Ψ in bar) (Slatyer, 1967; Milburn, 1979; Raschke, 1975; Schulze and Hall, 1982). The exact relationship between r_s and Ψ varies between different types of plants, and for the same plants grown under different conditions (Schulze, et al., 1982). However, as a general rule a decrease in leaf water potential results in stomatal closure, sometimes after a threshold level has been passed (Schulze, et al., 1982). As a first approximation we assume a linear relationship between stomatal conductance ($g_s=1/r_s$) and Ψ :

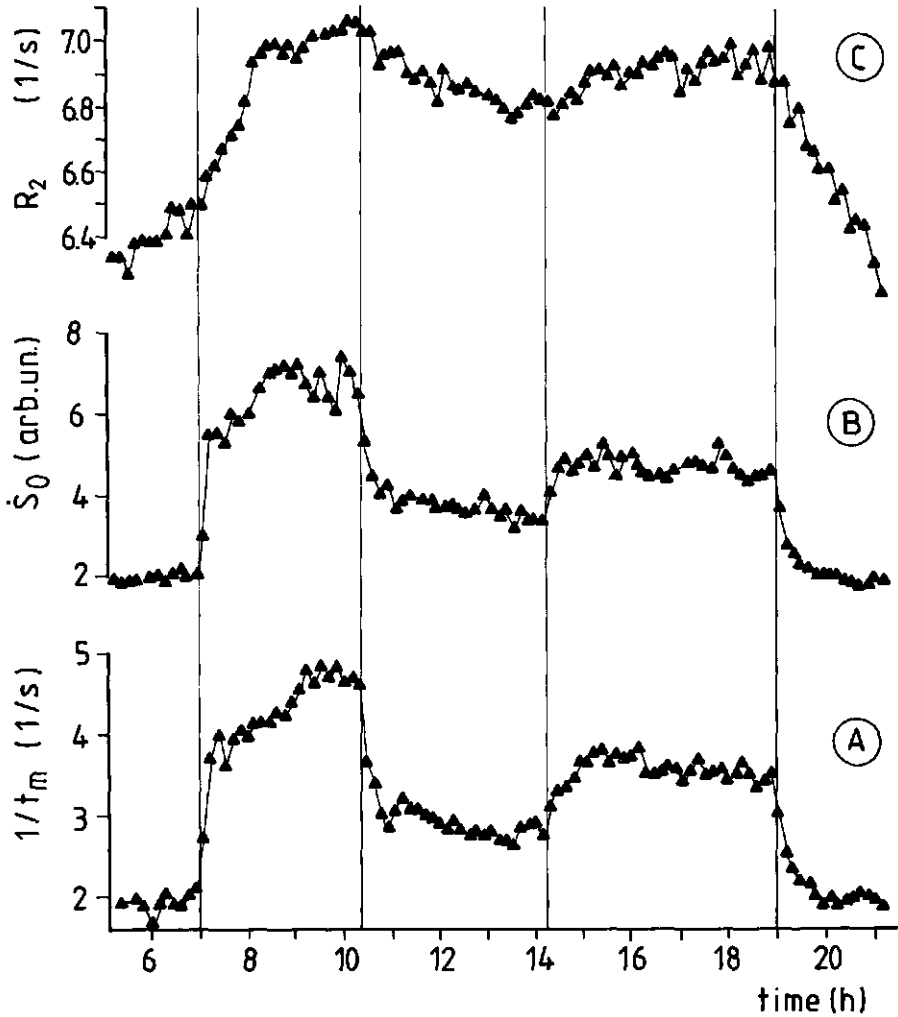


Figure 4

Effect of day/night and variation of relative humidity (rh) on linear water flow rate (Fig. 4A), volumetric flow rate (Fig. 4B) and water content/potential (Fig. 4C) of a gherkin plant. Conditions: radiant input: $95 \text{ W}\cdot\text{m}^{-2}$ (07.00 h - 19.00 h), $0 \text{ W}\cdot\text{m}^{-2}$ (before 07.00 h and after 19.00 h); air temperature: $20^\circ\text{C} \pm 1.5^\circ\text{C}$; root temperature: $20^\circ\text{C} \pm 0.5^\circ\text{C}$; rh: 60% (before 10.20 h and after 14.10 h), 95% (10.20 h - 14.10 h). Errors in rh were $\pm 10\%$.

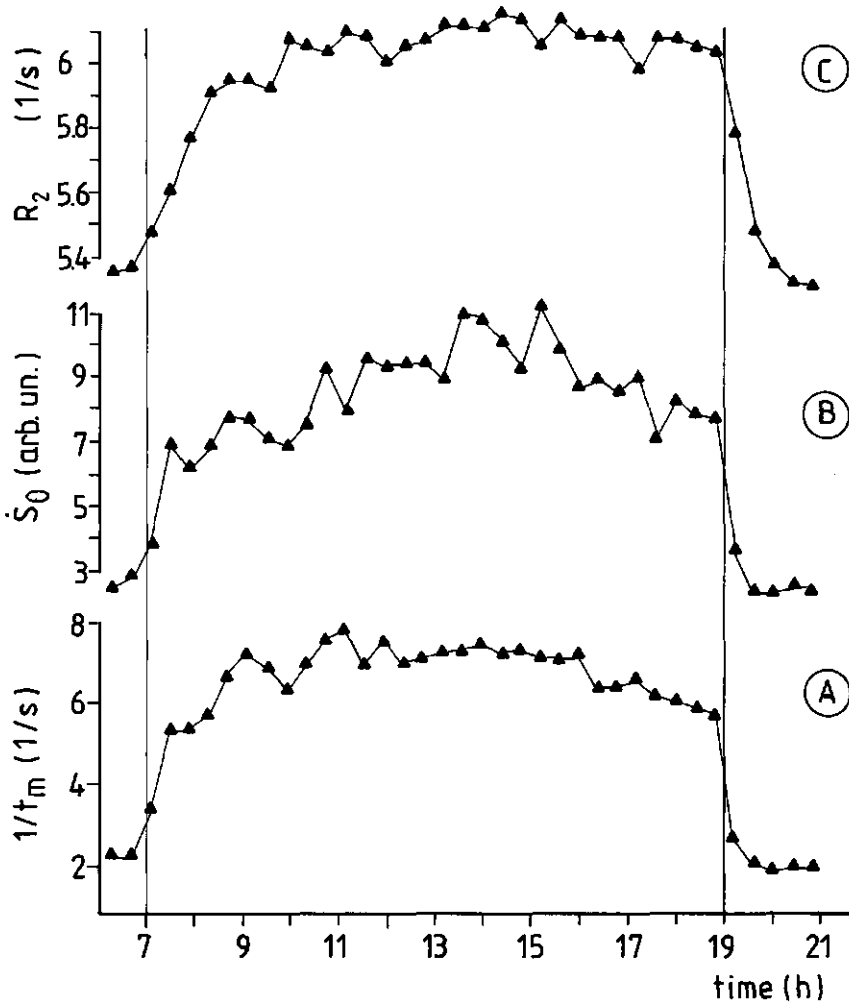


Figure 5

Effect of day/night on linear water flow rate (Fig. 5A), volumetric flow rate (Fig. 5B) and water content or potential (Fig. 5C) for the same plant as in Fig. 4. Conditions are identical with Fig. 4 except rh, which was $60\% \pm 10\%$ during the whole experiment. The scaling factor of Fig. 5B is identical to that of 4B.

$$g_s = L_s (\Psi - \Psi_c) \quad (7)$$

in which Ψ_c = water potential at which the stomata are closed and L_s ($m \cdot s^{-1} \cdot bar^{-1}$) = stomatal permeability coefficient. L_s is a function of light intensity, temperature, rh, CO_2 concentration and 'hormones'. Combination of eqs. (5) - (7) yields:

$$E = \frac{A_1 \Delta V}{r_c / [L_s r_c (\Psi - \Psi_c) + 1] + r_b} \quad (8)$$

The difference between the water potential of the external medium (Ψ_s) (e.g. of soil) and that of the plant is the driving force for water flow across the root (Slatyer, 1967), often supported by root pressure (P_r). Since of the hydraulic resistances within the plant the root is regarded as having the largest resistance (Weatherley, 1982), we assume the plant hydraulic resistance above the root to be zero, and thus no water potential gradient along the plant above the root. For water uptake (U , in $kg \cdot s^{-1}$) this leads to:

$$U = A_r L_r (\Psi_s + P_r - \Psi) \rho \quad (9)$$

in which L_r ($m \cdot s^{-1} \cdot bar^{-1}$) = water permeability coefficient of the root; A_r (m^2) = area of the membrane through which the water flows (related to the root area); ρ ($kg \cdot m^{-3}$) = density of liquid water. Values of L_r are typically around $10^{-8} m \cdot s^{-1} \cdot bar^{-1}$ (Slatyer, 1967). In Fig. 6 the relationships (8) and (9) are shown for a number of different values for r_c , L_s , ΔV and r_b . For Figs. 6A-D the following has been assumed: $A_1 = 1 m^2$, $\Psi_c = -10$ bar, $\Psi_s = -1$ bar, $P_r = 0.5$ bar and $A_r L_r = 7 \cdot 10^{-12} m^3 \cdot s^{-1} \cdot bar^{-1}$. The values for r_c , ΔV and r_b are chosen within physiologically feasible ranges, whereas the maximum value for L_s is chosen also in such a way that the maximum conductivity (at $\Psi = 0$ bar) falls within physiological ranges (Schulze *et al.*, 1982; Slatyer, 1967). It can be seen from these figs. that

(1) transpiration is very sensitive to r_b (Fig. 6A), L_s (Fig. 6B) and

ΔV (Fig. 6D);

- (2) unless $L_s = 0$, an increase in water potential leads to an increase in rate of transpiration and
- (3) for the same increase in Ψ the increase in E becomes smaller when Ψ becomes larger.

If $r_b \ll r_c [L_s r_c (\Psi - \Psi_c) + 1]$, however, a linear relationship between E and Ψ results:

$$E = A_1 \Delta V L_s (\Psi - \Psi_c) + A_1 \Delta V / r_c \quad (10)$$

For equilibrium:

$$E = U = Q_e \rho \quad (11)$$

with Q_e ($m^3 \cdot s^{-1}$) = equilibrium value of the flow rate Q . This also results in an equilibrium value for the water potential Ψ_e as is shown in Fig. 6D. Since air inside the sub-stomatal cavity can be considered as saturated with water vapour a linear relationship exists between ΔV and rh .

The results shown in Fig. 4 can now be explained using this model (eqs. (8) and (9), see also Fig. 7). During the dark period it is assumed that the stomata are closed ($L_s=0$). Eq. (8) then reduces to:

$$E = A_1 \Delta V / (r_c + r_b) \quad (12)$$

for this experiment: $A_1 = 0.918 \text{ m}^2$ (= 2x the projected area), $Q_e \cdot \rho = 4 \cdot 10^{-6} \text{ kg} \cdot \text{s}^{-1}$ and $\Delta V = 6.92 \text{ kg} \cdot \text{m}^{-3}$ ($rh = 60\%$ at 20°C ; leaves saturated with water vapour). Assuming the leaves to be at air temperature this leads to $r_b + r_c = 1600 \text{ s} \cdot \text{m}^{-1}$. Taking $r_b = 100 \text{ s} \cdot \text{m}^{-1}$ (a reasonable value for the rather large cucumber leaves and low wind speeds in the climate chamber; Nobel, 1974) this leads to $r_c = 1500 \text{ s} \cdot \text{m}^{-1}$, in fair agreement with literature values. (Schönherr, 1982, Slatyer, 1967). Transpiration during the dark period is represented by curve D in Fig. 7. From the intersection of curve U and transpiration curve D, Ψ can be obtained: $\Psi(1)$. Except for D, the curves in Fig. 7 can only yield qualitative

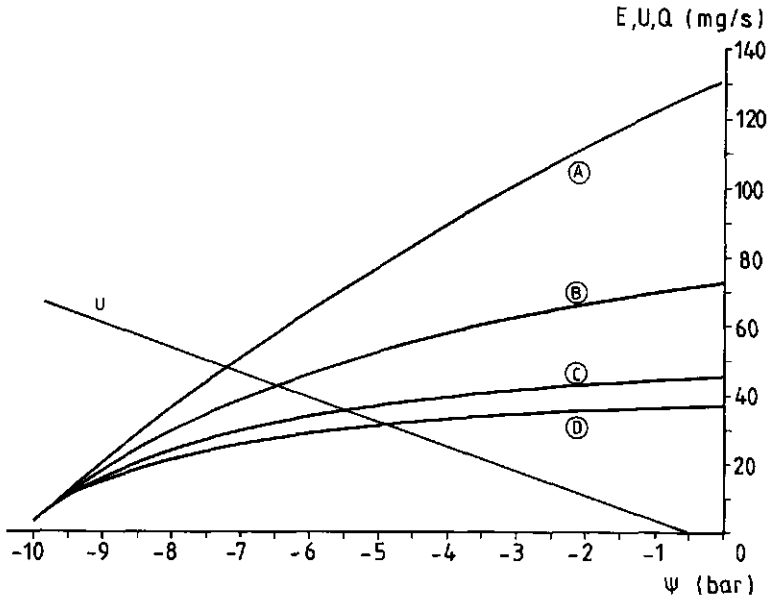


Fig. 6A

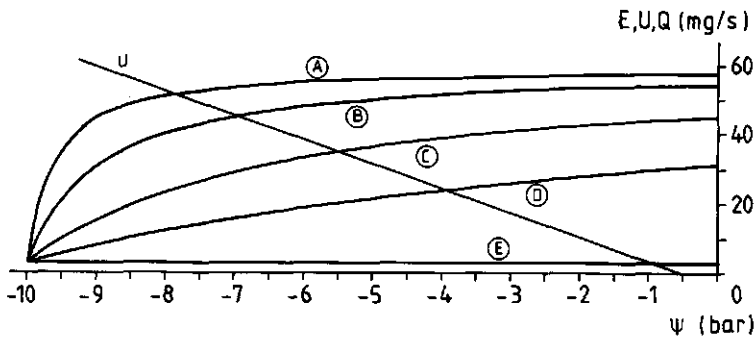


Fig. 6B

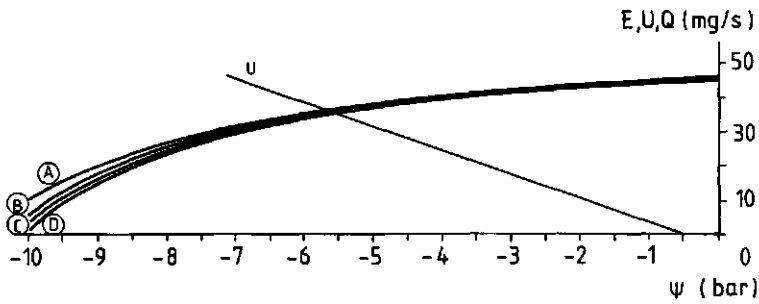


Fig. 6C

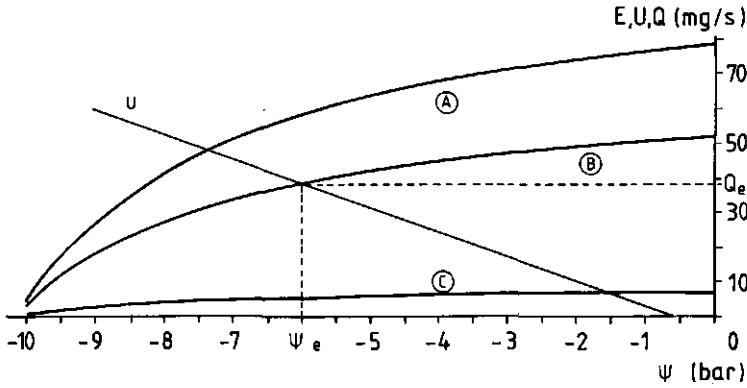


Fig. 6D

Figure 6

Effect of r_b (Fig. 6A), L_s (Fig. 6B), r_c (Fig. 6C) and ΔV (Fig. 6D) on transpiration according to eq. (8). A curve representing water uptake (U) according to eq. (9) is also drawn.

For all transpiration curves it has been assumed: $A_1 = 1 \text{ m}^2$ and $\Psi_c = -10 \text{ bar}$ and the leaf is saturated with water.

For U the following has been assumed: $\Psi_s = -1 \text{ bar}$, $P_r = 0.5 \text{ bar}$ and $A_r L_r = 7 \cdot 10^{-12} \text{ m}^3 \cdot \text{s}^{-1} \cdot \text{bar}^{-1}$.

Fig. 6A, effect of r_b :

$L_s = 0.003 \text{ m} \cdot \text{s}^{-1} \cdot \text{bar}^{-1}$, $r_c = 2000 \text{ s} \cdot \text{m}^{-1}$; $\Delta V = 6 \text{ gr} \cdot \text{m}^{-3}$; curves A, B, C and D: $r_b = 13, 50, 100, \text{ and } 130 \text{ s} \cdot \text{m}^{-1}$, respectively.

Fig. 6B, effect of L_s :

$r_b = 100 \text{ s} \cdot \text{m}^{-1}$; $r_c = 2000 \text{ s} \cdot \text{m}^{-1}$; $\Delta V = 6 \text{ gr} \cdot \text{m}^{-3}$; curves A, B, C, D and E: $L_s = 0.03, 0.01, 0.003, 0.001, \text{ and } 0 \text{ m} \cdot \text{s}^{-1} \cdot \text{bar}^{-1}$, respectively.

Fig. 6C, effect of r_c :

$L_s = 0.003 \text{ m} \cdot \text{s}^{-1} \cdot \text{bar}^{-1}$; $r_b = 100 \text{ s} \cdot \text{m}^{-1}$; $\Delta V = 6 \text{ gr} \cdot \text{m}^{-3}$; curves A, B, C and D: $r_c = 500, 1000, 2000 \text{ and } 5000 \text{ s} \cdot \text{m}^{-1}$, respectively.

Fig. 6D, effect of ΔV :

$L_s = 0.003 \text{ m} \cdot \text{s}^{-1} \cdot \text{bar}^{-1}$; $r_c = 2000 \text{ s} \cdot \text{m}^{-1}$; $r_b = 100 \text{ s} \cdot \text{m}^{-1}$; curves A, B and C: $\Delta V = 10.4$ (40% r.h. at 20°C), 6.9 (60% r.h. at 20°C) and 0.9 (95% r.h. at 20°C) $\text{gr} \cdot \text{m}^{-3}$, respectively.

Ψ_e and Q_e are the equilibrium values of Ψ and Q , respectively, resulting from U and transpiration curve B.

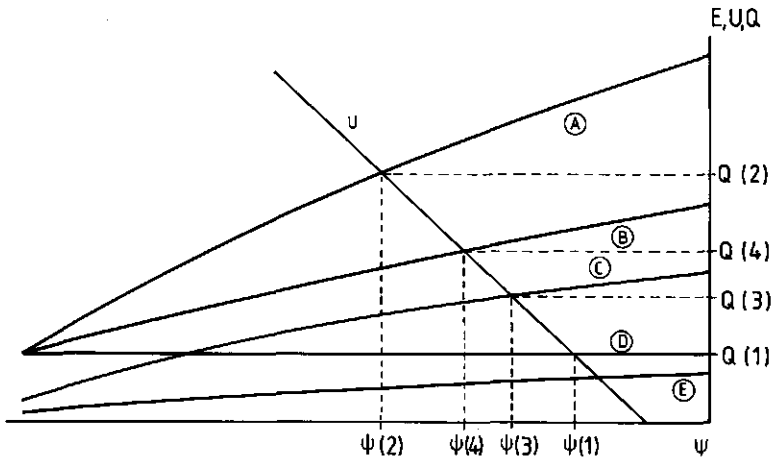


Figure 7

Qualitative representation of the experiments of Fig. 4 using eqs. (8) and (9). See text for explanation.

conclusions since the values of r_b , r_c , L_s and Ψ_c have been chosen rather arbitrarily, albeit within the above mentioned boundaries.

At 07.00 h the lights were turned on and the stomata opened. This is represented by curve A of Fig. 7, which shows that Ψ decreases $\Psi(1) \rightarrow \Psi(2)$ and Q increases $Q(1) \rightarrow Q(2)$ at the onset of illumination (leaf temperature is assumed to be unchanged). The predicted changes in Ψ and Q are in agreement with the results of Figs. 4 and 5.

At 10.20 h rh is increased to 95%, leading to an expected transpiration curve E in Fig. 7. With respect to curve A only ΔV has been changed from a value corresponding to $rh = 60\%$ to $rh = 95\%$ at constant air temperature. For curve E it has been assumed that L_s and leaf temperature remain unchanged. This is unlikely, because (Schulze *et al.*, 1982):

- (1) a dependence of stomatal aperture on humidity has been reported in literature, which means that also L_s may have increased at increasing rh (see eq. (7));
- (2) leaf energy balance will be changed; the increase in rh lowers transpiration, resulting in an increase of leaf temperature and thus of ΔV .

Both effect (1) and (2) cause transpiration to be higher than anticipated. That either one or both of these effects are present is confirmed by the observation that only minor changes in Q and Ψ were found in the range ca. 40% < r.h. < ca. 90%, whereas a large dependence of E was expected (see Fig. 6D) (not shown). It was not until rh became larger than ca. 90% that a significant change of Q and Ψ was observed. Both effect (1) and (2) have been incorporated in curve C of Fig. 7 (i.e. for both L_g and ΔV higher values have been used in curve C than in curve B), resulting in equilibrium values $\Psi(3)$ and $Q(3)$.

At 14.10 h rh is reduced to 60% again, leading to an increase of Q and a decrease of Ψ , as expected, but original levels of Q and Ψ are not reached. This is also illustrated by the behaviour of Q and Ψ in curves A and B of Fig. 7. For curve B in Fig. 7 it has been assumed that the original leaf temperature which existed before the period of 95% rh in Fig. 4 is restored. The only difference with curve A in Fig. 7 is a lower value of L_g .

At 19.00 h the dark period starts again. All changes in Ψ and flow rate due to variation of rh in Fig. 4 well exceed those during a day time period in which rh is not changed (Fig. 5).

In the experiments described in this paper only parameters directly affecting transpiration (eq. (8)) are considered. These parameters affect flow rate and water potential (or content) in opposite ways: when the flow velocity increases as a result of a change in L_g , r_b or ΔV , the water potential or content decreases and vice versa. In contrast, if uptake (eq. (9)) is considered, it can be predicted from Fig. 6 that the primary reaction of a plant to changes in L_r will be either a decrease or an increase in both water flow and water potential. Therefore the NMR method - being able to measure flowrate and changes in water potential in one and the same experiment - may serve as a tool to discriminate between factors affecting water balance in the root and the shoot. Effects of changes in L_r (e.g. induced by changes in root temperature) on Ψ and Q as well as on v are reported in a subsequent paper.

Acknowledgements

We are indebted to Mr. S. Zijlstra of the Institute of Plant Breeding for his kind gift of plant material, to Mr. P. Van de Sanden of the Centre for Agro-Biological Research for making available CO₂-measuring equipment, to Dr. J. Goudriaan of the Department of Theoretical Production Ecology for helpful discussions and private communication of material prior to publication, and to Professor D.W. Sheriff (CSIRO, Mount Gambier, Australia) for useful discussions.

Literature cited

- Belton, P.S. and Packer, K.J. 1974. Pulsed NMR studies of water in striated muscle III. The effects of water content. *Biochimica et Biophysica Acta*, 354, 305-314.
- Belton P.S. and Rattcliffe, R.G., 1985. NMR and compartmentation in biological tissues, in "Progress in NMR spectroscopy", Pergamon Press Ltd., Vol. 17, pp. 241-279.
- Farrar, T.C. and Becker, E.D., 1971. "Pulse and Fourier transform NMR". Academic Press Inc., New York.
- Fullerton, G.D., Potter, J.L. and Dornbluth, N.C., 1982. NMR relaxation of protons in tissues and other macromolecular water solutions. *Magnetic Resonance Imaging*, 1, 209-228.
- Gambhir, P.N., Agarwala, A.K., 1985. Simultaneous determination of moisture and oil content in oil seeds by pulsed Nuclear Magnetic Resonance. *Journal of the American Oil Chemists Society*, 62, 103-108.
- Gambhir, P.N., Panda, B.C. and Puri, R.K., 1983. Proton spin relaxation study of moisture and oil in seeds. *Indian Journal of experimental Botany*, 21, 460-461.
- Hall, A.E., 1982. "Physiological Plant Ecology II. Encyclopedia of Plant Physiology", Vol. 12B. Chapter 8. Lange, O.L., Nobel, P.S., Osmond, C.B., Ziegler, H., eds. Springer Verlag, Berlin.
- Hemminga, M.A., de Jager, P.A. and Sonneveld A., 1977. The study of flow by pulsed nuclear magnetic resonance. I. Measurement of flow rates in the presence of a stationary phase using a difference method. *Journal of Magnetic Resonance*, 27, 359-370.
- Hemminga, M.A. and de Jager, P.A., 1980. The study of flow by pulsed nuclear magnetic resonance. II. Measurement of flow velocities using a repetitive pulse method. *Journal of Magnetic Resonance*, 37, 1-16.
- Hughes, D.G. and Lindblom, G., 1974. Baseline drift in the Carr-Purcell-Meiboom-Gill pulsed NMR experiment. *Journal of Magnetic Resonance*, 13, 142-147.
- Jager, P.A. de, Reinders, J.E.A., Van As, H., 1986. Pulsed NMR system for automatic in vivo flow measurements. Proceedings of the 8th European Experimental NMR conference, 1986, Spa, Belgium, 53-54.

- Milburn, J.A., 1979. "Water flow in plants". Longman Group, London.
- Nobel, P.S., 1974. "Biophysical Plant Physiology". Chapter 7. Freeman and Company, San Francisco.
- Provencher, S.W. and Vogel, R.H., 1983. Regulation technique for inverse problems in molecular biology, in "Progress in Scientific Computing", Vol. 3, 304-319. Birkhauser, Boston.
- Raschke, K., 1975. Stomatal action. Annual Review of Plant Physiology, 26, 309-340.
- Reinders, J.E.A., Schaafsma, T.J. and Van As, H., 1987. Proton spin relaxation and diffusion of water in transport vessels of plants. Manuscript in preparation.
- Savitzky, A. and Golay, J.E., 1964. Smoothing and differentiation of data by simplified least squares procedures. Analytical Chemistry, 36, 1627-1639.
- Seiler, T., Trahms, L. and Wollensack, J., 1982. The distinction of corned water in free and bound fractions. Graefe's Archive for Clinical and Experimental Ophthalmology, 219, 287-289.
- Schönherr, J., 1982. "Physiological Plant Ecology II. Encyclopedia of Plant Physiology", Vol 12B, p. 159. Lange et al. eds. Springer Verlag, Berlin.
- Schulze, E.-D. and Hall, A.E., 1982. "Physiological Plant Ecology II. Encyclopedia of Plant Physiology", Vol 12B, Chapter 7. Lange et al. eds. Springer Verlag, Berlin.
- Slatyer, R.O., 1967. "Plant-Water relationships". Academic Press, London.
- Steiner, A.A., 1961. A universal method for preparing nutrient solutions of a certain desired composition. Plant and Soil, 15, 134-154.
- Van As, H., Van Vliet, P.A. and Schaafsma, T.J., 1980. ^1H -spin echo Nuclear Magnetic Resonance in plant tissue I. The effect of Mn(II) and water content in wheat leaves. Biophysical Journal, 32, 1043-1050.
- Van As, H., 1982. NMR, water and plants. Ph.D. thesis, Agricultural University, Wageningen.
- Van As, H. and Schaafsma, T.J., 1984. Noninvasive measurement of plant water flow by Nuclear Magnetic Resonance. Biophysical Journal, 45, 469-472.
- Van As, H. and Schaafsma, T.J., 1985. Flow in Nuclear Magnetic Resonance Imaging. "An Introduction to Biomedical Nuclear Magnetic Resonance". pp. 68-96. George Thieme Verlag, Stuttgart.
- Van As, H., Schaafsma, T.J. and Blaakmeer, J., 1986a. NMR of water flow and content in plants. Bruker Report, 1, 33-36.
- Van As, H., Schaafsma, T.J. and Blaakmeer, J., 1986b. Applications of NMR to water flow and -balance in plants. Acta Horticulturae, 174, 491-495.
- Van As, H. and Schaafsma, T.J., 1987. Measurement of flow by the NMR repetitive pulse method. Journal of Magnetic Resonance, 74, in press.
- Weatherley, P.E., 1982. "Physiological Plant Ecology II. Encyclopedia of Plant Physiology", Vol 12B. Chapter 3. Lange et al. eds. Springer Verlag, Berlin.

7.3 WATER BALANCE IN CUCUMUS PLANTS, MEASURED BY NUCLEAR MAGNETIC
RESONANCE, II

J.E.A. REINDERS, H. Van As, T.J. SCHAAFSMA

Dept. of Molecular Physics, Agricultural University,
De Dreijen 11, 6703 BC Wageningen, The Netherlands.

Abstract

Nuclear magnetic resonance (NMR) was used to investigate the effects of changes in root temperature, of changes in the area of root in contact with culture solution and of day/night rhythm on the water balance of a cucumber and a gherkin plant. Results are explained, in terms of water potential, flowrate and resistance using a previously presented model for the water balance. Results obtained by the NMR method are compared to those determined using a dendrometer. The results demonstrate that the NMR method can serve as a technique for discriminating between changes in water uptake by the roots and changes in transpiration.

Introduction

In a previous paper (I) (Reinders, Van As, Schaafsma, de Jager, 1987), a model for the water balance in plants has been introduced. The validity of this model could be verified by using pulsed proton NMR as a monitor for the effects of light and relative humidity (rh) on the linear and volume flow (Hemminga and de Jager, 1980; Van As and Schaafsma, 1987) as well as on the water potential or content (Van As Schaafsma and Blaakmeer, 1986a,b). The model predicts that effects of changes in shoot and root environment can be discriminated using the NMR method. In the present paper we report experiments carried out to test this prediction by changing the root environment only. In addition, we compare several experimental NMR parameters related to water potential,

and data from an apparatus that registers the thickness of the stem with an accuracy better than $1\mu\text{m}$: a linear variable differential transformer (LVDT) used as a dendrometer (Gensler, 1986). Since these NMR-parameters and the diameter of the stem are both affected by its water potential, we expected a correlation between the results obtained by both methods.

Theory

MODEL FOR WATER BALANCE IN PLANTS

In I the model for the water balance in plants was based on the following assumptions:

- the stomatal conductivity ($g_s=1/r_s$, r_s =stomatal resistance in $\text{s}\cdot\text{m}^{-1}$) is linearly proportional to the difference between the actual water potential (Ψ in bar) of the leaf and Ψ_c , the water potential at which the stomata are completely closed ($r_s=\infty$);
- the hydraulic resistance within the plant is zero above the root and therefore there is no water potential gradient along this part of the plant, and Ψ applies to the whole plant above the root;
- cuticular resistance (r_c in $\text{s}\cdot\text{m}^{-1}$) is in parallel with r_s and the boundary layer resistance (r_b in $\text{s}\cdot\text{m}^{-1}$) is in series with both r_s and r_c .

This leads to the following equation (see I) for transpiration (E , in $\text{kg}\cdot\text{s}^{-1}$):

$$E = \frac{A_l \Delta V}{r_c / [L_s r_c (\Psi - \Psi_c) + 1] + r_b} \quad (1)$$

in which: A_l = total Leaf area (m^2); L_s = stomatal permeability coefficient ($\text{m}\cdot\text{bar}^{-1}\cdot\text{s}^{-1}$) and ΔV = difference between the water vapour concentration of air in leaf air spaces and that of bulk air ($\text{kg}\cdot\text{m}^{-3}$).

Water uptake obeys the following equation:

$$U = A_r L_r (\Psi_s + P_r - \Psi) \rho \quad (2)$$

in which U = water uptake ($\text{kg}\cdot\text{s}^{-1}$); Ψ_s = water potential of the soil (here: Steiner solution); L_r = water permeability coefficient of the root ($\text{m}\cdot\text{s}^{-1}\cdot\text{bar}^{-1}$); P_r = root pressure (bar); A_r = area of the root membrane through which the water flows (m^2) and ρ = density of liquid water ($\text{kg}\cdot\text{m}^{-3}$).

For equilibrium:

$$E = U = Q_e \rho \quad (3)$$

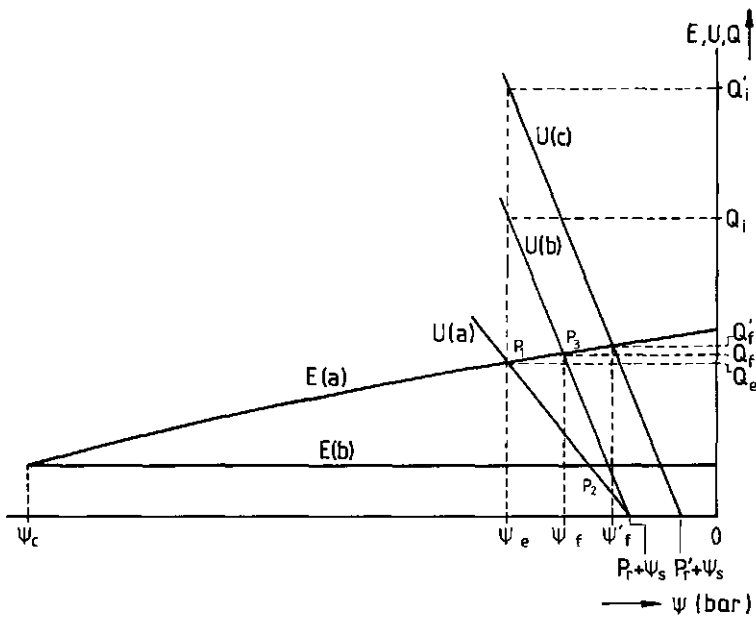


Figure 1

Schematic representation of transpiration (E) and water uptake (U) as a function of water potential (Ψ) according to eqs. (1) and (2). Q_e and Ψ_e are equilibrium values resulting from the curves $U(a)$ and $E(a)$. Increase in A_r or L_r leads to a new uptake curve $U(b)$, which causes initially a new flow rate Q_1 and results in new equilibrium values Q_f and Ψ_f . Increase in A_r and/or L_r , plus a change of P_r to P_r' leads to curve $U(c)$ with an initial flowrate Q_1' and final values Ψ_f' and Q_f' . $E(b)$ represents the transpiration curve during the night, when $L_s = 0$.

with Q_e = equilibrium value of the volume flow rate Q ($m^3 \cdot s^{-1}$). This results in an equilibrium value Ψ_e (see Fig. 1, the intersection of curves E(a) and U(a), which represent the curves for transpiration and water uptake, respectively). Eqs. 1-3 predict that factors which affect the transpiration curve (relative humidity (ΔV), light intensity (L_s), wind speed (r_b)) cause Q_e and Ψ to change in opposite directions (see Fig. 1). For example, when lights are turned off, L_s decreases and transpiration changes from E(a) to E(b), so that equilibrium points for Ψ and Q change from P_1 to P_2 (i.e. Ψ increases and Q decreases). By contrast, for uptake the model predicts that the primary reaction of the plant to a change in L_r or A_r is a change in water flow and water potential in the same direction (Fig. 1). When the uptake curve shifts from U(a) to U(b) the equilibrium point moves from P_1 to P_3 , i.e. both Q and Ψ increase.

In the following, we give the definitions P_w (= water content) = (fresh weight-dry weight)/dry weight, and R_w (= relative water content) = (fresh weight-dry weight)/(turgid weight-dry weight). The turgid weight is obtained by floating the tissue in water until water uptake has fallen below a predetermined value.

Materials and methods

NUCLEAR MAGNETIC RESONANCE

The NMR flow experiments have been described in detail in previous papers (Hemminga and de Jager, 1980; Van As and Schaafsma, 1984; Van As and Schaafsma, 1987). These experiments yield a time-dependent NMR-signal ($S(t)$, see I) from which we obtain the (mean) linear flow velocity (v , in $m \cdot s^{-1}$) and the volumetric flow velocity Q ($m^3 \cdot s^{-1}$). Calibration constants used for these derivations are identical to those in paper I.

The relaxation time T_2 , obtained from the decay of the transverse magnetization (Farrar and Becker, 1971), provides information on water content and water potential of the plant (see I). In I an effective decay rate ($R_2 = T_2^{-1}$) was defined as the weighted average of three

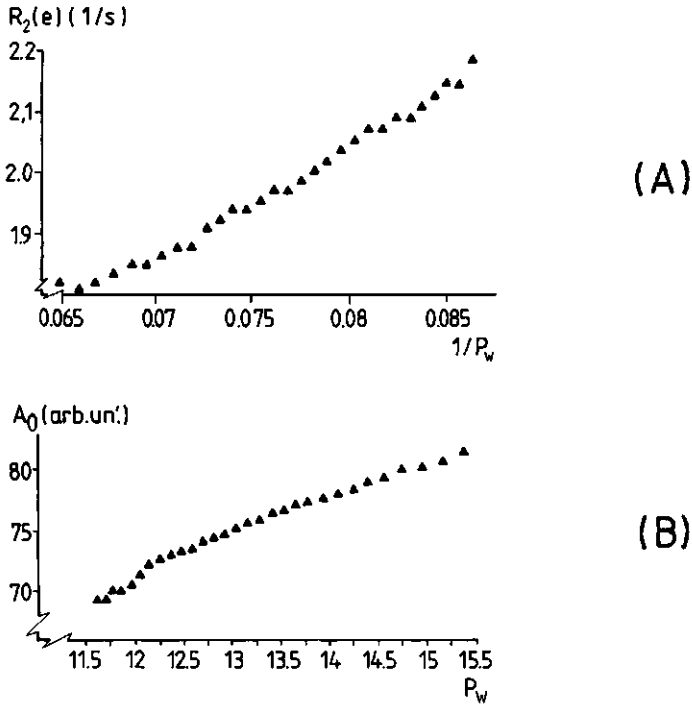


Figure 2

Relationships between $R_2(e)$ and $1/P_w$ (Fig. 2A) and between A_0 and P_w (Fig. 2B) for a cucumber stem segment during dehydration in the rf coil. For further details see Materials and Methods.

relaxation times that can be obtained from a multi-exponential analysis of the transverse magnetization decay curves (Van As, Schaafsma and Blaakmeer, 1986a,b). In the present paper this average decay rate is denoted as $R_2(av)$ (in s^{-1}). $R_2(av)$ exhibits an approximately linear dependence on $1/P_w$. Alternatively, the time at which the signal amplitude has decayed to a fraction $1/e$ of its initial value (here denoted as $T_2(e)$, $R_2(e) = 1/T_2(e)$) can be used as a parameter to monitor P_w . In Fig. 2A the relationship between $R_2(e)$ and $1/P_w$ for a cucumber stem segment is shown for a range of physiologically relevant values of P_w , corresponding to a relative water content of 100% - 75%. Similarly to

$R_2(av)$, $R_2(e)$ was found to be linearly dependent of the experimental value of $1/P_w$. An advantage of $R_2(e)$ as compared to $R_2(av)$ is that it can be obtained very easily, whereas $R_2(av)$ requires time-consuming computer calculations. Therefore, we have used $R_2(e)$, and for comparison $R_2(av)$, to monitor P_w .

The initial signal amplitude (A_0) of the relaxation curves, defined as the amplitude extrapolated to $t=0$, is found to be proportional to P_w (see Fig. 2B) for the same range of P_w -values as in Fig. 2A. Since under our experimental conditions, the first datapoint of transverse magnetization decay curve is obtained at $t = 6.5$ ms, A_0 does not contain any contribution of protons with relaxation times shorter than a few milliseconds, including those present in the dry matter. Provided the plant dry weight remains unchanged (no growth), A_0 is expected to be proportional to P_w . During our experiments with a duration of ca. 1 day, the dry weight is assumed to be constant. A_0 can only be used in a comparative way because the plant's dry weight is unknown.

DENDROMETER

A linear variable differential transformer (LVDT, type HBM W1/E5, Höttinger Baldwin Messtechnik) (Gensler, 1986) was used to measure the absolute thickness of a plant stem. This has been shown to be related to plant water content (Klepper, Browning, Taylor, 1971) and potential (Huck, Klepper, 1977) of the plant. Growth also causes changes in LVDT-output. During the duration of our experiments (ca. 1 day), the change in LVDT output, due to growth, can be neglected with respect to variations, due to changes in water content.

EXPERIMENTAL CONDITIONS

Detailed descriptions of plant material, plant environment and measurements are given in I. All of these and signal evaluation procedures were the same in this study, unless otherwise indicated. Plants were greenhouse hydro cultures of cucumbers and gherkins (Cucumis sativus L.) grown at the Institute of Horticultural Plant Breeding in

Wageningen in October - December 1986. The air temperature was ca. 18/20°C. During this period light/dark periods and light intensity were determined by natural illumination. Relative humidity was about 60%. Before each experiment the plants were exposed to a 12 h light period (07.00 to 19.00 h) and a 12 h dark period. Relative humidity was 65±10%, air temperature 20±1.5°C, root temperature 20±0.5°C, and radiant input 95 W·m⁻². Steiner solution was circulated through a reservoir controlled thermostatically to ± 0.1°C. U was varied in two different ways:

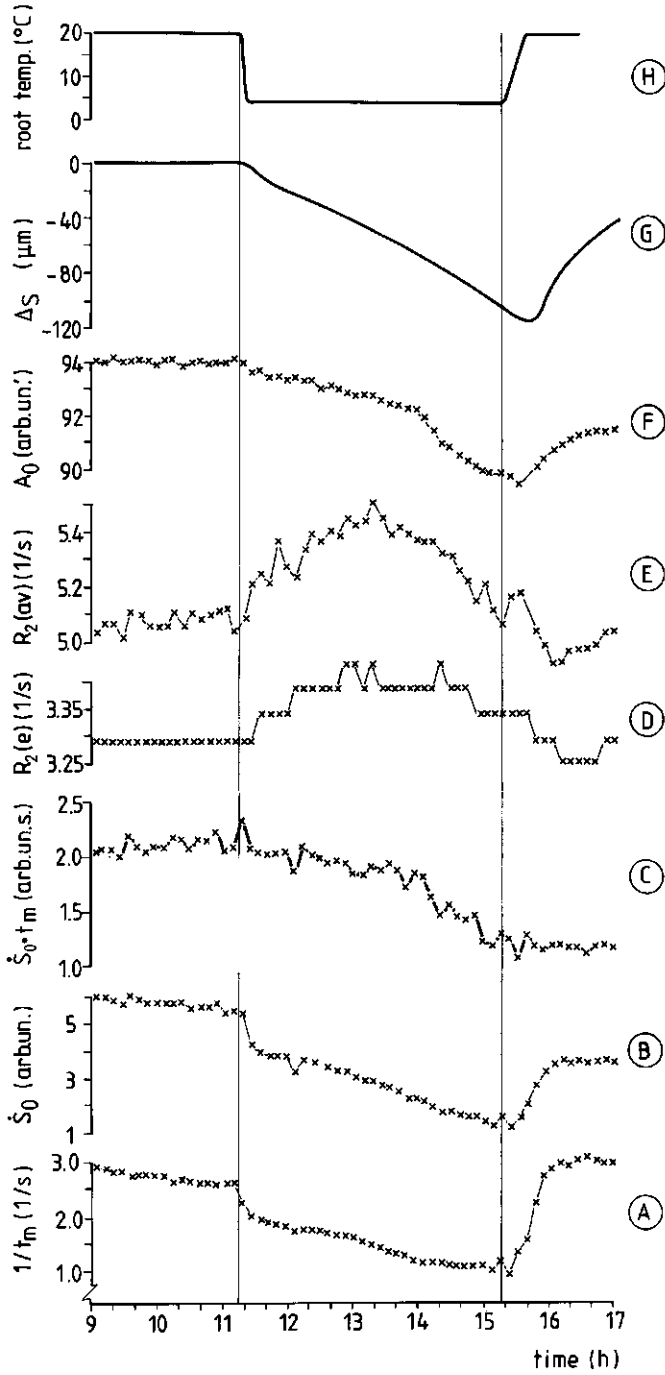
- a) by changing root temperature and
- b) by changing the area of root in contact with Steiner solution by varying the water level in the root container.

The LVDT was positioned on the stem just above the floor of the climate chamber and ca. 0.5 m above the NMR probe. Its output was monitored simultaneously with the NMR signals.

Values of $R_2(e)$ and A_0 , used to obtain the relationships $R_2(e) - 1/P_w$ and $A_0 - P_w$, were calculated from NMR relaxation curves obtained at regular time intervals for a stem segment during dehydration, while it remained in the rf coil. The values of P_w were obtained by weighing at regular intervals a second stem segment. This was cut from a region adjacent to the first, and allowed to dehydrate in the rf coil immediately after the first one, and under the same conditions. Data from both experiments were combined to give the desired relationships between P_w and $R_2(av)$ or $R_2(e)$.

Figure 3 (page 123)

Effect of variation of root temperature (Fig. 3H) of a hydroculture plant on linear water flow rate $v \propto 1/t_m$ (Fig. 3A), volumetric water flow rate $Q \propto \dot{S}_0$ (Fig. 3B), effective area available for flow $A = Q/v \propto \dot{S}_0 t_m$ (Fig. 3C) and water content or potential, determined in various ways: from NMR relaxation data (Figs. 3D-F) and using a dendrometer (Fig. 3G). Δ_S = difference in stem thickness, compared to the thickness at night. See text for further details.



Results and discussion

Fig.3 shows effects on a number of parameters of reducing and later increasing U by lowering and then raising the root temperature of a cucumber plant. The reduction in root temperature resulted in a rapid decrease of v and Q , followed by a more gradual decrease (Figs. 3A and 3B). The water content gradually decreased according to Figs. 3F and 3G. During the first few hours, this is also indicated by Figs. 3D and 3E. After this, however, $R_2(av)$ and $R_2(e)$ decrease, apparently in contrast with Figs. 3F and 3G. Cooling the roots results in a decrease in L_r (Slatyer, 1967; Tranquillini, 1982) due to 1) an increased viscosity (η) of the water and 2) a reduced metabolic activity of the root cells. Additionally, Ψ and Q may be influenced by a change in L_s , since prolonged exposure to 4°C causes a gradual closure of the stomata, mediated by abscisic acid (ABA) (Raschke, 1975). A reduction in L_s causes Ψ to increase and reduction in L_r causes Ψ to decrease, as can be derived from Fig. 1. If this model is correct, the overall effect is clearly dominated by L_r , as can be seen in Figs. 3F and 3G.

Dividing the simultaneous values of \dot{S}_0 (Fig. 3B) and $1/t_m$ (Fig. 3A), yields a measure for the effective area (A) available for flow (Fig. 3C). The values of A and the amplitude A_0 (Fig. 3F) are found to be highly correlated in the period 9.00-15.00 h. Note, that the change in slope in the A_0 -curve at ca. 14.00 h (Fig. 3F) corresponds to a similar change in the slope of the $\dot{S}_0 \cdot t_m$ curve (Fig. 3C) at the same time.

By comparing Figs. 3C and 3F we can conclude that the decrease of $\dot{S}_0 \cdot t_m$ and A_0 is not due to changes in stomatal resistance, induced by changing the root temperature. This can be excluded, since an increase of stomatal resistance would result in an increase of A_0 , contrary to observation. Therefore, the observed changes in A_0 and $\dot{S}_0 \cdot t_m$ are both ascribed to changes in the root resistance.

Note also, that $\dot{S}_0 \cdot t_m$ refers to the area, available for flow in the stem. If the rate of water transport in all xylem vessels would change in an identical manner (e.g. due to a change in root resistance), this would not result in a change of A. The observed change of A implies that part of the water-conducting system is lost for transport, due to the

exposure of the root to low temperatures. This loss is irreversible as can be seen from the curve in Fig. 3C at $t > \text{ca. } 15.00 \text{ h}$.

The effects on A, v and Q, represented in Figs. 3C, A and B, demonstrate the power of the NMR method, when applied to water transport in intact plants.

The decrease in $R_2(e)$ and $R_2(av)$ in Figs. 3D and 3E after the plant has been exposed to 4°C for a few hours can be explained by a temperature effect on the relaxation times which has been observed in various biological tissues (Belton, Packer and Sellwood, 1973; Yoshizaki, Maruyama, Yamada, Nishikawa and Morimoto, 1983; Niccolai, Rossi and Tiezzi, 1983; Kälväräinen, Sukhanova and Goryunov, 1983; Bottomley, Foster, Argersinger and Pfeifer, 1984). For cucumber tissue a temperature dependence of the transverse relaxation time was observed in our laboratory (Hilhorst, 1978). A cucumber stem segment was exposed to a decreasing temperature from 12°C to -10°C . Between 12°C and 0°C a linear increase of T_2 was observed of about 10 %, which is of the same order of magnitude as changes due to variation in water content. Based on this analysis, the curves of $R_2(av)$ and $R_2(e)$ presented here, result from two (opposing effects: 1) a decrease in water content leading to an increase of $R_2(e)$ and $R_2(av)$ and 2) a decrease of temperature of the tissue, due to the upward flow of cold water resulting in a gradual decrease of $R_2(av)$ and $R_2(e)$. After a few hours the net behaviour is dominated by the latter effect. The initial reaction following an increase of the water temperature from 4°C to 20°C is as expected: an increase of both the flow rate and the water content. The behaviour of $R_2(av)$ and $R_2(e)$, due to a rise in temperature, is again a combination of the aforementioned effects. After re-establishing a root temperature of 20°C , Q and the water content equilibrate at a value smaller than that before the start of the experiment (results not shown), whereas v reaches a value which is even higher than before the root cooling experiment as discussed before.

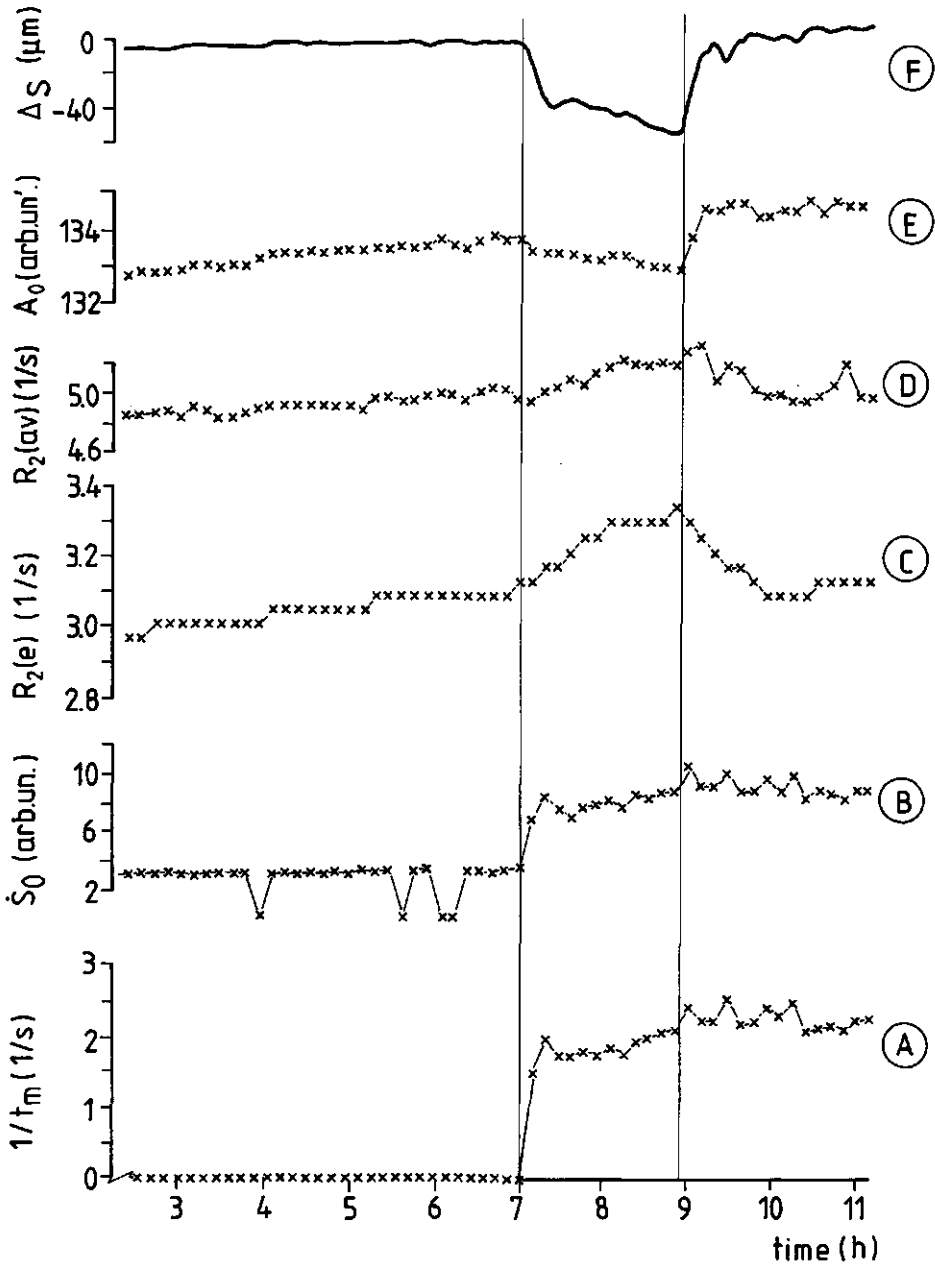
A second experiment demonstrates for a gherkin plant the effect of a change of night to day as well as an increase in U, resulting from an increase in the root area in contact with Steiner solution (Fig. 4). At 07.00 h the light was turned on and at 08.55 h Steiner solution was

added to the reservoir containing the roots so that a larger fraction of the roots was in contact with the solution than previously, equivalent to an increase in A_r and perhaps in P_r in eq. (2). The change night to day causes the expected fall in Ψ and increase in Q , as discussed before. The increase in root area in contact with Steiner solution resulted in an increase in Ψ (as expected), while flow rate hardly increased. This can be explained by assuming that the value of the slope of the transpiration vs. Ψ curve ($E(a)$) is much smaller than the slope for $U(a)$ vs. Ψ (Fig. 1). With P_r constant an increase in A_r causes the slope ($A_r L_r$) of U vs. Ψ to increase ($U(a)$ to $U(b)$ in Fig. 1. This causes a transient flow Q_i , which decreases to a final flow Q_f , slightly higher than the initial Q_e , and a final water potential Ψ_f which is considerably higher than the initial Ψ_e . An increase in both P_r and A_r results in uptake curve $U(c)$, transient flow Q_i' , and final flow and Ψ Q_f' and Ψ_f' , respectively. Thus a change in A_r leads to Ψ and Q changing in the same directions, as we observed. When applying Fig. 1 to the decrease of root temperature in Fig. 3, (i.e. the uptake curve changes from $U(b)$ to $U(a)$ and the transpiration curve is represented by $E(a)$) we would expect a large decrease in Ψ and a relatively small decrease in Q . The opposite is observed, however. Within the model, the drop in Q can be accounted for by a fast decrease in L_s , thus preventing a large fall in water potential.

Assuming $L_s=0$, then it is possible to calculate r_c and r_b from the equilibrium flow rate in the dark, because we know A_l and ΔV . For the plant, used in the experiment of Fig. 4, these values are: $A_l = 1.1 \text{ m}^2 \pm 10\%$ (2x the projected area) and $\Delta V = 6 \text{ gr} \cdot \text{m}^{-3} \pm 10\%$ (relative humidity of air 65% at 20°C and leaves saturated with water vapour at air temperature). With $Q = 6 \text{ } \mu\text{l} \cdot \text{s}^{-1} \pm 20\%$ (Fig. 4B): $r_c + r_b = 1100 \pm 330$

Figure 4 (page 127)

Effects of change night to day (07.00 h) and of watering the plant (08.55 h) on water flow and content/potential, measured in various ways. After solution was added, a larger part of the roots was in contact with the Steiner solution than before. See text and Fig. 3. for further details.



$\text{s}\cdot\text{m}^{-1}$. Assuming boundary layer resistance (r_b) is $100 \text{ s}\cdot\text{m}^{-1}$ (Nobel, 1974), then r_c is $1000 \pm 330 \text{ s}\cdot\text{m}^{-1}$, which is in fair agreement with literature values (Schönherr, 1982; Slatyer, 1967).

Fig. 4 shows some discrepancies between different measured variables (Fig. 4C-F) all of which should reflect the water potential. In the following, the main observations are summarized. In some cases a tentative explanation is offered. The change night to day causes a sharp increase in flow rate (Figs. 4A and 4B) and a sharp decrease in stem thickness (Fig. 4F). The decrease in water content, however, as determined by A_0 (Fig. 4E) is much less pronounced than the reduction in stem diameter, whereas $R_2(e)$ and $R_2(av)$ (Figs. 4C and 4D) do not show a sharp increase, but only slow changes. Perhaps the variation of stem thickness is (to a certain extent) caused by a change in the diameter of the pith cavity. Addition of solution caused an immediate increase in water content as determined by A_0 and Δ_S (Figs. 4E and 4F). Note that the equilibrium dendrometer reading and A_0 after addition of Steiner solution were larger than at night (Figs. 4E and 4F), whereas $R_2(av)$ and $R_2(e)$ declined steadily after solution was added. This gradual decline (increase in water potential or content) might result from a (radial) redistribution of water in the stem caused by local water potential gradients. When the plant was in darkness (before 07.00 h) Figs. 4C and 4D indicate a decrease in water content, whereas Fig. 4E indicates an increase and Fig. 4F hardly shows any change in stem diameter. Although some of the observed effects are not completely understood, the ability to monitor effects of small environmental changes is a common advantage of the LVDT and the NMR flow measurements. The small variations of the LVDT signal around 10.00 h are coincident with those of $1/t_m$ (Fig. 4A) and \dot{S}_0 (Fig. 4B). In order to get more quantitative information on the plant (model) it will be advantageous to combine NMR with other techniques (e.g. porometry).

Acknowledgements

We are indebted to Mr. S. Zijlstra of the Institute of Plant Breeding for his kind gift of the plant material, to Mr. G.T. Bruggink of

the Department of Horticultural Plant Breeding for making available the dendrometer and to Prof. D.W. Sheriff (CSIRO, Mount Gambier, Australia) for useful discussions.

Literature cited

- Belton, P.S., Packer, K.J. and Sellwood, T.C., 1973. Pulsed NMR studies of water in striated muscle II. Spin-lattice relaxation times and the dynamics of the non-freezing fraction of water. *Biochimica et Biophysica Acta*, 304, 56-64.
- Bottomley, P.A., Foster, T.H., Argersinger, R.E. and Pfeifer, L.M., 1984. A review of normal tissue hydrogen NMR relaxation times and relaxation mechanisms from 1-100 MHz: Dependence on tissue type, NMR frequency, temperature, species, excision and age. *Medical Physics*, Vol. 11, No. 4, 425-448.
- Farrar, T.C. and Becker, E.D., 1971. "Pulse and Fourier Transform NMR". Academic Press Inc., New York.
- Fullerton, G.D., Potter, J.L. and Dornbluth, N.C., 1982. NMR relaxation of protons in tissues and other macromolecular water solutions. *Magnetic Resonance Imaging*, 1, 209-228.
- Gensler, W.G., 1986. "Advanced Agricultural Instrumentation Design and Use". pp. 457-476. Gensler, ed. Martinus Nijhoff Publishers, Dordrecht, Netherlands.
- Hemminga, M.A. and de Jager, P.A., 1980. The study of flow by pulsed nuclear magnetic resonance. II. Measurement of flow velocities using a repetitive pulse method. *Journal of Magnetic Resonance*, 37, 1-16.
- Hilhorst, M.H., 1978. Spin echo metingen aan plantaardig materiaal. M.Sc. Thesis. Agricultural University, Wageningen.
- Huck, G.M. and Klepper, B., 1977. Water relations of cotton. 2. Continuous estimates of plant water potential from stem diameter measurements. *Agronomical Journal*, 69, 593-597.
- Käiväräinen, A.I., Sukhanova, G. and Goryunov, A.S., 1984. Changes in water properties in Serum Albumin solutions induced by alterations in protein flexibility. NMR studies. *Folia biologica (Praha)*, 84-92.
- Klepper, B., Browning, D. and Taylor, H.M., 1971. Stem diameter in relation to plant water status. *Plant Physiology*, 52, 565-568.
- Niccolai, N., Rossi, C. and Tiezzi, E., 1983. Water proton spin-lattice relaxation behaviour in heterogeneous biological systems. *Chemical Physics Letters*. Vol. 96, No. 2, 154-156.
- Nobel, P.S., 1974. "Biophysical Plant Physiology". Chapter 7. Freeman and company, San Francisco.
- Raschke, K., 1975. Stomatal action. *Annual Review of Plant Physiology*, 26, 309-340.
- Reinders, J.E.A., Van As, H., Schaafsma, T.J., de Jager, P.A., 1987. Water balance in Cucumis plants, measured by Nuclear Magnetic Resonance, I. Submitted to *Journal of Experimental Botany*.
- Schönherr, J., 1982. "Physiological Plant Ecology II. Encyclopedia of Plant Physiology", Vol. 12B. p. 159. Lange, O.L., Nobel, P.S., Osmond, C.B., Ziegler, H., eds. Springer Verlag Berlin.
- Slatyer, R.O., 1967. "Plant-water relationships". Academic Press, Lon-

- don.
- Tranquillini, W., 1982. "Physiological Plant Ecology II. Encyclopedia of Plant Physiology", Vol 12B. Chapter 11. Lange et al. eds. Springer Verlag, Berlin.
- Van As, H., 1982. NMR, water and plants. Ph.D. thesis. Agricultural University, Wageningen.
- Van As, H. and Schaafsma, T.J., 1984. Noninvasive measurement of plant water flow by nuclear magnetic resonance. *Biophysical Journal*, 45, 469-472.
- Van As, H., Schaafsma, T.J. and Blaakmeer, J., 1986a. NMR of water flow and content in plants. *Bruker Report*, 1, 33-36.
- Van As, H., Schaafsma, T.J. and Blaakmeer, J., 1986b. Applications of NMR to water flow and -balance in plants. *Acta Horticulturae*, 174, 491-495.
- Van As, H., Schaafsma, T.J., 1987. Measurement of flow by the NMR repetitive pulse method. *Journal of Magnetic Resonance*, 74, in press.
- Yoshizaku, K., Maruyama, Y., Yamada, S., Nishikawa, H. and Morimoto, T., 1983. Application of Nuclear Magnetic Resonance on the study of water in muscle. *Journal of the Kyoto Prefectural University of Medicine*, 92(2), 209-218.

7.4 Miscellaneous experiments

In previous sections the emphasis was on experiments and results in connection with a model for the plant water balance. In this section additional experiments are presented, some of which are relevant to this model, whereas also experiments are reported, which yield interesting information on related subjects.

Fig. 1 shows the behaviour of water flow (Figs. 1A,B), effective area available for flow (Fig. 1F), and water content (Figs. 1C,D,E,G) during several day-night periods in which no external parameters were changed except the light intensity. The first part of Fig. 1 (D1 - D4) shows the effects occurring immediately after transport. These effects are described in more detail in the discussion of Fig. 2, which shows these effects in a more pronounced way. It can be seen from Fig. 1 that during the day, Q and v (Figs. 1A,B) are larger than during the night and that according to Figs. 1C, D and G the water content or potential is decreased during the day. The decrease of the stem diameter (i.e. to more negative values of Δ_S) corresponds in general to a lower water content (or potential) (see Chapter 2). The continuous increase in A_0 during D1 - D4 (Fig. 1E) is probably a growth effect. The increase in A_0 , however, appears to be larger during the night than during the day. In fact, this could indicate a decrease of the water content or potential during the day. Growth can also be noticed as an increase of Δ_S in the inset of Fig. 1G. A small effect, due to the day-night cycle, can be found in Fig. 1F, suggesting changes in the area available for flow. This does not necessarily have to be a real effect, since it may result from slightly too high values of $1/t_m$ for low velocities (see Chapter 6). It can be seen from Figs. 1A and B that the flow rate does not remain constant during the day. Q and v usually reach a maximum after some hours in the light and then decrease again, a tendency which is followed by the relaxation rate, but is not noticeable in Δ_S .

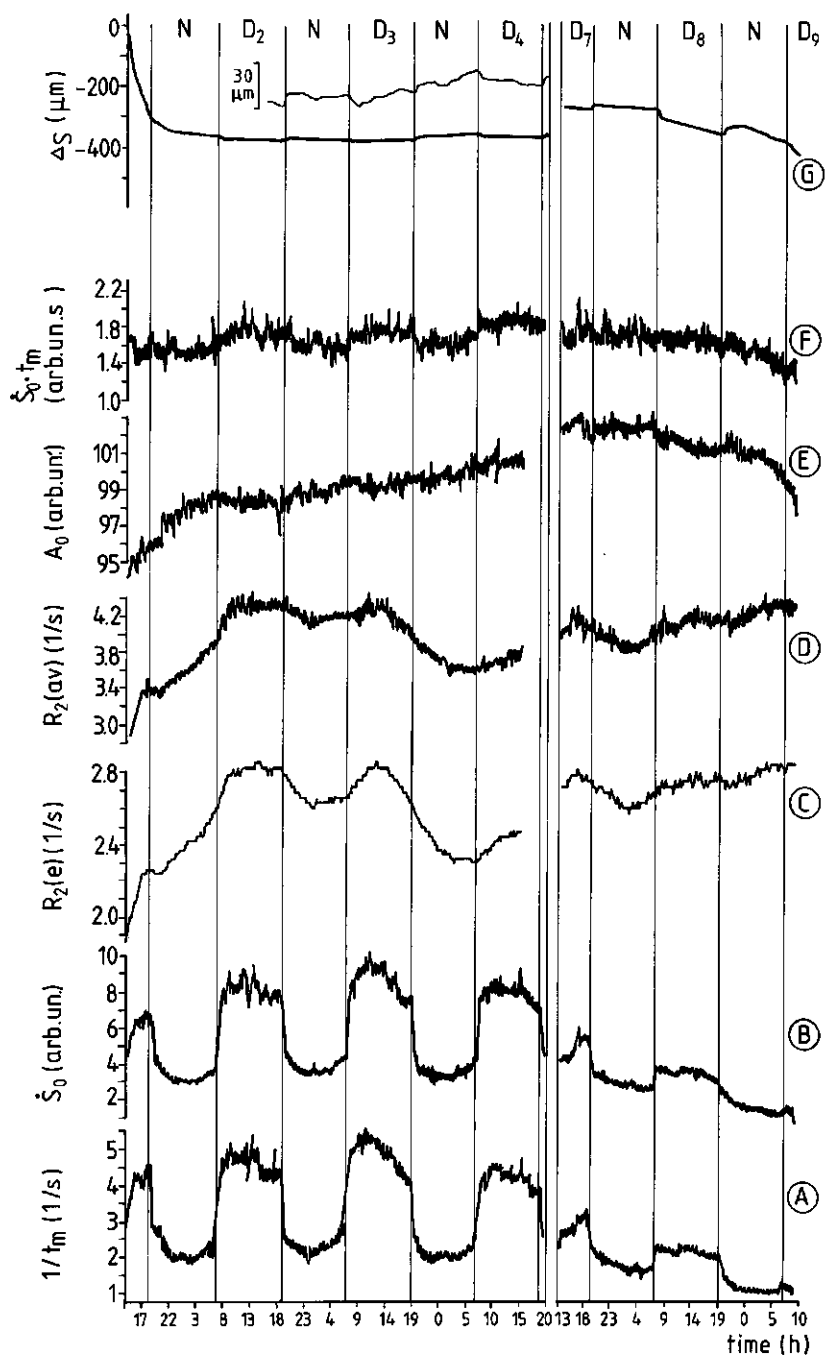
The last part of Fig. 1 shows the result of an accidental population of white flies in the climate chamber. During D7 - D9 this population increased. The infestation of white fly can be clearly seen in all measured parameters. The flow rate (Figs. 1A,B) as well as the water

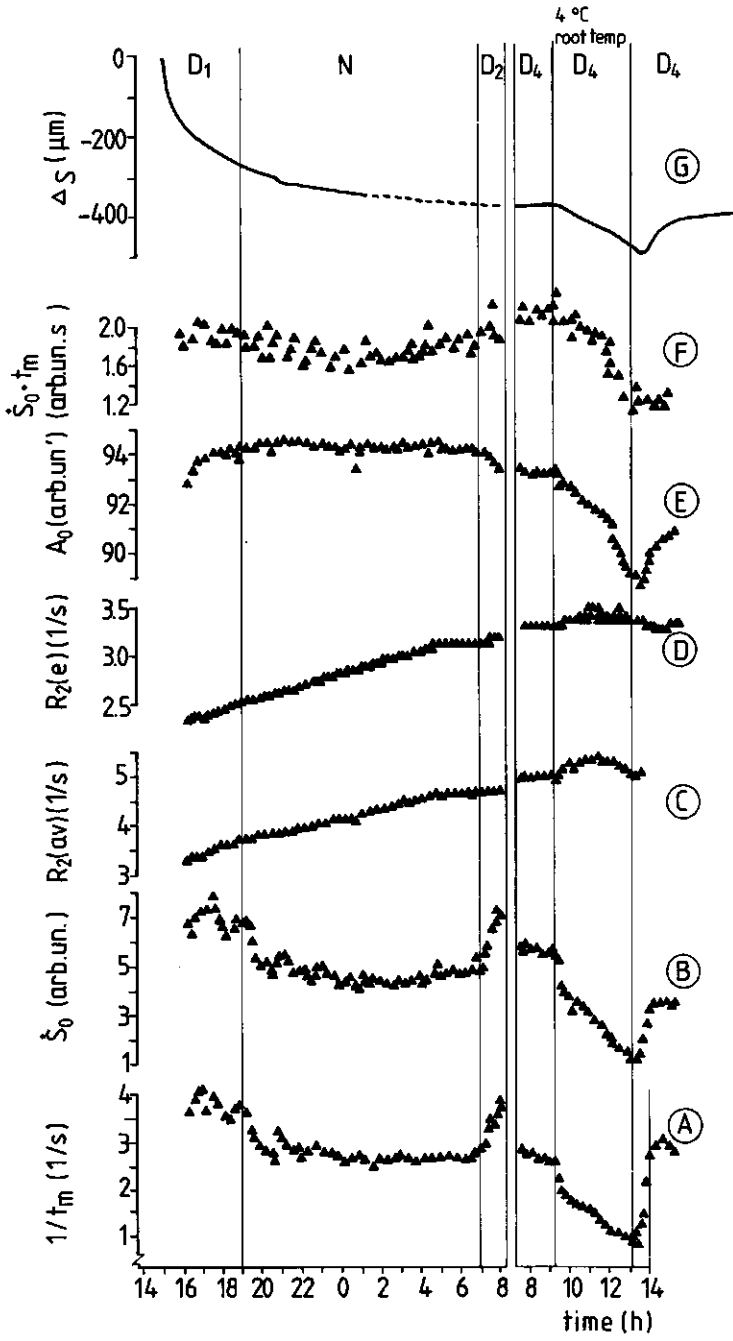
content or potential (Figs. 1C,D,E,G) decreased, indicating that the resistance for water uptake increased more than that for transpiration. Note that A decreased as well.

Fig. 2 consists of two parts. The first (D1 and D2) shows the response of various parameters of a cucumber plant immediately after it has been transferred from the greenhouse, where it was grown, to the climate chamber. The second part (D4), shows the root cooling experiment, described in the previous section, conducted on the same cucumber plant. They have been also included in Fig. 2 to make a comparison of the size of the changes during D₁ and D₂ with those of the root-cooling experiments. The same parameters related to water flow and content that were discussed in Fig. 1 are shown. In Fig. 2G it can be seen that a large decrease in stem thickness occurs after transporting the plant. This decrease continues for several hours and is almost unaffected by the change day-night. The dashed part of curve 2G has been extrapolated since during this period the LVDT output was outside the scale of the recorder, and readjustment was not carried out. The relaxation rates in Figs. 2C and 2D react in a parallel way as Δ_S . This is in contrast with A_0 in Fig. 2E, however, which shows a slight increase during the first hours, then hardly changes during the night and decreases slightly when the lights are switched on (D₂). The different behaviour of A_0 on one hand and the relaxation rate and Δ_S on the other, has been observed in many cucumber and gherkin plants, and can also be seen in Fig. 1. Although Δ_S and the relaxation times decreased during the first hours, the flow rate (Figs. 2A,B) appears not to be affected. Only day-night changes affected the flow rates. The total decrease in Δ_S after starting

Figure 1 (page 133)

Response of linear flow velocity (Fig. 1A), volumetric flow velocity (Fig. 1B), water content/potential (Fig. 1C,D,E,G) and effective area available for flow (Fig. 1F) to day-night changes. Climatological conditions: radiant input: 95 W/m² during the day (D), 0 during the night (N); air temperature: 20°C ±1.5°C; root temperature: 20°C ±0.5°C; rh: 65% ±10%. A part of the LVDT output (Δ_S) has been enlarged and is shown in an inset in Fig. 1G.





the experiment is about 3 times the decrease that was observed during the root cooling experiment (second part of Fig. 2G). Nevertheless, no wilting occurred, whereas the root cooling experiments resulted in wilting of the plant. Therefore, the decrease in Δ_S is unlikely to be exclusively a result of water loss. It may also be due to adaptations of the stem to forces exerted by the LVDT and/or forces resulting from the different position of the plant in the climate chamber with respect to the greenhouse (e.g. a change of the dimensions of the pith cavity). The fact that this always results in a decrease of the relaxation times indicates that the relative amount of free water decreased (see Chapter 6). In terms of the diffusion model of Chapter 4 it may be concluded that the cell (vacuole) geometry and/or dimensions change.

Assuming a con-flow profile and using the calibration constants K_v and K_q as given in Chapter 6, we obtain:

$$A = A(\text{nmr}) = Q/v = (K_q/K_v)(\dot{S}_0 t_m) = 0.72 \dot{S}_0 t_m \quad (1)$$

in which A is expressed in mm^2 , \dot{S}_0 in the arbitrary units used in all figures and t_m is in s. For the cucumber plant of Fig. 2 an average value of $(\dot{S}_0 t_m)$ of 1.94 (arb.un.·s) was found, resulting in $A(\text{nmr}) = 1.41 \pm 0.2 \text{ mm}^2$. From microscopic measurements a value of $A(\text{micr}) = 2.43 \text{ mm}^2$ was found, which results in a ratio $A(\text{nmr})/A(\text{micr}) = 0.58$. For other plants ratios of $A(\text{nmr})/A(\text{micr})$ between 0.5 and 0.8 were found, in agreement with earlier observations [1]. Note that:

- 1) the real flow profile (i.e. K_v) in a plant may differ from a con-flow profile;

Figure 2 (page 134)

Response of the same parameters as in Fig. 1 for a cucumber plant:

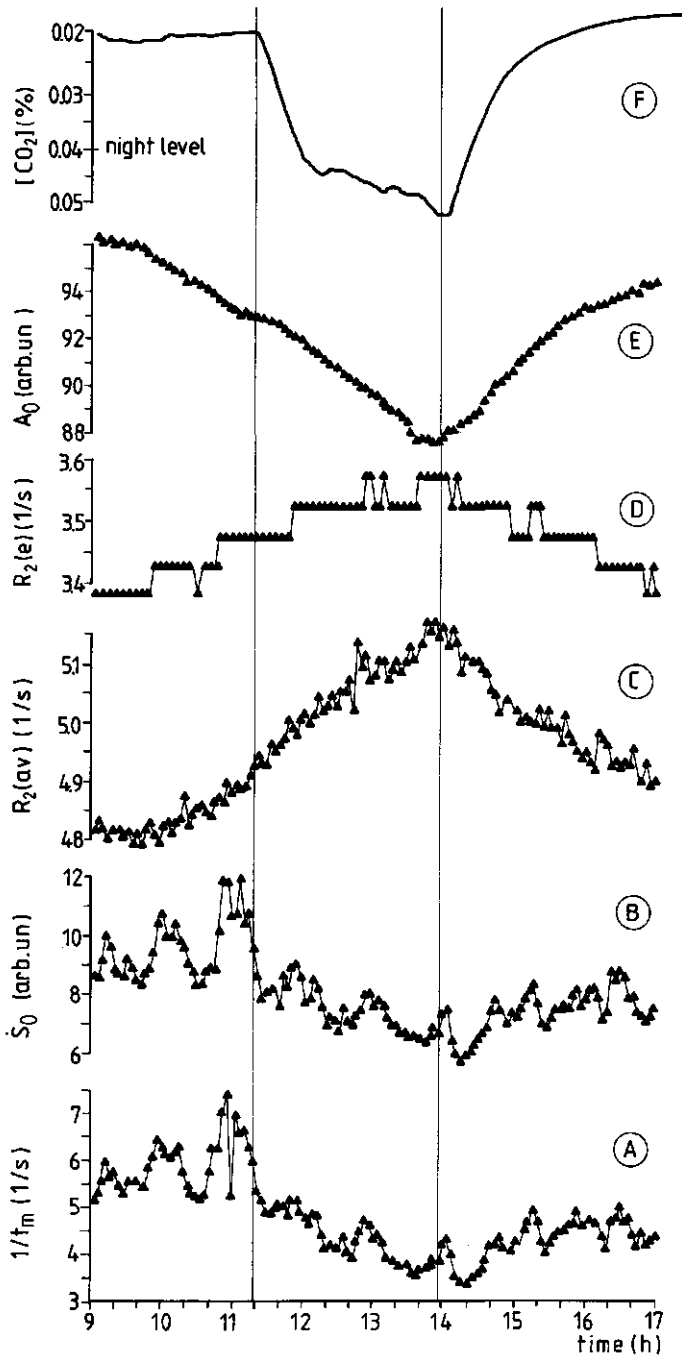
- 1) immediately after transport of the plant to the climate chamber (D1-D2), and
 - 2) to a decrease of the root temperature from 20 °C to 4 °C (D4).
- Climatological conditions are the same as in Fig. 1.

- 2) water, flowing through narrow vessels as well as water near the vessel wall is not seen in the flow experiment due to too low values of T_2 and/or flow velocity [Chapter 6];
- 3) there may be non-conducting vessels [2-6].

Fig. 3 shows the effect of an increase in CO_2 concentration both inside and outside the climate chamber for a gherkin plant on water content (Figs. 3C-E) and flow (Figs. 3A,B). Between 11:17 h and 13:57 h CO_2 from a cylinder was injected into the room where the experiments were carried out, leading to a change of climate chamber CO_2 concentration shown in Fig. 3F. These values, which are around 0.05%, are somewhat higher than the indicated 0.04% night level. CO_2 concentrations outside the chamber (where the roots are) also increased, but to an unknown degree, and the effects on water content and flow rate are likely to be the result of the combined effects of CO_2 on stomata and roots. Since CO_2 has a high solubility in water it can easily come into contact with the roots surrounded by well-aerated Steiner solution. Elevated CO_2 concentrations result in an increase in both stomatal resistance and root resistance [7]. Both these effects lead to a reduction of the flow rate (Figs. 3A,B), but because they act on opposite ends of the plant its water content or potential is affected in opposite ways. Figs. 3C-E show that the increased CO_2 concentration resulted in a reduction of the water content and potential, thus leading to the conclusion that resistance for water uptake increases more than for transpiration. An effect of the increased CO_2 concentration can hardly be seen in Fig. 3E. Both flow velocity and water content or potential decreased until the CO_2 concentration declined again at about 14.00 h. The resulting effect on the water content or potential (Figs. 3C-E) was much more pronounced

Figure 3 (page 137)

Effect of an increasing CO_2 concentration (Fig. 3F) on linear flow rate (Fig. 3A), volumetric flow rate (Fig. 3B) and water content or potential (Figs. 3C,D,E) for a gherkin plant. Both roots and shoot were exposed to an increased CO_2 concentration. Climatological conditions are the same as in Fig. 1.



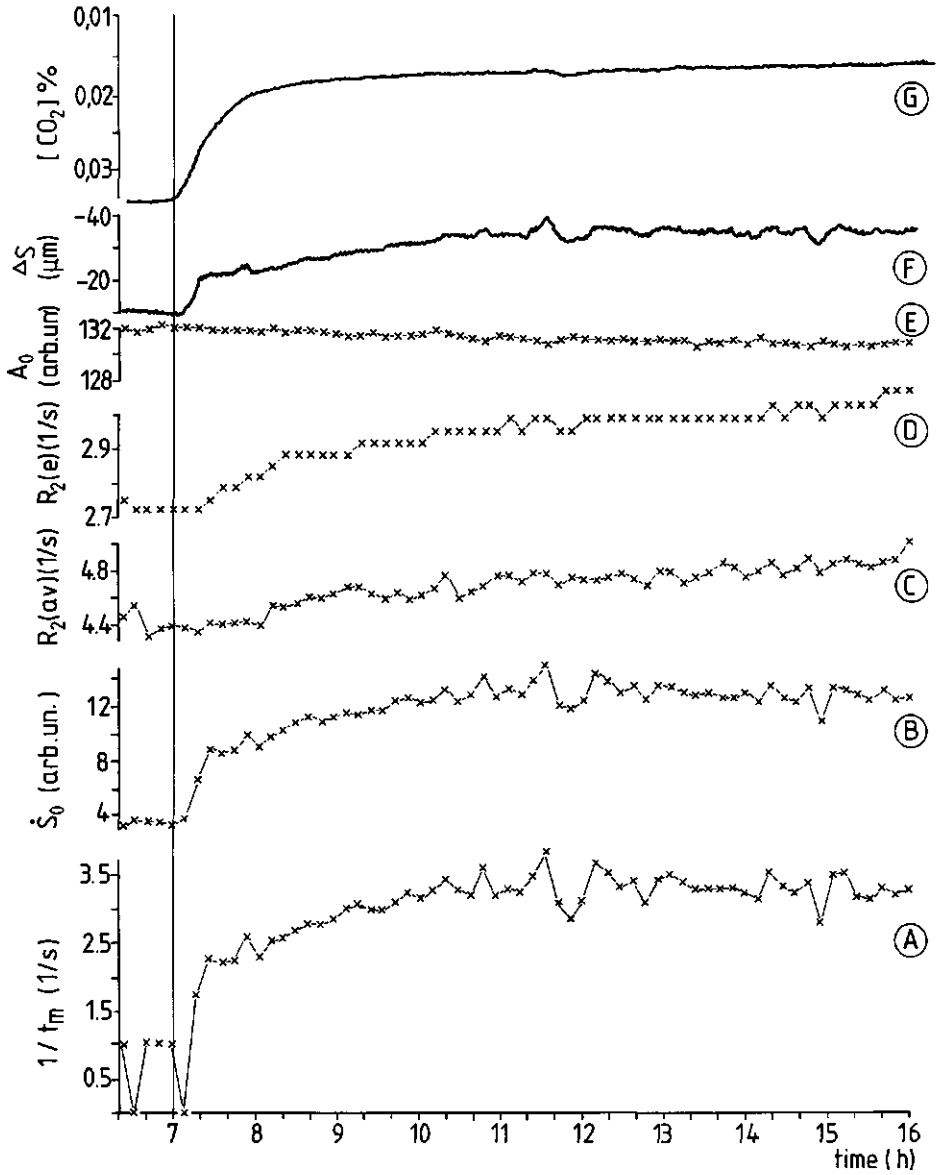


Figure 4 (page 138)

Illustration of the correlation between various measured parameters: linear flow rate (Fig. 4A), volumetric flow rate (Fig. 4B) and water content or potential (Fig. 4C-F). The CO₂ concentration is also shown (Fig. 4G). At 7.00 h illumination was switched on. Note that the sign of A_3 in Fig. 1F is inverted with respect to that in Figs. 1 and 2 to emphasise the correlation between various parameters.

than that on the flow rate (Figs. 1A,B), although both increased. The flow rate did not return to the original value which it had before the CO₂ concentration was increased. This might be caused by the 'daily rhythm' of the plant. During the day, if no environmental conditions are changed, water flow does not remain constant, but is often lower at the end of the day (Figs. 1A and B). The effective area available for flow showed no significant variation during the experiment and is not included in Fig. 3. Stem thickness was not monitored.

Fig. 4 is included to show the correlation that can be observed between various parameters during part of the day. When the lights were switched on v and Q increased (Figs. 4A,B) and A_3 and the CO₂ concentration (Figs. 4F,G) decreased. The relaxation rates (Figs. 4C,D) increased slowly, indicating a decrease in water content and potential. A_0 , however, did not change significantly. A showed no significant variations and is not included in Fig. 4. A very high correlation between the flow rates and A_3 is observed (e.g. the fluctuations around 12:00 hrs), which can also be seen in the CO₂ concentration. This high correlation between parameters, obtained with completely different methods, indicates the high accuracy with which changes in linear and volume flow velocity can be observed.

7.5 References

- [1] H. Van As and T.J. Schaafsma, 1984. *Bioph. J.*, 45, 469-472.
- [2] A.A. Jeje, M.H. Zimmermann, 1979. *J. Exp. Bot.* 30, 817-827.
- [3] M.H. Zimmermann, C.L. Brown, 1971. "Trees: structure and function". Springer Verlag, New York.
- [4] M.H. Zimmermann, J. McDonough, 1978. "Plant Disease". Horsfall et al., eds. Academic Press, London. Vol. 3, 117-40.
- [5] M.H. Zimmermann, 1978. *Can. J. Bot.* 56, 2286-2295.
- [6] J.A. Petty, 1978. *J. Exp. Bot.* 29, 1463-1469.
- [7] R.O. Slatyer, 1967. "Plant-Water relationships". Academic Press, London.

SUMMARY

=====

Water is one of the most important constituents of a plant. It is the medium in which many biological reactions take place and nutrients are transported throughout the plant in aqueous solutions. Because it serves as a hydrogen donor in photosynthesis water can be considered as one of the building blocks of the plant structure. Water plays an essential role in plant temperature regulation and is an important supporting structure, especially in non-woody plants. The study of plant-water relations is an important discipline in plant physiology, and many methods are available to study water content, water potential and water flow in plants. Chapter 1 contains a summary of the most frequently used techniques. All techniques measure only a single variable: water content, water potential or water flow. Most of the techniques are destructive and invasive, which does not apply to Nuclear Magnetic Resonance (NMR).

For over 25 years NMR has been used to obtain information on the water content of biological tissue. At the Department of Molecular Physics the Repetitive Pulse (RP) NMR method has been used as a technique to measure water flow since 1974. The method has shown to be successful when applied to cucumber, pumpkin, and gherkin plants.

NMR has the following advantages:

- it is non-destructive and non-invasive;
- it permits almost simultaneous measurements of linear water flow, volumetric water flow and water content over long periods of time with a time resolution of a few seconds;
- from a combination of volumetric and linear water flow the effective total cross-sectional area available for flow can be calculated.

The intrinsic low sensitivity of NMR and high costs of the equipment are disadvantages of the method. Provided sufficient attention is paid to data acquisition and processing, the method can be made sensitive enough to obtain physiologically relevant data.

The goal of the work presented in this thesis was to evaluate the

significance of the NMR techniques in the field of plant physiology, in particular plant-water relations.

Chapter 2 contains NMR theory, and defines the concepts used in describing the water status of plants, as well as the combination of NMR and plant-water relations.

Materials and methods are described in Chapter 3. Particular attention has been paid to a home-built NMR probe and stabilization system for the main magnetic field ('lock').

Experiments with respect to the magnetic properties of the plant material are described in Chapters 4 and 5. These experiments were carried out for further understanding of the possibilities and limitations of the method, as well as improvement of the NMR technique and equipment.

When applied to plants with narrow xylem vessels, the NMR flow technique proved to be unsuccessful. This is due to a too short transverse relaxation time (T_2) in such vessels. A model relating T_2 to the xylem vessel diameter is presented in Chapter 4. It is assumed in this model that the xylem vessel walls contain 'relaxation sinks'. This means that the protons of the water molecules lose their magnetization (=relaxation) created in the experiment upon contact with the vessel wall, which makes them undetectable with the RP NMR technique. The effectiveness of this process is proportional to the value of a parameter H . The probability for a water molecule to reach the wall is determined by diffusion processes. A larger distance to the wall results in a longer time required for a molecule to reach the wall. The overall result is that T_2 of water in narrow vessels is shorter than in wide vessels. Using this information, it was possible to calculate in Chapter 6 that a well defined flow signal can only be observed in xylem vessels with a diameter of at least ca. 90 μm , using the experimental conditions described in this thesis.

The magnetic properties of the plant stem as a whole are discussed in Chapter 5. The rationale behind this was that a signal of stationary water was observed during a flow experiment. Theoretically this should not be so, because the magnetization of the stationary water in the upper coil half should be counterbalanced by that of the lower half.

This, however, was not found to be completely correct for plants, resulting in the presence of a background signal in addition to the flow signal. The observed NMR spectra of cucumber stem segments were found to be dependent on the orientation of the stem with respect to the magnetic field direction. The angular dependence could be explained by the presence of local magnetic susceptibility differences within the stem. These result in local magnetic field gradients, leading to a background signal due to stationary water in a flow experiment, and a decrease of T_2 . The latter effect increases the lower boundary of the diameter of xylem vessels in which flow signals can be detected. The line widths of the spectra showed a quadratic dependence on the main magnetic field. This does not agree with literature data, and is not yet understood. In the design of NMR flow meters this effect should be taken into account.

In Chapter 6 the influence of different flow profiles on the NMR flow curves is discussed. Because a plant contains many xylem vessels with different diameters, the flow profile is different from that of a system consisting of capillaries with equal diameters, which is used for calibration. The influence on calibration constants and possible adjustments are considered. The influence of relaxation times (see Chapter 4) and stationary water on the flow curves as derived from computer simulations is discussed as well. It was shown that variations in linear flow velocity of more than 5-10%, variations in volumetric flow velocity of more than 10-20%, and variations in water potential down to ca. 1 bar could be reliably detected by NMR. Experimental procedures to obtain quantitative information on flow rate and T_2 are described as well.

In Chapter 7 water balance studies carried out on the stem of water cultures of intact cucumber and gherkin plants are described. In some experiments NMR results are compared with those obtained with a dendrometer. The following environmental conditions were varied: relative humidity, light intensity, CO_2 concentration of air and root medium, root temperature, and root area in contact with surrounding medium.

Using the NMR techniques it was possible to discriminate between parameters affecting water uptake by the root and transpiration at the leaf surface. If the resistance for water uptake increased more than for

transpiration, both water flow and content decreased. By contrast, if the resistance for transpiration increased more than for water uptake, the water content increased and the water flow decreased. This can also be concluded from the model for water balance in plants, which was formulated in Chapter 7, on the basis of experimental data.

SAMENVATTING

=====

Water is een van de belangrijkste bestanddelen van een plant. Het dient ondermeer als medium voor biologische reacties, is het transportmiddel voor nutriënten, is leverancier van waterstof in de fotosynthese, speelt een belangrijke rol bij de temperatuurregulatie van de plant en geeft, met name aan niet-houtachtige planten, mechanische stevigheid. De studie van de waterhuishouding van planten vormt dan ook een belangrijke tak van de plantenfysiologie en er bestaan vele methoden ter bestudering van het watergehalte, de waterpotentiaal en de waterstroming in planten. Hoofdstuk 1 bevat een opsomming van de belangrijkste methoden. Vele van de genoemde technieken zijn destructief of vergen de inbreng van "markerings" stoffen. Bovendien zijn ze niet in staat om zowel waterstroming als watergehalte (of waterpotentiaal) in één experiment te meten. Deze nadelen heeft kernspinresonantie niet.

Kernspinresonantie (NMR; van het Engelse: Nuclear Magnetic Resonance) is een techniek die al circa 25 jaar bekend is als meetmethode voor het watergehalte. Bij de vakgroep Moleculaire Fysica wordt sinds 1974 NMR gebruikt als methode om stroomsnelheden van water te meten. De methode blijkt goed toepasbaar te zijn op komkommerachtigen, zoals pompoen, augurk en komkommer.

Als voordelen van de gebruikte NMR techniek kunnen worden aangevoerd:

- de methode is niet destructief en behoeft geen toevoeging van markeringsstoffen;
- de volume snelheid (ml/s), lineaire snelheid (m/s) en het watergehalte kunnen vrijwel gelijktijdig met een tijdsresolutie van enkele seconden en over lange periodes worden bepaald;
- uit volume snelheid en de lineaire snelheid kan het totaal doorstroomde oppervlak van de xyleemvaten in de stengel worden berekend.

De intrinsieke lage gevoeligheid van NMR en de hoge kosten van de apparatuur zijn de belangrijkste nadelen van deze techniek. Mits voldoende aandacht wordt besteed aan de acquisitie en verwerking van de

NMR-signalen, is de methode echter gevoelig genoeg voor de meting van fysiologisch relevante grootheden.

Het doel van dit proefschrift is aan te geven welke waarde de NMR techniek heeft voor de beantwoording van plantenfysiologische vragen met betrekking tot de waterhuishouding.

In hoofdstuk 2 wordt een theoretische uiteenzetting gegeven van NMR en de begrippen die betrekking hebben op de waterhuishouding in planten. Tevens wordt de theoretische basis gelegd voor de combinatie van NMR en waterhuishouding.

Hoofdstuk 3 geeft een overzicht van de gebruikte materialen en methoden en beschrijft de constructie van een zend- en ontvangstspoel en een apparaat ter stabilisering van het magneetveld ("lock"-systeem).

De hoofdstukken 4 en 5 bespreken de magnetische eigenschappen van het plantenmateriaal. Deze werden bestudeerd om de gebruikte meet-technieken en apparatuur te verbeteren en tevens om meer inzicht te verkrijgen in de mogelijkheden en beperkingen van de NMR-methodes.

De NMR stromingsmetingen bleken niet succesvol te zijn wanneer ze werden toegepast op planten met te nauwe transport- of xyleemvaten. De oorzaak hiervan ligt in het feit dat de transversale relaxatietijd (T_2) te kort is. In hoofdstuk 4 wordt een model gepresenteerd dat een verband geeft tussen T_2 en de straal van de xyleemvaten. In dit model wordt er vanuit gegaan dat de wand van een xyleemvat relaxatieputten bevat, d.w.z. dat de protonen van de watermoleculen hun in het experiment opgelegde magnetisatie verliezen (=relaxeren) als ze de wand bereiken. Als gevolg daarvan zijn deze protonen niet meer detecteerbaar m.b.v. de gebruikte techniek. De snelheid waarmee deze relaxatie plaats vindt, is evenredig met de waarde van een parameter H , die de effectiviteit van de relaxatieputten weergeeft. Diffusieprocessen bepalen de kans waarmee een watermolecuul de wand bereikt. Een grotere afstand tot de wand heeft tot gevolg dat een molecuul langere tijd nodig heeft om de wand te bereiken. Dit heeft tot gevolg dat de relaxatiesnelheid van de protonmagnetisatie van het water in nauwe xyleemvaten korter is dan in wijde xyleemvaten. Met de informatie uit dit hoofdstuk kon in hoofdstuk 6 worden berekend dat met de in dit proefschrift beschreven apparatuur een xyleemvatdiameter van minimaal circa 90 μm nodig is om goed gedefinieerde stro-

mingssignalen te kunnen waarnemen.

In hoofdstuk 5 staan de magnetische eigenschappen van de komkommerstengel als geheel centraal. Achtergrond van deze studie was het feit dat een signaal van stationair water zichtbaar was bij de meting van stromend water. In theorie wordt het stationaire water niet gedetecteerd bij een stromingsmeting omdat de magnetisaties van het water in de onderste en bovenste spoelhelften elkaar opheffen. Bij planten is dit echter niet volledig het geval, waardoor een stoorsignaal ten gevolge van stilstaand water ontstaat. De waargenomen afhankelijkheid van het NMR-spectrum van de orientatie van de stengel t.o.v de magneetveldrichting wordt in hoofdstuk 5 verklaard m.b.v. magnetische susceptibiliteitsverschillen in het weefsel. Deze leiden tot lokale magnetische veldgradienten, die enerzijds aanleiding geven tot het ontstaan van een stationair-water signaal en anderzijds een verkortende invloed hebben op T_2 van het stromende water. Dit laatste effect heeft een verhoging tot gevolg van de ondergrens voor de diameter van de xyleemvaten waarin een stromingssignaal kan worden waargenomen. De gemeten spectrale lijnbreedte bleek kwadratisch met de waarde van het magneetveld toe te nemen. Dit is niet in overeenstemming met literatuurgegevens en voorsnog niet begrepen. Bij het ontwerpen van NMR stromingsmeters moet met deze gegevens rekening gehouden worden.

In hoofdstuk 6 wordt ondermeer de invloed van stromingsprofielen op de stromingsmetingen beschouwd. Een plant bevat immers vele xyleemvaten met verschillende diameters. Dit leidt tot een ander stromingsprofiel dan voor een systeem van capillairen met uniforme diameter zoals dit wordt gebruikt bij calibrering, waardoor aanpassing van de calibratieconstanten vereist is. Ook werd m.b.v computersimulaties de invloed van de relaxatietijden (zie hoofdstuk 4) en het stilstaande water op de stromingssignalen onderzocht. Er werd aangetoond dat variaties in lineaire snelheid van meer dan 5-10%, van variaties in volume snelheid van meer dan 10-20% en variaties van minimaal ca. 1 bar in de waterpotentiaal betrouwbaar met NMR kunnen worden gemeten. Ook worden de experimentele procedures beschreven ter verkrijging van kwantitatieve gegevens m.b.t. stromingssnelheid en T_2 .

Hoofdstuk 7, tenslotte, bevat watertransport- en watergehaltemetin-

gen aan waterculturen van intacte komkommer- en augurkenplanten. In een aantal gevallen werden de watergehalte metingen aan de stengel van de intacte plant vergeleken met de resultaten die werden verkregen met een stengeldiktemeter. De volgende omgevingscondities werden gevarieerd: relatieve luchtvochtigheid, lichtintensiteit, CO_2 -concentratie van lucht en voedingsoplossing, worteltemperatuur en het worteloppervlak in contact met de voedingsoplossing.

Het bleek mogelijk te zijn om met de NMR techniek onderscheid te maken tussen effecten die invloed hebben op de opname van water in de wortel en effecten die de transpiratie aan het bladoppervlak beïnvloeden. Indien de weerstand voor opname meer toenam dan voor transpiratie, leidde dit tot een afname van zowel de stroomsnelheid als het watergehalte in de stengel. Nam echter de weerstand voor transpiratie meer toe dan voor opname, dan was een toenemend watergehalte en een afnemende stroomsnelheid het gevolg. Een en ander blijkt ook uit het model voor de waterhuishouding in planten dat werd geformuleerd n.a.v. de experimenten in hoofdstuk 7.

CURRICULUM VITEA

Johannes Engelbert Andreas Reinders werd op 5 juli 1958 in Horst (L.) geboren. Van 1964 tot 1970 volgde hij basisonderwijs aan de St. Hubertusschool te Hegelsom. In 1976 legde hij eindexamen Atheneum B af aan het Peelland college te Deurne.

In datzelfde jaar begon hij de studie Moleculaire Wetenschappen aan de Landbouwhogeshool te Wageningen. Zijn afstudeervakken waren Moleculaire Fysica (verzwaard hoofdvak) en Dierfysiologie (hoofdvak). Zijn praktijktijd bracht hij door aan de "State University of New York, Department of Chemistry", in Stony Brook, New York, USA.

Hij studeerde in 1983 af, waarna hij gedurende 4 jaar in dienst was van de Landbouwhogeschool en op de vakgroep Moleculaire Fysica het onderzoek verrichtte dat tot dit proefschrift leidde.